

## **Novel Coatings for Enhancement of Light-Emitting Diodes (LEDs)**

**October 28, 2006**

**Sponsored by  
Defense Advanced Research Projects Agency (DOD)  
Advanced Technology Office**

**ARPA Order T169**

**Issued by U. S. Army Aviation & Missile Command Under  
Contract No. W31P4Q-05-C-R017**

### **Distribution Statement**

Approved for public release, distribution unlimited.

**Final Report (CDRL A006)**

**Science Applications International Corporation**  
**1710 SAIC Drive**  
**McLean, Virginia 22102**

**Effective Date of Contract**  
**October 21, 2004**

**Contract Expiration Date**  
**October 31, 2006**

**Reporting Period**  
**October 21, 2004 – October 28, 2006**

**Principal Investigator**  
**Russell Smilgys**  
**(703) 676-4056**

**DISCLAIMER**

The views and conclusions contained in this document are those of the authors and should not be interpreted as representing the official policies, either expressed or implied, of the Defense Advanced Research Projects Agency, the U.S. Army Aviation & Missile Command, or the U.S. Government.

## REPORT DOCUMENTATION PAGE

Form Approved  
OMB No. 0704-0188

The public reporting burden for this collection of information is estimated to average 1 hour per response, including the time for reviewing instructions, searching existing data sources, gathering and maintaining the data needed, and completing and reviewing the collection of information. Send comments regarding this burden estimate or any other aspect of this collection of information, including suggestions for reducing the burden, to Department of Defense, Washington Headquarters Services, Directorate for Information Operations and Reports (0704-0188), 1215 Jefferson Davis Highway, Suite 1204, Arlington, VA 22202-4302. Respondents should be aware that notwithstanding any other provision of law, no person shall be subject to any penalty for failing to comply with a collection of information if it does not display a currently valid OMB control number.

PLEASE DO NOT RETURN YOUR FORM TO THE ABOVE ADDRESS.

1. REPORT DATE (DD-MM-YYYY) 28-10-2006	2. REPORT TYPE CDRL A006, Final Report	3. DATES COVERED (From - To) 21-10-2004 to 28-10-2006		
4. TITLE AND SUBTITLE Novel Coatings for Enhancement of Light-Emitting Diodes (LEDs)		5a. CONTRACT NUMBER W31P4Q-05-C-R017		
		5b. GRANT NUMBER		
		5c. PROGRAM ELEMENT NUMBER		
6. AUTHOR(S) Dr. Russell V. Smilgys Dr. Neri Shatz Dr. John Bortz		5d. PROJECT NUMBER		
		5e. TASK NUMBER		
		5f. WORK UNIT NUMBER		
7. PERFORMING ORGANIZATION NAME(S) AND ADDRESS(ES) Science Applications International Corporation 1710 SAIC Dr McLean, VA 22102		8. PERFORMING ORGANIZATION REPORT NUMBER		
9. SPONSORING/MONITORING AGENCY NAME(S) AND ADDRESS(ES) U.S. Army Aviation & Missile Command Redstone Arsenal, AL 35898-5248		10. SPONSOR/MONITOR'S ACRONYM(S)		
		11. SPONSOR/MONITOR'S REPORT NUMBER(S)		
12. DISTRIBUTION/AVAILABILITY STATEMENT Approved for public release; distribution unlimited.				
13. SUPPLEMENTARY NOTES				
14. ABSTRACT This report summarizes work performed by Science Applications International Corporation (SAIC) in fulfillment of a contract with the Defense Advanced Research Projects Agency. SAIC's partner in this work was Lumileds, a major manufacturer of high power LEDs. Since SAIC did not have a contractual relationship with Lumileds - which was agreed to by all parties at the beginning - SAIC's performance on some tasks was ultimately limited by Lumileds' cooperation. One task was to investigate novel coatings that could protect and improve the performance of light emitting diodes (LEDs). Another task was to investigate methods to improve the stability and performance of a phosphor coating on an LED die. The final task was to develop original designs that could improve the external quantum efficiency of LEDs.				
15. SUBJECT TERMS				
16. SECURITY CLASSIFICATION OF: a. REPORT U		17. LIMITATION OF ABSTRACT UU	18. NUMBER OF PAGES 128	19a. NAME OF RESPONSIBLE PERSON Dr. Russell V. Smilgys
b. ABSTRACT U		c. THIS PAGE U		19b. TELEPHONE NUMBER (Include area code) (703) 676-4056

## Table of Contents

Summary.....	1
Task Results.....	2
Task 1. Deposit and evaluate coatings on bare LED dies without phosphor supplied by Lumileds: Non-functional dies.....	2
Task 2. Deposit and evaluate coatings on bare LED dies without phosphor supplied by Lumileds: Functional dies.....	2
Task 3. Evaluate effectiveness of dielectric coating to stabilize the performance of LEDs with respect to harsh environmental exposure – with phosphor.....	14
Task 4. Investigate techniques to improve the external quantum efficiency of LEDs..	17
Appendix A. Report by consultant Dr. Krupke on phosphors.....	18
Appendix B. PowerPoint presentation of Task 4 results.....	26

## Summary

This report summarizes work performed by Science Applications International Corporation (SAIC) in fulfillment of a contract with the Defense Advanced Research Projects Agency. SAIC's partner in this work was Lumileds, a major manufacturer of high power LEDs. Since SAIC did not have a contractual relationship with Lumileds - which was agreed to by all parties at the beginning - SAIC's performance on some tasks was ultimately limited by Lumileds' cooperation.

One task was to investigate novel coatings that could protect and improve the performance of light emitting diodes (LEDs). SAIC's technical strength in coatings is an alumina coating deposited by a physical vapor deposition technique called ion beam assisted deposition (IBAD). Lumileds defined a problem of interest to be prevention of corrosion on the submount of an LED die. SAIC designed and built fixturing to handle Lumileds' LED wafers, then coated samples. The coating process yielded dies with a strongly adhered alumina coating that was unaffected by solvents, furnace firing, and thermal shock. The last batch of dies coated in 2005 showed the same protective properties as well as no loss in electrical or light emission properties, according to accounts of testing performed by Lumileds. Unfortunately this early success was not pursued because Lumileds underwent a change in ownership around July 2005, during which it suspended its collaboration with SAIC. By the time Lumileds was ready to resume the collaboration in May 2006, it had already solved the corrosion problem by other means.

Another task was to investigate methods to improve the stability and performance of a phosphor coating on an LED die. One of Lumileds' products is a white light LED that consists of a blue die with a yellow phosphor. The phosphor coating is a relatively thick coating consisting of phosphor particles embedded in a silicone binder. The goal of this task was to find a phosphor that could function within an alumina coating. Our consultant's analysis revealed that the fundamental physics of phosphor emission severely limits the number of potential candidates. We found that commercial phosphor powders with high quantum efficiency are too large to embed in an alumina coating. We synthesized a nanoscale yellow phosphor when no vendor could be found. Unfortunately that phosphor yielded poor quantum efficiency. In the end we failed to develop a method to improve phosphor performance on an LED die, albeit with a modest effort in exploring other phosphor possibilities.

The final task was to develop original designs that could improve the external quantum efficiency of LEDs. SAIC's strength in this area is a proprietary nonimaging optics code. In consultation with Lumileds, SAIC developed designs for five different optical elements that collect and project light from a LED. The simulations showed that the designs achieve a significant improvement in performance compared to Lumileds original dome design.

## Task Results

### ***Task 1. Deposit and evaluate coatings on bare LED dies without phosphor supplied by Lumileds: Non-functional dies***

Prior to the start of the contract we anticipated that Lumileds would have non-functional dies that SAIC could use to perform preliminary optimization of the coating process. As it happened, Lumileds decided to supply only functional dies; therefore this task was immediately bypassed.

### ***Task 2. Deposit and evaluate coatings on bare LED dies without phosphor supplied by Lumileds: Functional dies***

On November 24, 2004 SAIC received from Lumileds three diced wafers, for a total of 12 samples. Two of the wafers had a circuit element bonded next to the flip chip (style B). The third wafer lacked the extra element and contact pads around the edge of the wafer (style A).

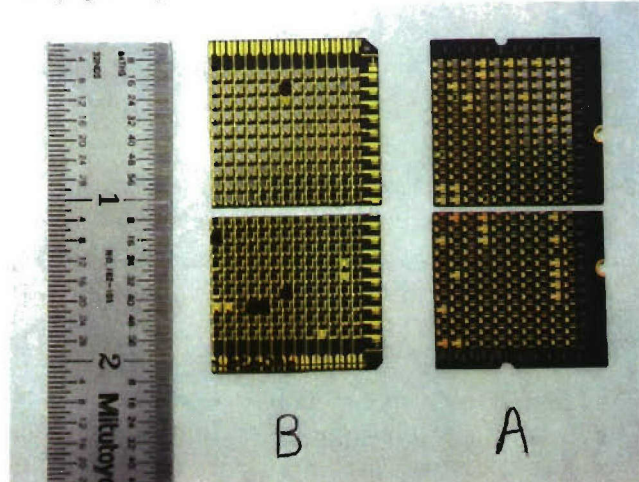


*Figure 1. Two samples of each 'style' of diced LED wafer received from Lumileds. Style B has electrical pads on its front surface to light individual LEDs. The style A sample on the right has only back surface pads.*

At the kick off meeting on November 8, 2004, Scott Kern said he was interested to have an alumina coating deposited to protect the submount from corrosion. The flip chips are bonded above the submount with a small gap underneath. While most of the submount is exposed when a sample is mounted normal to the deposition beam, regions around the base of the flip chip could be shadowed. The reason is that the alumina evaporant follows a line-of-sight path from source to substrate. To achieve better coverage around the base, we built a fixture that holds a sample at angle with respect to the evaporation source. The angle can be varied from 0° to 90°. Based on the packing density of flip chips on a submount, we estimate that the optimal angle is between 20° and 40°. To further increase coating uniformity, we included sample spinning.



*Figure 2. View inside coating chamber looking down at fixtures built to coat LED samples. The horizontal bar across the middle suspends three fixtures that hold samples at an angle with spinning. The three angles set are 40°, 30°, and 20°, left to right respectively. The two circles beneath the fixtures are holes in a panel to pass the evaporant beam from below. A window to look into the chamber is located at the top left of the picture.*

Two coating runs were performed on 6Dec04 and 9Dec04 using the new fixture. Two samples of style A were coated in the first run, and two samples of style B in the second run. A third sample of style B was loaded in the chamber during 9Dec04 and left uncoated as a control.

#### **Coating Run 6Dec04**

Two samples of a style A wafer were coated with alumina by ion beam assisted deposition (IBAD):

Sample ID	Deposition Rate	Coating Thickness	Mounting Angle
6Dec04P1	1.9 nm/s	3150 nm	20°
6Dec04P2	1.9 nm/s	2250 nm	40°

The most important variables in the process are the deposition rate of alumina and the ion source parameters. These parameters were set based on a ‘recipe’ developed several years ago for coating advanced solar reflective materials. For that contract the alumina coating protected silver from tarnishing. The optimal recipe for protection of a LED submount might be different. For example, the solar reflective material was a flat

sheet, whereas the LED samples have surface texture. To take this into account we mount the samples at a skewed angle in the coating chamber. The nominal deposition rate and thickness are stated for a surface with normal incidence to the evaporant beam, but the actual rate and thickness will depend on the local geometry of the surface texture. If the sample surface were flat, the coating thickness would be 1080 nm and 1450 nm for samples P1 and P2, respectively. An additional complexity is that the ion source is incident at an angle.

The alumina coating is transparent and thin. By eye, the only indication of its presence is a slightly darker color in coated regions compared to the uncoated edge where the submount was masked. Under an optical microscope at 100x power the coating is not visible.

#### **Fire sample 6Dec04P1 in tube furnace**

As a first test, sample 6Dec04P1 was progressively heated in a tube furnace according to the following protocol:

Step	Temperature [°C]	Time [minutes]
1	250	5
2	350	15
3	425	15

The coated side of the sample showed no effect from this treatment. However, the uncoated backside showed discoloration after heating to 425°C. Sample 6Dec04P2 was heated to 155°C and showed no effect.

Both samples were evaluated for functional LEDs using a current limited power supply set to 3 volts and 100 mA. Since the style A wafer lacks contact pads on its front surface, we built a simple test gig to make electrical contact one row at a time on the backsurface. For sample 6Dec04P2 whole rows light as brightly as an uncoated control. For sample 6Dec04P1, whole rows light, but the LEDs are dimmer than an uncoated style A sample.

#### **Coating Run 9Dec04**

Three samples of a style B wafer were loaded in the coating chamber, but only two were coated with alumina by IBAD:

Sample ID	Deposition Rate	Coating Thickness	Sample Mounting Angle
9Dec04P1	1.9 nm/s	4500 nm	20°
9Dec04P2	1.9 nm/s	7200 nm	40°

The samples were evaluated for functional LEDs using a current limited power supply set to 3 volts and 100 mA. The samples were not baked prior to testing. The style B wafer does not require a gig to test for LED functionality because front surface contact

pads are present. A single LED is addressed by contacting its respective row and column pads. For sample 9Dec04P1 80% of the LEDs light as brightly as an uncoated style B sample, 10% light but are dimmer, and 10% partially light. Partial lighting is characterized by only one or two of the three ‘zones’ lighting on a single LED.

For sample 9Dec04P2 a significant degradation of its electrical characteristics occurred. When a pair of row and column pads are contacted, multiple LEDs light instead of just one. Those LEDs protected by a mask from coating light as a complete row, whereas those that are coated light either whole or partial rows or columns, depending on the particular pair of pads contacted. Either due to degradation or spreading of the available power across multiple LEDs, the LEDs on 9Dec04P2 were also dimmer.

The uncoated control sample that was loaded into the chamber showed some darkening where its surface was not masked. Its LEDs light brightly.

#### **Coating Run 23Dec04**

The purpose for this run was to explore whether it is better for the LEDs to be electrically isolated from or shorted to ground during deposition. This could be important because the deposition process uses an ion beam. Two samples were mounted on aluminum blocks that are connected to chamber ground. The LED pads on the sample at Position 1 were electrically shorted out to the block using silver paint. The LED pads at Position 2 were electrically isolated from the block using Kapton tape. Both samples were individually coated with alumina by ion beam assisted deposition (IBAD).

The ion source was operated on a mixture of argon and a proprietary gas. Compared to previous runs, the ion beam power was reduced by a factor of  $\sin(40^\circ)$  to account for the reduced deposition rate when a surface is held at an angle during deposition.

A piece of glass slide was used to mask a portion of each sample. After deposition the thickness of the coating on the slide was measured by fitting the optical transmission.

Sample ID	Deposition Rate	Coating Thickness	Sample Mounting Angle
23Dec04P1	2 nm/s	2 $\mu$ m	40°
23Dec04P2	2 nm/s	2 $\mu$ m	40°

Unexpectedly, the silver paint tightly bonded sample 23Dec04P1 to the aluminum block. It had to be soaked in acetone to break it free. The flip chip side of the sample showed contamination with small particles, as viewed under an optical microscope at 50x. The LEDs on this sample were tested one at a time using a current limited power supply (3 volts and 0.1 amps). All the LEDs light and draw the full current, however, in some cases, more than one LED lights, which suggests shorting between LEDs. This might have been caused by the silver paint not being completely removed after coating, or an electrical overload caused by the ion source during deposition.

Sample 23Dec04P2 was mounted without silver paint. The flip chip side is clean and free of particles. The coating is most clearly distinguished at the transition between coated and uncoated regions. The coating itself appears glassy, and successfully covers the submount and gold electrical traces. The coated submount appears slightly darker colored than bare submount.

One thing we noticed using an optical microscope is an appearance of granularity on the underside of many flip chips. The effect is not perfectly correlated with the alumina coating, but more coated flip chips show granularity than do uncoated ones. In figure 3 granularity is evident on the left hand side flip chip compared to the right hand side one. In the four vertical bands under the flip chip, there is increased scattering of light. The bright spot of light located in the second band from the left is not due to granularity. Instead this is caused by a dimple in the top surface, possibly caused when the flip chip was mounted. Although not evident here, it is evident in SEM images.

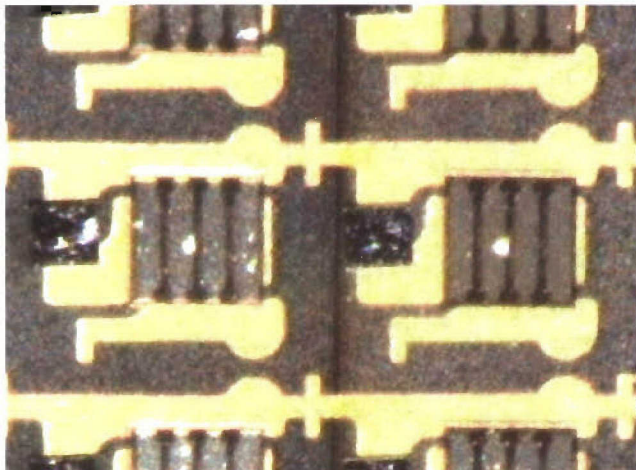


*Figure 3. Video still frame of sample 23Dec04P2. The vertical line down the middle is the transition between the coated region on the left and the uncoated region on the right. Each flip chip has four bands that light. The coated flip chip shows increased underside granularity compared with the uncoated flip chip.*

### **Electrical testing of 23Dec04P2**

All of the LEDs on sample 23Dec04P2 light and draw 0.1 amps.

### **Coating Run 28Dec04**

The purpose for this run was to investigate the use of oxygen as the ion source feed gas instead of the proprietary gas. The motivation for this change was that the coating on the glass slide in the previous run was slightly tinted, which suggested incomplete oxidation.

Two samples of a Style B wafer were mounted onto the aluminum blocks using Kapton tape for electrical isolation. A piece of glass slide was used to mask a portion of each sample from coating. Later the coating thickness on the glass slide was measured by fitting the optical transmission spectrum.

Sample ID	Deposition Rate	Coating Thickness	Sample Mounting Angle
28Dec04P1	2 nm/s	2 $\mu$ m	40°
28Dec04P2	$\leq$ 2 nm/s	3 $\mu$ m	40°

Under an optical microscope, both samples appeared clean with a glassy alumina coating.

### Electrical testing of 28Dec04P2

All of the LEDs on sample P2 were tested using a current limited power supply. All of the uncoated LEDs draw 0.1 amps and appear by eye to light brightly. The coated LEDs vary in their current draw from 70 to 100 milliamps, with the majority drawing 70 mA amps and lighting less brightly.

### Fire sample 28Dec04P1 in tube furnace

Sample P1 was subjected to firing in a tube furnace open to air according to the protocol:

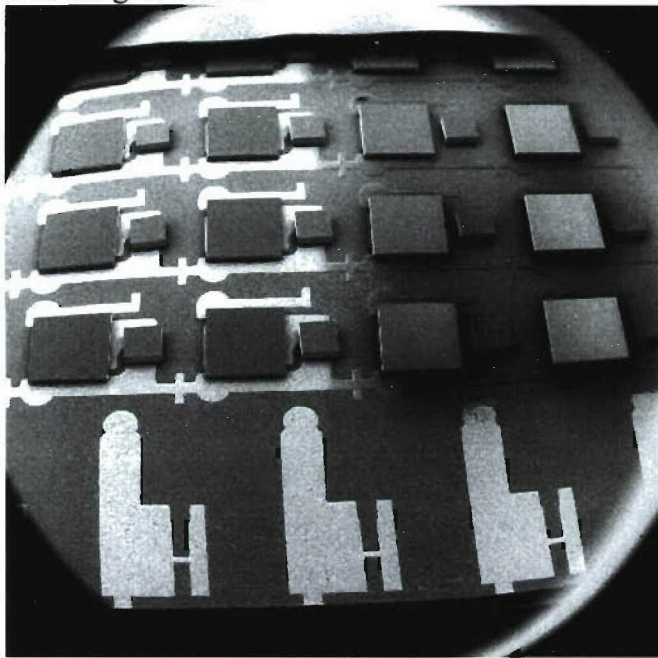
Step	Temperature [°C]	Time [minutes]
1	250	6
2	350	15
3	420	15

After Step 1 the sample was inspected under an optical microscope (50x). The coating showed no damage. About 20% of the LEDs were retested, and all appeared to light brightly by eye. After Step 2 all of the LEDs were retested. All lit, but none as brightly as after Step 1. Some LEDs were initially bright then dimmed after a moment. Again, the coating showed no damage. After Step 3 the sample was quickly pulled from the furnace to maximize the thermal shock. The sample cooled from 420°C to 100°C in about 30 seconds. Again, the coating showed no sign of flaking or cracking. All the LEDs continued to light individually, but still dimmer than after Step 2. All of the LEDs drew less than 10 mA amps at 3 volts. Some of the LEDs light fewer than the four 'bands' present on each flip chip.

### SEM Analysis of 28Dec04P1-after furnace firing

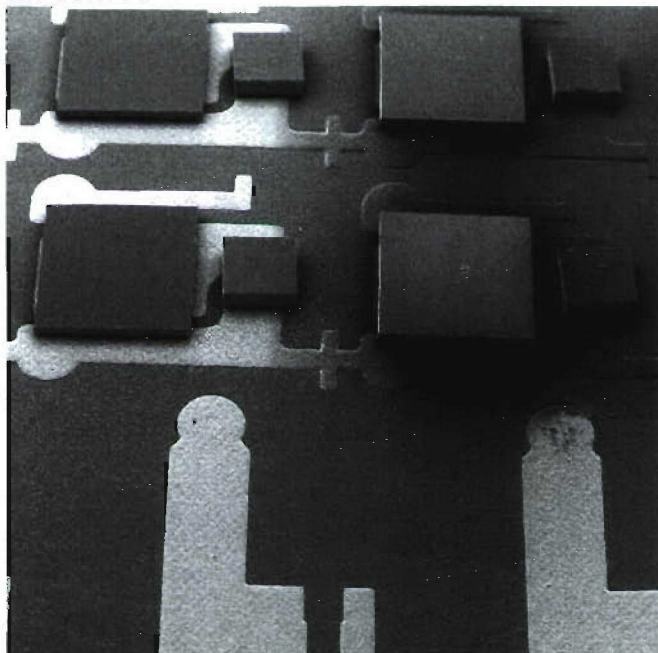
Sample 28Dec04P1 was analyzed using the SEM at SAIC- after the sample had been through the furnace firing protocol. Figure 4 is a broad view of the sample using the lowest magnification available. The distorted view is due to the low magnification. A matrix (four columns wide and three rows deep) of flip chips is visible. Three electrical contact pads for the wafer are visible at the bottom of the image. The entire region of the sample in the image has been sputtered coated with gold to prevent beam charging. The two columns on the right were coated with alumina, the two columns on the left are un-coated. The remarkable difference between the two is that the gold electrical traces in the uncoated region show a bright contrast against the darker insulating submount. The reason for the contrast is that the alumina coating is electrically insulating and it lowers the secondary electron emission from the underlying gold traces. The absence of bright con-

trast on the right two columns of flip chips is evidence that the alumina coating has uniformly covered the gold traces.



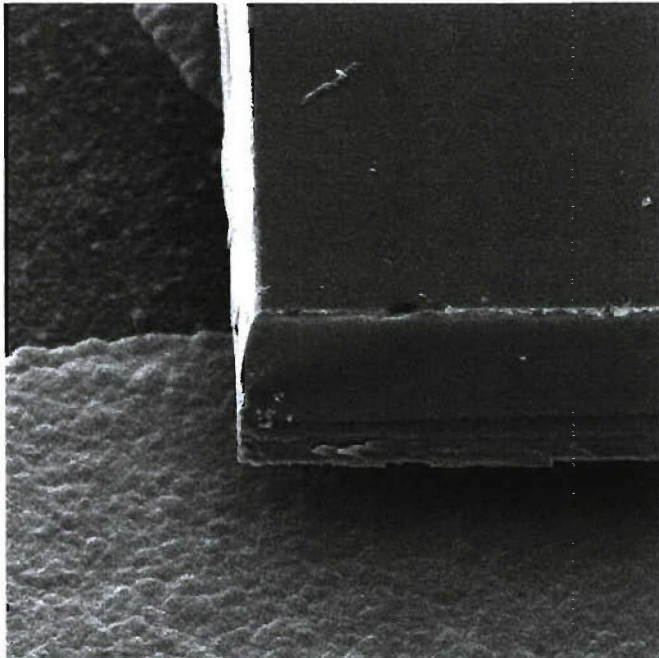
*Figure 4. SEM view of sample 28Dec04P1- after furnace firing.*

Figure 5 is a closer view at the border between uncoated and alumina coated regions. The uncoated region was masked by a glass slide during deposition, as were the electrical contacts at the bottom.



*Figure 5. Closer view of border between uncoated and alumina coated regions.*

Figures 6 and 7 compare the corners of flip chips that were uncoated and coated with alumina.



*Figure 6. Corner of flip chip in region uncoated with alumina.*

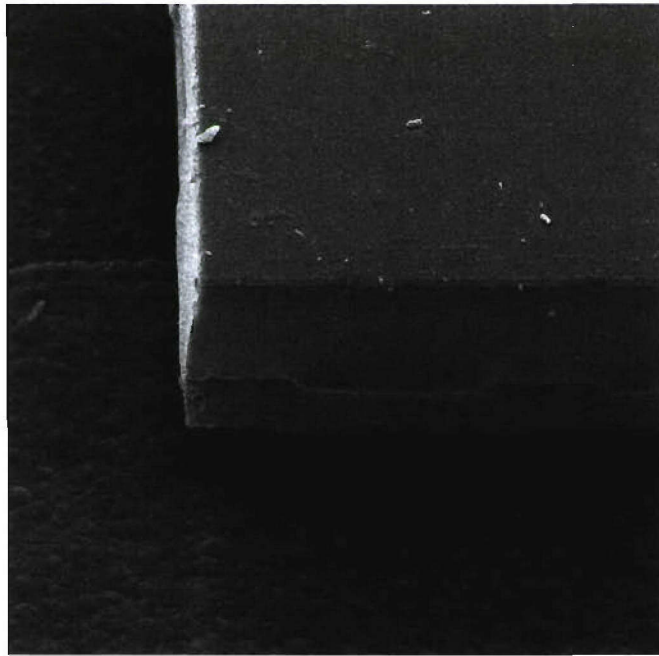


*Figure 7. Corner of flip chip in region coated with alumina.*

Figures 8 and 9 show a gold trace that is coated with alumina at the top, but uncoated at the bottom. A glass slide was used to mask the wafer prior to alumina coating. These figures show that the alumina coating remains strongly bound to the trace and submount-even after having been fired to 420°C.

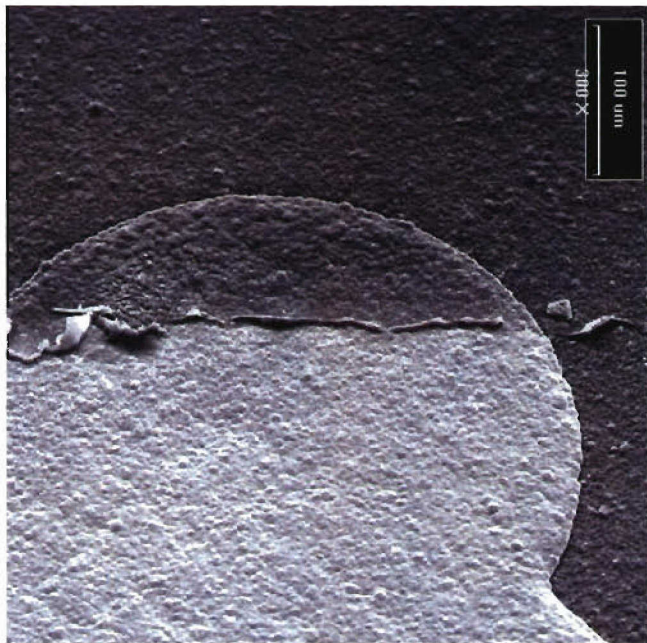


Figure 8. View of gold trace partially coated with alumina. The bottom portion of the trace was masked by a glass slide during alumina deposition. The fragments of alumina coating present at the border were created when the glass slide was torn away from the wafer.

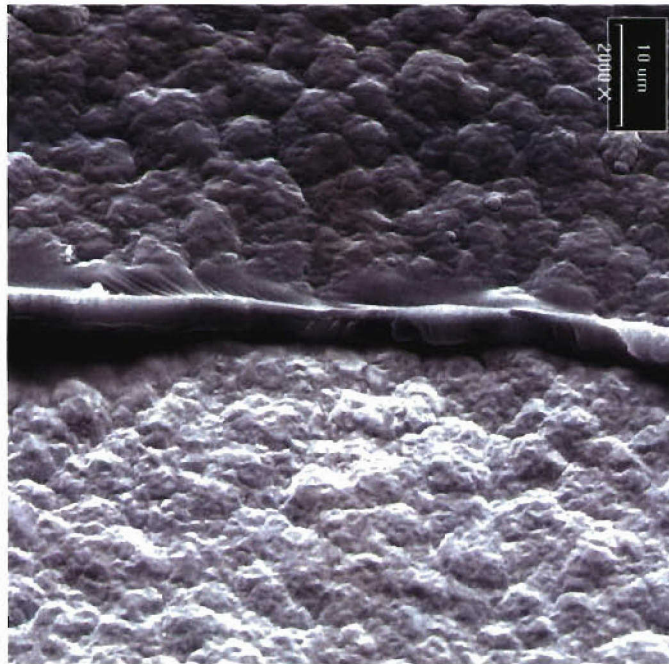
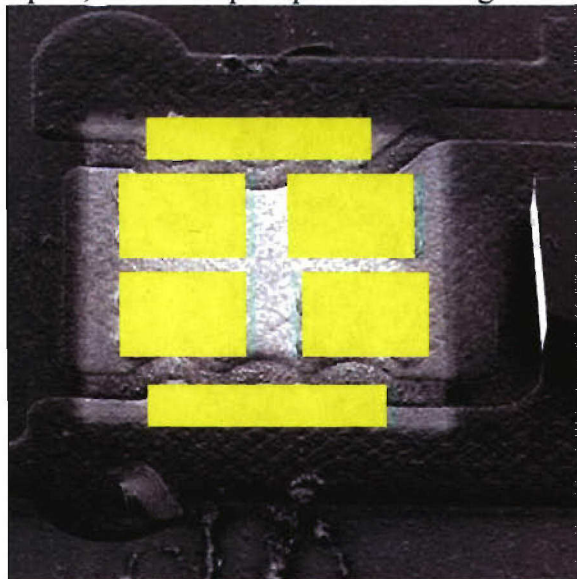


Figure 9. Detail from Figure 6 over gold trace. The alumina coating extends from the top of the frame to the middle. The horizontal band in the middle of the frame is a cross sectional view of the alumina coating where it was turned up in contact with the glass slide mask. The coating is two microns thick. Even after having been fired to 420°C, the alumina coating remains well adhered to the gold trace.

After the sample had been sputter coated with gold, a flip chip was removed from a region that was alumina coated. Figure 10 shows that a high contrast “shadow” remains where the flip chip is missing. This is evidence that the alumina coating does not extend beneath the flip chip. This is expected because the alumina coating deposition follows a line-of-sight path, and the flip chip masks the region beneath itself.



*Figure 10. The flip chip has been removed to reveal a bright contrast shadow.*

#### **Thermal shock test of 28Dec04P1**

The sample 28Dec04P1 was tested for resistance of the alumina coating to thermal shock. The sample had already been furnace fired and sputter coated with gold. The thermal shock test consisted of plunging the whole sample into a cup of liquid nitrogen, waiting until bubbling stopped, removing the sample from the cup, placing it in a ziplock bag, and waiting until it warmed to room temperature. This sequence of steps was repeated four times. (The purpose of the ziplock bag was to minimize water condensation on the cold sample while it warmed.) Then the sample was viewed using the SEM. The result was that the alumina coating remained fully adhered, with no sign of damage. Figure 11 is a low magnification view of coated and uncoated regions. The darker contrast in coated regions is evidence that the alumina coating remains in place.

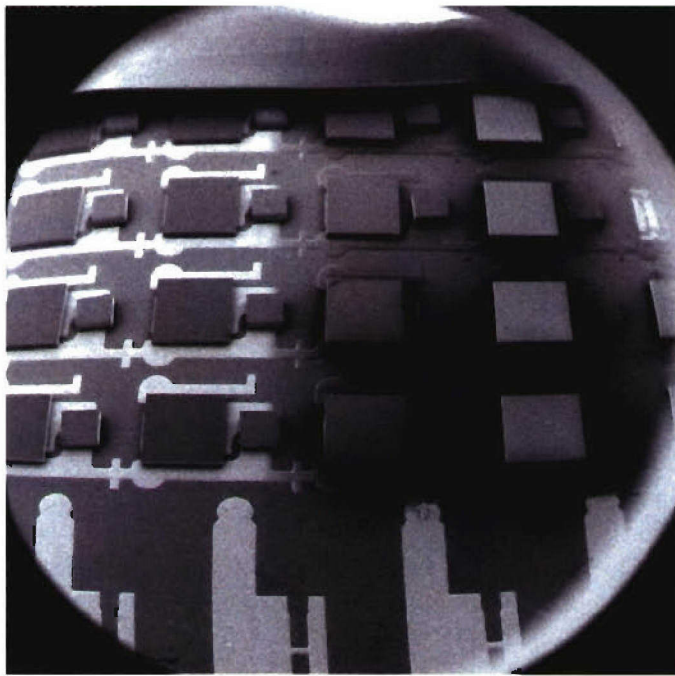


*Figure 11. View of sample 28Dec04P1 after thermal shock test. The test consisted of rapidly cycling the sample from room temperature to liquid nitrogen four times. The lack of bright contrast on the electrical traces around the two columns of flip chips on the right, which were coated with alumina, is evidence that the alumina coating remains in place.*

#### **Coating Run 19Jan05**

The purpose for this run was to explore whether it is better for the LEDs to be electrically isolated from or shorted to ground during deposition. This could be important because the deposition process uses an ion beam. Two samples were mounted on aluminum blocks that are connected to chamber ground. The LED pads on the sample at Position 1 were electrically shorted out to the block using silver paint. The LED pads at Position 2 were electrically isolated from the block using Kapton tape. Both samples were individually coated with alumina by ion beam assisted deposition (IBAD).

A piece of glass slide was used to mask a portion of each sample. After deposition the thickness of the coating on the slide was measured by fitting the optical transmission.

Sample ID	Deposition Rate	Coating Thickness	Sample Mounting Angle
23Dec04P1	2 nm/s	2 $\mu$ m	40°
23Dec04P2	2 nm/s	2 $\mu$ m	40°

#### **Electrical testing of 23Dec04P2**

All of the LEDs on sample 23Dec04P2 light and draw 0.1 amps.

#### **Coating Run 28Dec04**

The purpose for this run was to investigate the use of oxygen as the ion source feed gas instead of the proprietary gas. The motivation for this change was that the coating on the glass slide in the previous run was slightly tinted, which suggested incomplete oxidation.

Two samples of a Style B wafer were mounted onto the aluminum blocks using Kapton tape for electrical isolation. A piece of glass slide was used to mask a portion of each sample from coating. Later the coating thickness on the glass slide was measured by fitting the optical transmission spectrum.

Sample ID	Deposition Rate	Coating Thickness	Sample Mounting Angle
28Dec04P1	2 nm/s	2 $\mu\text{m}$	40°
28Dec04P2	$\leq$ 2 nm/s	3 $\mu\text{m}$	40°

### Electrical testing of 28Dec04P2

All of the LEDs on sample P2 were tested using a current limited power supply. All of the uncoated LEDs draw 0.1 amps and appear by eye to light brightly. The coated LEDs vary in their current draw from 70 to 100 milliamps, with the majority drawing 70 mA amps and lighting less brightly.

### Summary of LED Dies Coated in March/April 2005

Lumileds supplied to SAIC 12 new samples for coating on February 23, 2005. The samples were half of a whole Type B wafer, or 1" x 2" in size. Since the new samples were twice as large as the previous samples, we fabricated two new holders from machinable ceramic. The purpose for the ceramic holder was to electrically isolate the LEDs from ground during deposition. The new holders were large enough to accommodate a whole wafer. For these runs a blank piece of glass slide was mounted next to the sample as a witness. After deposition the thickness of the coating on the slide was measured by fitting the optical transmission.

#### Summary of samples coated in 2005

SAIC Sample ID	Coating Thickness	Lumileds ID#	Comment
15Mar05P1	1.8 $\mu\text{m}$	050114-26	
15Mar05P2	1.8 $\mu\text{m}$	050114-26 Top	
17Mar05P1	3.4 $\mu\text{m}$	050114-32	
17Mar05P2	4.6 $\mu\text{m}$	050114-32 Top	Reduced %T in blue
21Mar05P1	2.1 $\mu\text{m}$	050114-30	Reduced %T in blue
21Mar05P2	1.7 $\mu\text{m}$	050114-30 Top	
24Mar05P1	1.7 $\mu\text{m}$	050114-29	
24Mar05P2	1.7 $\mu\text{m}$	050114-29 Top	
28Mar05P1	2.0 $\mu\text{m}$	050114-28 Top	
28Mar05P2	2.6 $\mu\text{m}$	050114-28	
2April05P1	0.7 $\mu\text{m}$	050114-27 Top	
2April05P2	2.6 $\mu\text{m}$	050114-27	Coating flaking on flip chip

On April 7, 2005 Russell Smilgys delivered 12 half wafers (Type B) coated with alumina to Lumileds. Xina Quan reported that of the four wafers she tested, all showed only minor changes in performance. Her employment ended at Lumileds before she could test all of the coated wafers. Scott Kern reviewed the data and decided that further evaluation of the alumina coating as a protective barrier was warranted.

About May 2005 Scott Kern stopped responding to phone calls and messages. SAIC later learned that Lumileds was acquired by Philips Lighting and that Scott was instructed to suspend his interaction with SAIC. SAIC placed Task 2 into suspension while Lumileds completed its change in ownership. Scott finally reported in April 2006 that he was ready to resume the interaction with SAIC, however, in the mean time Lumileds had solved the problem of corrosion of the LED submount-the motivation for the task in the first place. The new technical point of contact assigned by Scott was unable to identify a new problem that novel coatings could address, so no further work was done on this task.

***Task 3. Evaluate effectiveness of dielectric coating to stabilize the performance of LEDs with respect to harsh environmental exposure - with phosphor***

The anticipated scope for this task included development of a coating process able to embed phosphor particles into the IBAD alumina coating. The outline for the task was as follows:

- e. Develop coating process at SAIC to embed phosphor into alumina coating
  1. Co-evaporate alumina and YAG:Ce and/or other phosphor system onto sapphire substrates
  2. Evaluate the coating at SAIC:
    - i. Perform compositional analysis
    - ii. Measure spectral output of embedded phosphor coating under appropriate illumination
- f. If successful, co-evaporate and deposit alumina and YAG:Ce phosphor onto functional LEDs
- g. Evaluate optical performance of coated dies at SAIC
- h. Deliver coated dies to Lumileds for optical and environmental evaluation

SAIC hired the consultant Dr. William Krupke to scope out in detail the physics of the problem and identify potential solutions. Dr. Krupke was formerly Deputy Associate Director at Lawrence Livermore National Laboratory (LLNL) for 20 years. At LLNL he co-founded the Laser Directorate and was responsible for the development and execution of the Laboratory's Inertial Confinement Fusion (ICF) and Atomic Vapor Laser Isotope Separation (AVLIS) national R&D programs. Since he left LLNL in 1999 he has been a full time consultant to high-growth start-up companies, including Novalux, Crystal Photonics, and Photera.

We had Dr. Krupke investigate the feasibility of item e. and review the literature to determine if a solution might already have been reported. He delivered an eight page report.

Here is a summary of his results and recommendations. His full report may be found in Appendix A.

Three approaches to solving item e. were investigated: 1. Direct ion doping of alumina films for yellow phosphor functionality, 2. Embedding Ce:YAG phosphor particles in alumina thin films, 3. Embedding other blue-absorbing, yellow-emitting phosphor particles in alumina thin films.

#### Approach 1

The first approach would be the most desirable because the doped ion would be co-evaporated with the alumina. A difficult constraint on this approach is that the alumina coating is relatively thin. It is not practical to deposit an alumina coating more than 10,000 nm thick, so the doping and conversion efficiency of the ion would need to be high. Krupke showed that the peak absorption transition cross-section would need to be no less than  $10^{-18} \text{ cm}^2$ , assuming a maximum ion doping density of  $10^{21} \text{ cm}^{-3}$ . Transition metal d-d transitions meet this condition; however, a review of the literature found that none of the transition metal ions known to fluoresce in an alumina host possess appropriate absorption and emission features. Rare earth f-d transitions are also strong enough. Two candidate dopants are  $\text{Ce}^{+3}$  and  $\text{Eu}^{+3}$ . Again, a review of the literature found that these two ions also have the wrong absorption and emission features in an alumina host. In summary, Dr. Krupke was unable to identify any candidate ion for direct embedding in an alumina film that would meet the necessary criteria for a practical alumina phosphor that efficiently emits yellow radiation when excited by a blue LED. This approach was dropped.

#### Approach 2

The second approach is to embed Ce:YAG phosphor particles in an alumina coating. There are precedents for this type of phosphor particle embedding so it is a more promising approach. Dr. Krupke believes phosphor particles on the order of 100 to 1000 nm in size can be loaded with a sufficient density of  $\text{Ce}^{+3}$  to meet the goal. The simplest implementation would be to build up a multilayered coating consisting of layer of “sprinkled” phosphor particles, followed by a layer of alumina, and so on. To attempt this approach SAIC would need a supply of nanoparticle Ce:YAG phosphor.

As a first step we acquired samples of two yellow phosphors from Phosphor Technology in the smallest particle size offered.

PTL GRADE	CHEMICAL COMPOSITION	CIE COLOUR COORDINATES		MEDIAN PARTICLE SIZE (MICRON)
QMK58/N-C1	$\text{Y}_3\text{Al}_5\text{O}_{12}:\text{Ce}$	0.412	0.544	8.0
QMK58/F-C1	$\text{Y}_3\text{Al}_5\text{O}_{12}:\text{Ce}$	0.412	0.544	3.5

We built a test stand to measure the emission from these phosphors under pumping by blue LEDs with emission centered at 430 nm and 460 nm. Figure 12 shows the emission

spectra for phosphor QMK58/FC1 pumped by the 460 nm LED. The thickness of the phosphor layer was adjusted to allow some of the pump beam to transmit.

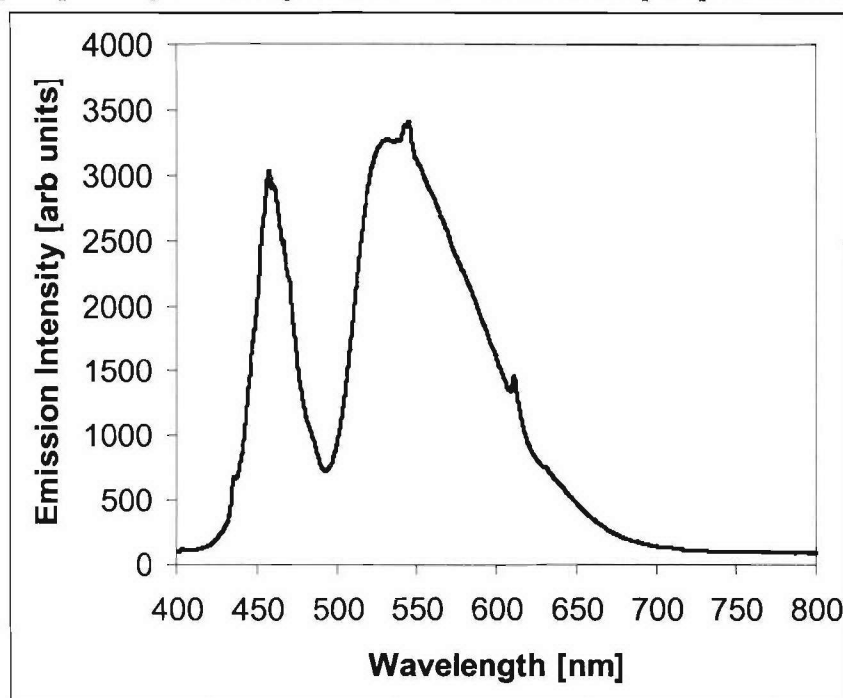


Figure 12. Transmission spectrum of YAG:Ce phosphor pumped by 460 nm LED. The thickness of the phosphor layer was adjusted to allow some of the pump beam to transmit.

While these commercial phosphor exhibit excellent quantum efficiency, they are not practical to embed in an alumina coating. The reason is that the maximum practical thickness for an alumina coating is only 6 microns, which is too thin to cover and seal particles that are almost as large or larger. Ideally the phosphor particles would be at the nano-scale.

We were unable to find a commercial vendor for nanoparticle yellow phosphor, so we synthesized a nanoscale YAG:Ce<sup>3+</sup> phosphor following a published recipe (“The crystal structure and spectra of nano-scale YAG:Ce<sup>3+</sup>,” Qian Li, Lian Gao, and Dongsheng Yan, *Materials Chemistry and Physics*, **64** (2000) 41). In brief:

Nanoscale powders of cerium-doped yttrium aluminum garnet (YAG ( $\text{Y}_3\text{Al}_5\text{O}_{12}$ ):Ce<sup>3+</sup>) were prepared by a gel-based synthesis. Appropriate ratios of the metal nitrates (0.1 M Al, 0.06 M Y, 0.001 M Ce) were dissolved in a citric acid-stabilized solution of acrylamide monomer (6%) and crosslinker (2%). Polymerization was initiated with ammonium persulfate at 80°C, leading to the formation of a turbid, slightly-elastic gel, that was placed in an open alumina crucible in a tube furnace, and heated at 2°C /min in air to an ultimate temperature of 900°C. The temperature was maintained at 900°C for 2 hours, and then cooled to room temperature. The resulting pale yellow nanopowder was obtained in 83% yield.

We found that the resultant nano-scale phosphor showed poor quantum efficiency compared to commercial yellow phosphors, which are micron scale in size. We did not pursue this approach further.

### Approach 3

The third approach is to co-deposit sub-micron particles of a crystalline phosphor other than Ce:YAG. The idea is to find a phosphor with superior properties such as a higher excitation cross-section, higher doping solubility, higher quantum efficiency, or better optical or mechanical properties for embedding in an alumina coating. A review of the literature found two candidates-a SiAlON host matrix doped with  $\text{Eu}^{+2}$ , and  $\text{Eu}^{+2}:\text{Sr}_2\text{SiO}_4$ . We were unable to locate a vendor so this approach was not pursued.

### ***Task 4. Investigate techniques to improve the external quantum efficiency of LEDs***

The results from this task are found in a PowerPoint presentation in Appendix B.

Appendix A Report by consultant Dr. Krupke

**SAIC LED Phosphor Report Section: Alternative phosphor implementations**  
Rev 2.

**Approach 1. Direct ion doping of alumina films for yellow phosphor functionality.**

A first alternative phosphor implementation is the possibility of directly doping the amorphous alumina film with ions capable of efficiently absorbing  $\sim 460$  nm blue light generated by the LED, and efficiently converting the absorb energy into nominally  $\sim 580$  nm yellow light, thereby producing a white light output similar in character to a conventional white light LED employing a conventional  $\text{Ce}^{3+}$  doped YAG phosphor. The demand absorption and emission wavelengths, and desired alumina film thickness of 5-10 microns, places rather restrictive spectroscopic criteria on candidate dopant ions. Key criteria are listed in Table A1.

Table A1. Nominal spectroscopic criteria for color conversion ions doped into alumina.

symbol	parameter	value (range)	unit
$\lambda_{a,p}$	peak absorption transition wavelength	450-470	nm
$\alpha_{a,p}$	peak absorption coefficient*	>1000	$\text{cm}^{-1}$
$\Delta\lambda$	absorption transition halfwidth**	>10	nm
$\sigma_{a,p}$	peak absorption transition cross-section***	$10^{-18}$ - $10^{-17}$	$\text{cm}^2$
$\rho$	ion doping density***	$10^{21}$ - $10^{20}$	$\text{cm}^{-3}$
$\lambda_{e,p}$	peak emission transition wavelength	570-590	nm
$\eta$	radiative emission efficiency	>50	%

\* provides a peak absorbance of unity (one e-folding) in a 10 micron thick film.

\*\* match or exceed LED blue emission spectral width ( $\sim 10$  nm FWHM).

\*\*\*product of peak transition cross-section and ion density equals  $1000 \text{ cm}^{-1}$ .

The rather high value of peak absorptivity,  $\alpha_{a,p} > 1000 \text{ cm}^{-1}$ , is necessary to ensure a reasonably high absorbed fraction of LED blue light upon passing through the  $\sim 10$  micron thick alumina film. Since

$$\alpha_{a,p} = \rho \sigma_{a,p} = 1000 \text{ cm}^{-1} \quad (1)$$

the peak transition absorption cross-section determines the doping density that must be incorporated into the film (implicitly, it is also requires that, at that concentration, the fluorescence efficiency of the ion remains usefully high). Since the mean substitutional cation site density in alumina is  $\sim 2 \times 10^{22} \text{ cm}^{-3}$ , and fluorescing ions are generally self-quenched when doped into dielectric host media at a concentrations of several tens of percent, it is reasonable to restrict the maximum anticipated ion doping density to  $<\sim 10^{21} \text{ cm}^{-3}$ . From Eq. (1) this restricts the peak absorption transition cross-section to no less than  $10^{-18} \text{ cm}^2$ . An ion with a peak absorption transition cross-section as high as  $10^{-17} \text{ cm}^2$  would lower the needed doping ion concentration to  $10^{20} \text{ cm}^{-3}$ , or  $\sim$  a few atomic cation

percentage of the host film. Such a lower doping is considerably less likely to alter the desired protective mechanical and thermal properties of the alumina film.

The third restriction listed in Table A1, namely, the >10 nm spectral halfwidth of the ion absorption feature (matching or exceeding the ~10 nm spectral emission bandwidth typical of blue LEDs), further restricts the type of electronic transitions employed and candidate dopant ions. This restriction is expressed [1] by the relationship for electric dipole transitions of an ion embedded in a dielectric solid with an index of refraction, n:

$$\sigma_{a,p} [\text{cm}^2] = 10^{-7} f \lambda [\text{cm}]^2 \{12 \pi c n^2 (g_u/g_l) \Delta\lambda [\text{nm}]\}^{-1} \quad (2)$$

where  $\sigma_{a,p} [\text{cm}^2]$  is the peak absorption cross-section of the transition with wavelength  $\lambda [\text{cm}]$ , f is the transition oscillator strength,  $g_u$ ,  $g_l$  are respectively, the degeneracies of the upper and lower energy levels of the transition,  $\Delta\lambda [\text{nm}]$  is the absorption transition linewidth, and  $c [\text{cm/sec}]$  is the speed of light.

The oscillator strength, f, is determined by the parity of the wavefunctions of the initial and final electronic levels involved in the transition, and their spatial extensions in the host material. Many ions are known to absorb in the near UV and deep blue spectral region, and to fluoresce in the visible, when doped in dielectric solid. Rare earth ions such a  $\text{Ce}^{3+}$  and  $\text{Eu}^{2+}$  absorb and emit in parity allowed f-d transitions, while many other trivalent rare earth ions absorb and emit in parity forbidden f-f transitions. Similarly, most transition metal ions that fluoresce do so in parity-forbidden d-d transitions. Although strictly forbidden in the free ion, such transitions become partially allowed when the ion is embedded in a dielectric solid as a result of configuration parity mixing by the host medium ligand fields. Extensive spectroscopic studies of electronic transitions of transition metal ions ( $\text{TM}^{2+, 3+}$ ) and rare earth ions ( $\text{RE}^{2+, 3+}$ ) in dielectric solids manifest the typical transition oscillator strengths listed in Table A2. Using Eq. (2), typical peak absorption cross-sections are estimated and also listed in Table A2.

Table A2. Typical oscillator strengths of visible transitions of ions in dielectric solids

ion type	type	f-range	Bandwidth, nm	typical peak absorption, $\text{cm}^2$
rare earth	f-d	$10^{-3}$ - $10^{-2}$	40	$10^{-19}$ - $10^{-18}$
rare earth	f-f	$10^{-7}$ - $10^{-6}$	1	$10^{-22}$ - $10^{-20}$
transition	d-d	$10^{-3}$ - $10^{-2}$	40	$10^{-19}$ - $10^{-18}$

\*assumes a transition wavelength of 460 nm in a medium with refractive index n = 1.6

Clearly, from oscillator strength data of Table A2 combined with the spectroscopic restrictions of Table A1, as a class target ions are rare earth ions with f-d transitions and d-d- transitions of the transition metal ions. The rare earth ions with weaker f-f- transitions, although manifesting excellent fluorescence properties, cannot be utilized in the present application because of the small film thickness to be utilized.

Because the d-electrons of both the rare earth ions and the transition metal ions interact strongly with the ligands of a dielectric host, the absorption and emission transition wavelengths will vary substantially with dielectric host composition and structure. The energy separations between the  $4f^n$  and  $4f^{n-1}3d^1$  configurations of the trivalent and divalent rare earth ions have been reported by Dieke [3], and the splitting and shifting of the lowest lying (longest wavelength absorption and emission f-d transitions of  $Ce^{3+}$  and  $Eu^{2+}$  ions in various dielectric solids has been extensively reported by Dembros [4-7]. Sugano et. al. have reviewed the  $3d^n$  electronic energy levels of transition metal ions in dielectric solids and the characteristics of electronic transitions in dielectric solids [8].

Based on available spectroscopic literature, only two rare earth ions possessing f-d transitions survive as plausible candidate ions that may meet the full set of restricted values discussed above. These are listed in Table A3.

Table A3. Candidate dopant ions for a thin film alumina phosphor.

Ion type	Ion (valance)	Configurations
rare earth metal	$Ce^{3+}$	$4f^1-4f^03d^1$
rare earth metal	$Eu^{2+}$	$4f^6-4f^53d^1$

Note that none of the transition metal ions known to fluoresce in an alumina environment possess appropriate absorption and emission features required for present purposes. Regarding the specific rare earth ions listed in Table A3, in addition to possessing potentially adequately strong transitions located in the required spectral region, incorporation of adequately high ion concentrations in alumina films must be feasible with adequate purity of ion valence state under film deposition conditions. Further, the ions must manifest useful fluorescence efficiency.

Given that the  $Ce^{3+}$  has been widely utilized to produce broadband green-yellow emission in garnet crystals we first consider its use as a dopant in alumina films. The incorporation of trivalent rare earth ions in alumina has been studied most extensively in recent years using erbium,  $Er^{3+}$ , ions as the dopant ion. Interest has centered on producing 1550 nm emission in alumina single crystals (sapphire) and in amorphous alumina thin films. Because trivalent rare earth ions strongly prefer oxygen coordination numbers  $>6$  (and as high as 9 or 10), direct substitution in Al lattice sites of sapphire is difficult because the Al sites are 6-fold coordinated, and the  $Ce^{3+}$  radius (1.03 Å) is much larger than the  $Al^{3+}$  radius (0.53 Å). Nonetheless, substantial concentrations of  $RE^{3+}$  in alumina have been realized using several synthesis routes, including ion implantation followed by annealing [9], sol gel synthesis [10], and combustion synthesis [11]. Using these methods,  $RE^{3+}$  ion concentrations in excess of  $10^{20} \text{ cm}^{-3}$  have been reported, especially in amorphous thin films wherein the oxygen coordination number can exceed 6. Turning specifically to  $Ce^{3+}$ , the limited spectroscopic data for  $Ce^{3+}$  ions in alumina [12, 13] places the lowest-lying f-d absorption feature at wavelength of  $\sim 300$  nm, and emission in the near ultraviolet  $\sim 386$  nm, consistent with the large bandgap of alumina. Thus  $Ce^{3+}$  ion in alumina fails to meet the requirements set out in Table A1. The  $Eu^{2+}$  ions doped into various types of crystals are known to produce broadband blue, green, yellow, orange and red fluores-

cence [7]. In general, the more covalent bonding of oxygen-containing crystals might be expected to shift to the red the transitions responsible for  $\text{Eu}^{2+}$  ion absorption and emission transition observed in fluorides. Jaffe [14] reports for  $\text{Eu}^{2+}:\text{Al}_2\text{O}_3$  an absorption peak at a wavelength of 380 nm and an emission peak at a wavelength of 480 nm. Thus the  $\text{Eu}^{2+}$  ion in alumina fails to meet the requirement set out in Table A1.

As summarized in Table A1, we have identified no ion candidates for direct incorporation in alumina films that meet the necessary criteria for a practical alumina phosphor that efficiently emits yellow radiation when excited by blue LED emission.

Table A4. Assessment candidate dopant ions for a yellow alumina phosphor.

Ion	Comment
$\text{Ce}^{3+}$	absorption feature too far in the ultraviolet; no emission reported in alumina
$\text{Eu}^{2+}$	stabilization of divalent state unreported in alumina
$\text{TM}^{2+, 3+}$	no fluorescing ions in the yellow spectral region

### Approach 2. Embedding Ce:YAG phosphor particles in alumina thin films.

A second alternative phosphor implementation is to co-deposit Ce:YAG blue absorbing-yellow emitting phosphor particles and embed them in the alumina film. There are precedents for this type of active particle implementation in thin films [15]. Since an alumina film in the 5-10  $\mu\text{m}$  thickness range is desired, the Ce:YAG (or other) phosphor particles should have a mean diameter that is a small fraction of this physical thickness, say  $< 1\mu\text{m}$ , and possibly as small as 100 nm. In order to maintain the same absorbance for blue light in this composite film as achieved in the thicker ( $\sim 25\mu\text{m}$ ) conventional Ce:YAG phosphor coating, it will be necessary to increase the concentration of  $\text{Ce}^{3+}$  ions in the YAG crystalline phosphor several-fold above that utilized in conventional Ce:YAG phosphor powders. Figure 1 shows the lowest lying  $4\text{f}^1-4\text{f}^05\text{d}^1$  blue absorption transition of  $\text{Ce}^{3+}$  in YAG [16]. The peak blue excitation transition cross-section of  $\text{Ce}^{3+}$  in YAG is  $0.7 \times 10^{-18} \text{ cm}^2$  and its spectral bandwidth is 40 nm. A peak absorption coefficient of  $1000 \text{ cm}^{-1}$  therefore requires a  $\text{Ce}^{3+}$  ion density  $1.3 \times 10^{21} \text{ ion/cc}$ , or about 7 atomic percent. Because of the larger atomic radius of the  $\text{Ce}^{3+}$  ion (1.03 Å) compared to that of the  $\text{Y}^{3+}$  ion it replaces (0.89 Å) in the YAG lattice, the distribution coefficient of  $\text{Ce}^{3+}$  ions in YAG is fairly small ( $< 0.2$ ), so that the achievable Ce doping concentration in YAG depends sensitively on the kinetic pathway (synthesis process) chosen to prepare the doped sub-micron powders. Also, it will be necessary limit the doping concentration of  $\text{Ce}^{3+}$  ions in YAG to avoid any significant self-quenching effect. Given the recent interest in the use of Ce:YAG phosphor powders for use in white light LEDs, there is now an extensive literature describing the preparation and spectroscopic characteristics of Ce:YAG powders produced by a variety of methods [17-23]. This literature suggests that sub-micron sized Ce doped YAG particles can be successfully prepared.

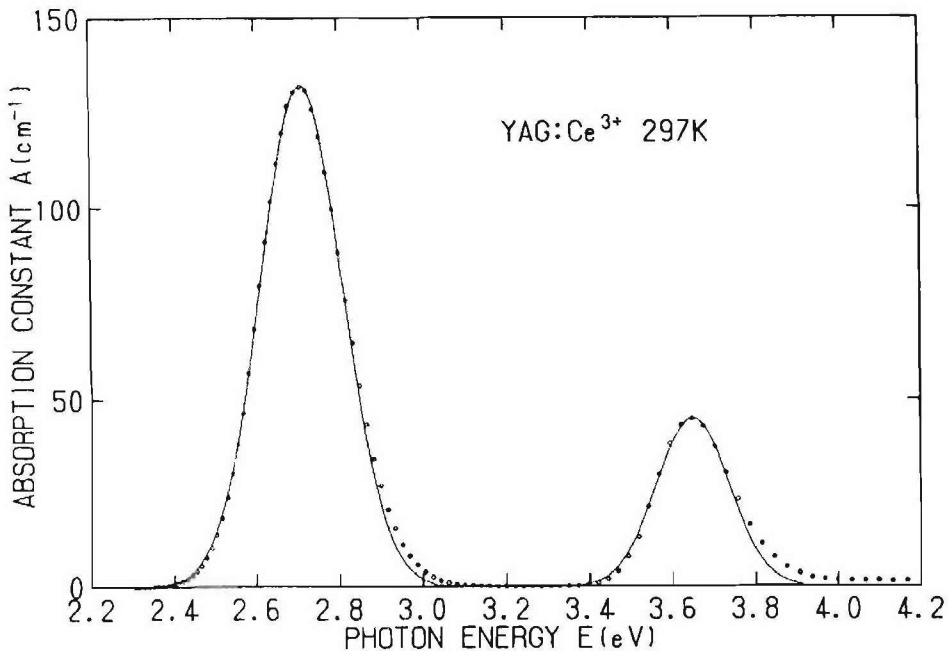


Figure A1. Lower lying  $4f^1-4f^05d^1$  blue absorption transitions of  $\text{Ce}^{3+}$  in YAG [16].  $\text{Ce}^{3+}$  ion concentration in crystal =  $1.77 \times 10^{20}$  ions/cc (1.28% of  $\text{Y}^{3+}$  sites in YAG).

**Approach 3. Embedding other blue-absorbing, yellow-emitting phosphor particles in alumina thin films.**

A third phosphor implementation alternative is to co-deposit sub-micron particles of a crystalline phosphor other than Ce-YAG, possessing superior conversion characteristics for the production of alumina-coated white LEDs. The sought superiority might appear in one or more forms: 1) higher blue transition excitation cross-section (requiring a lower doping density to achieve an effective thin film absorption coefficient of  $1000 \text{ cm}^{-1}$ ); 2) higher doping solubility in the dielectric host matrix; 3) higher quantum efficiency for emission in the yellow spectral region; 4) better crystalline morphology, optical, and mechanical characteristics for embedding in alumina thin films. A review of the phosphor literature [24-26] coupled with the rather restrictive conditions of Table A1, greatly limit the prospects for such an alternative phosphor (to Ce:YAG). However, a recent report by Swakumma, et. al. [27] indicates a SiAlON host matrix doped with divalent europium,  $\text{Eu}^{2+}$  is a promising candidate for this purpose. Figure 2 shows the absorption and emission spectra of  $\text{Eu}^{2+}$  doped SiAlON. The peak absorption cross-section in the blue spectral region was not reported, and will have to be determined in future work. Several papers have been published on the preparation of luminescent SiAlON phosphor powders [28-30], and will be drawn upon in the present work.

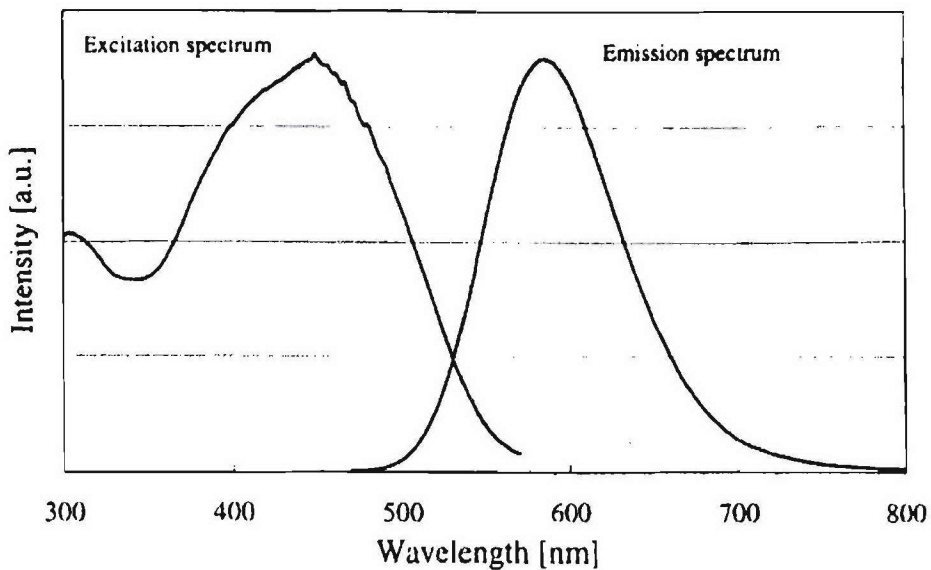


Figure A2. Excitation and emission spectra of the yellowish orange Ca:Eu:SiAlON phosphor [27]. The excitation wavelength is 450 nm for the emission spectrum, and the emission monitoring wavelength is 585 nm for the excitation spectrum.

A second  $\text{Eu}^{2+}$  doped blue-absorbing, yellow-emitting phosphor of potential utility in the present application is  $\text{Eu}^{2+}:\text{Sr}_2\text{SiO}_4$  [31], and will also be further examined.

### References:

1. L. J. F. Broer, L. J. Gorter, J. Hoogschagen, *Physica*, **11**, 231 (1945).
2. A. G. Mitchell and M. W. Zemansky, “Resonance Radiation and Excited Atoms”, p97, Cambridge Press, 1961.
3. Gerhard Dieke, “Spectra and Energy Levels of Rare Earth Ions in Crystals”. Interscience Publishers, John Wiley & Sons, New York, N. Y., 1968.
4. P. Dorenbos, “The 5d level positions of the trivalent lanthanides in inorganic compounds”, *J. Lumines.*, **91**, 155-176 (2000).
5. P. Dorenbos, “5d level energies of  $\text{Ce}^{3+}$  and the crystalline environment. IV aluminates and “simple” oxides”, *J. Lumines.*, **99**, 283-299 (2002).
6. P. Dorenbos, “Optical basicity, interpreted by means of  $\text{Ce}^{3+}$  5d level spectroscopy in ionic crystals”, *J. Non-crystalline Solids*, **324**, 220-229 (2003).

7. P. Dorenbos, "Energy of the first  $4f^7$ - $4f^65d$  transition of  $\text{Eu}^{2+}$  in inorganic compounds", *J. Lumines.*, **104**, 239-260 (2003).

8. S. Sugano, Y. Tanabe, H. Kamimura, Multiplets of Transition Metal Ions in Crystals", Academic Press, New York, 1970.

9. M. Iwaki, Makoto Kumagai, Keiko Aono, "Ion-beam-induced luminescence of Tb-implanted sapphire", *Nuc. Inst. And Methods in Phys. Res.*, **B127/128**, 488-491 (1997).

10. T. Ishizaka, Y. Kurokawa, "Optical properties of rare-earth ion ( $\text{Gd}^{3+}$ ,  $\text{Ho}^{3+}$ ,  $\text{Pr}^{3+}$ ,  $\text{Sm}^{3+}$ ,  $\text{Dy}^{3+}$ , and  $\text{Tm}^{3+}$ )-doped alumina films prepared by the sol-gel method", *J. Luminescence*, **92**, 57-63 (2001).

11. O. Ozuna, G. A. Hirata, J. McKittrick, "Luminescence enhancement in  $\text{Eu}^{3+}$ -doped  $\alpha$ - and  $\gamma$ -  $\text{Al}_2\text{O}_3$  produced by pressure-assisted low-temperature combustion synthesis", *Appl. Phys. Letters*, **84**, 1296-1298 (2004).

12. L. A. Bondar, A. A. Kolpakova, L. Y. Markovskii, A. N. Sokolov, L. E. Tarasova, N. A. Toropov, *Bull. Acad. Sci. Phys. Ser.*, **33**, 877 (1969)

13. Keiko Aono, Hiroshi Tioda, Kenichi Terashima, Masaya Iwaki, "Annealing effects on luminescence from Ce-implanted  $\alpha$ - $\text{Al}_2\text{O}_3$ ", *Nuc. Inst. And Methods. In Phys. Res.*, **B175-177**, 580-584 (2001).

14. P. M. Jaffe, *J. Electrochem. Soc.: Solid State Sci.*, **116**, 629 (1969).

15. Y. G. Liu, H. Y. Xu, R. Mu, D. O. Henderson, Y. M. Lu, J. Y. Zhang, D. Z. Shen, X. W. Fan, C. W. White, "Production, structure, and optical properties of  $\text{ZnO}$  nanocrystals embedded in  $\text{CaF}_2$  matrix", *Appl. Phys. Letters*, **83**, 1210-1213 (2003).

16. T. Tomiki, T. Kohatsu, H. Shimabukuro, Y. Ganaha, " $\text{Ce}^{3+}$  centers in  $\text{Y}_3\text{Al}_5\text{O}_{12}$  (YAG) single crystals. II", *J. Phys. Soc. Japan*, **61**, 2382-2387 (1992).

17. Q. Li, L. Gao, D. Yan, "The crystal structure and spectra of nanoscale YAG:Ce $^{3+}$ ", *Matls. Chem. Phys.*, **64**, 41-44 (2000).

18. C. H. Lu, C. H. Hong, R. Jagannathan, "Luminescent  $\text{Y}_3\text{Al}_5\text{O}_{12}:\text{Ce}^{3+}$  nanoparticles-low temperature sol-gel synthesis and critical preparative parameters", *J. Matl. Sci. Letters*, **21**, 1489-1492 (2002).

19. S. Lee, S. Y. Seo, "Optimization and yttrium aluminum garnet:Ce $^{3+}$  phosphors for white light-emitting diodes by combinatorial chemistry method", *J. Electrochem. Soc.*, **149**, J85-J88 (2002).

20. Y. Pan, M. Wu, Q. Su, "Tailored photoluminescence of YAG:Ce phosphor through various methods", *J. Phys. Chem. Solids*, **65**, 845-850 (2004).

21. Y. Pan, M. Wu, Q. Su, "Comparative investigation on synthesis and photoluminescence of YAG:Ce phosphor", *Matls. Sci. Eng.*, **B106**, 251-256 (2004).

22. Y. Zhou, J. Lin, M. Yu, S. Wang, H. Zhang, "Synthesis-dependent luminescence properties of  $Y_3Al_5O_{12}:RE^{3+}$  ( $RE=$ Ce, Sm, Tb) phosphors", *Materials Letters*, **56**, 628-636 (2002).

23. R. A. Rodriguez-Rojas, E. De la Rosa-Cruz, L. A. Diaz-Torres, P. Salas, R. Melen-drez, M. Bsrboza-Flores, M. A. Meneses-Nava, O. Barbosa-Garcia", Preparation, photo- and thermo-luminescence characterization of  $Tb^{3+}$  and  $Ce^{3+}$  doped nanocrystalline  $Y_3Al_5O_{12}$  exposed to UV-radiation", *Optical Materials*, **25**, 285-293 (2004).

24. S. Kamiya, H. Mizuno, "Phosphors for lamps", Chapter 5, Section 6, 389-432, *Phosphor Handbook*, S. Shionoya, W. M. Yen, editors, CRC Press.

25. T. Kojima, "Phosphors for plasma displays", Chapter 10, Section 1, 623-636, *Phosphor Handbook*, S. Shionoya, W. M. Yen, editors, CRC Press.

26. R. Mueller-Mach, G. O. Mueller, M. R. Krames, "Phosphors materials and combinations for illumination grade white pcLED", *SPIE* **5187**, 115-122 (2004).

27. K. Sakuma, K. Omichi, N. Kimura, M. Ohashi, D. Tanaka, N. Hirosaki, Y. Yamamoto, R. J. Xie, T. Suehiro, "Warm-white, light-emitting diode with yellowish orange  $\alpha$ -SiAlON ceramic phosphor", *Optics Letters*, **29**, 2001-2003 (2004).

28. H. Mandal, M. J. Hoffman, "Preparation of multiple-cation  $\alpha$ -SiAlON ceramics containing lanthanum", *J. Am. Ceram. Soc.*, **82**, 229-232 (1999).

29. R. J. Xie, M. Mitomo, K. Uheda, F. F. Xu, Y. Akimune, "Preparation and luminescence of calcium- and rare-earth ( $R=$ Dy, Tb, and Pr)- co-doped  $\alpha$ -SiAlON ceramics", *J. Am. Ceram. Soc.*, **85**, 1229-1234 (2002).

30. J. W. H. van Krevel, J. W. T. van Rutten, H. Mandal, H. T. Hintzen, R. Metselaar, "Luminescence properties of terbium-, cerium-, or europium-doped  $\alpha$ -SiAlON ceramics", *J. Solid State Chemistry*, **165**, 19-24 (2002).

31. J. S. Kim, J. Y. Kang, P. E. Jeon, J. C. Choi, H. L. Park, T. W. Kim, "GaN-based white-light-emitting diodes fabricated with a mixture of  $Ba_3MgSi_2O_8:Eu^{2+}$ ", *Japanese. J. Appl. Phys.*, **43**, 989-992 (2004).

## Appendix B

# Final report: Optimal design of LED die-bonded micro-optics

Prepared by Dr. Neri Shatz and Dr. John Bortz

Science Applications International Corporation  
November 11, 2005

## Optimal design of LED die-bonded micro-optics



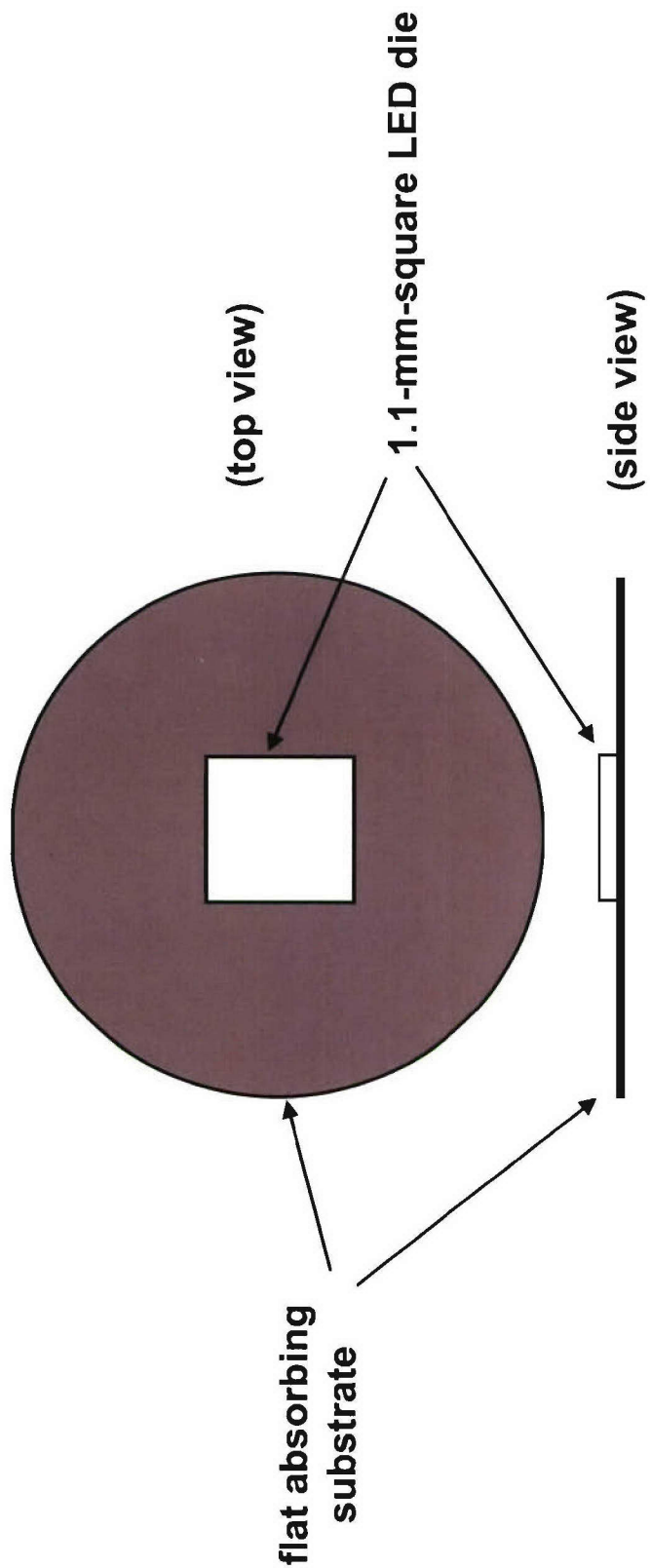
An Employee-Owned Company

- Current LEDs incorporate encapsulant dome shapes that are **not optimized for light extraction and disperse flux over  $2\pi$  steradians.**
- Higher flux-extraction and collection efficiencies may be achievable by optimizing the design of a micro-optic element bonded directly onto the die.
- In addition to improving extraction and collection efficiencies, pre-compressing the LED output would potentially improve flux-transfer efficiency of the downstream optics, as well as simplifying their design and consequently reducing manufacturing costs.
- The specifications of this design problem were developed in consultation with Lumileds Lighting.
- Goal of design is to couple flux from an LED die into a beam having a  $45^\circ$  half angle over a 3-mm-diameter exit aperture.
- Source modeled as a Lambertian emitter.

## Source model

- The source is 1.1-mm-square, 0.1-mm-thick white light LED die.
- Source is Lambertian emitter, which emits flux from the top and 4 sides of the die.
- Die will be assumed to lie on a flat, perfectly absorbing substrate.
- Radiance assumed to be spatially uniform over entire emitting surface.
- Refractive index: 1.50 (for axisymmetric designs).
- Refractive index later revised to 1.51, which was used for non-axisymmetric designs.

- Total source étendue for refractive index of 1.50:  $11.66 \text{ mm}^2\text{-sr}$ .
- Total source étendue for refractive index of 1.51:  $11.82 \text{ mm}^2\text{-sr}$ .



## Target model

---



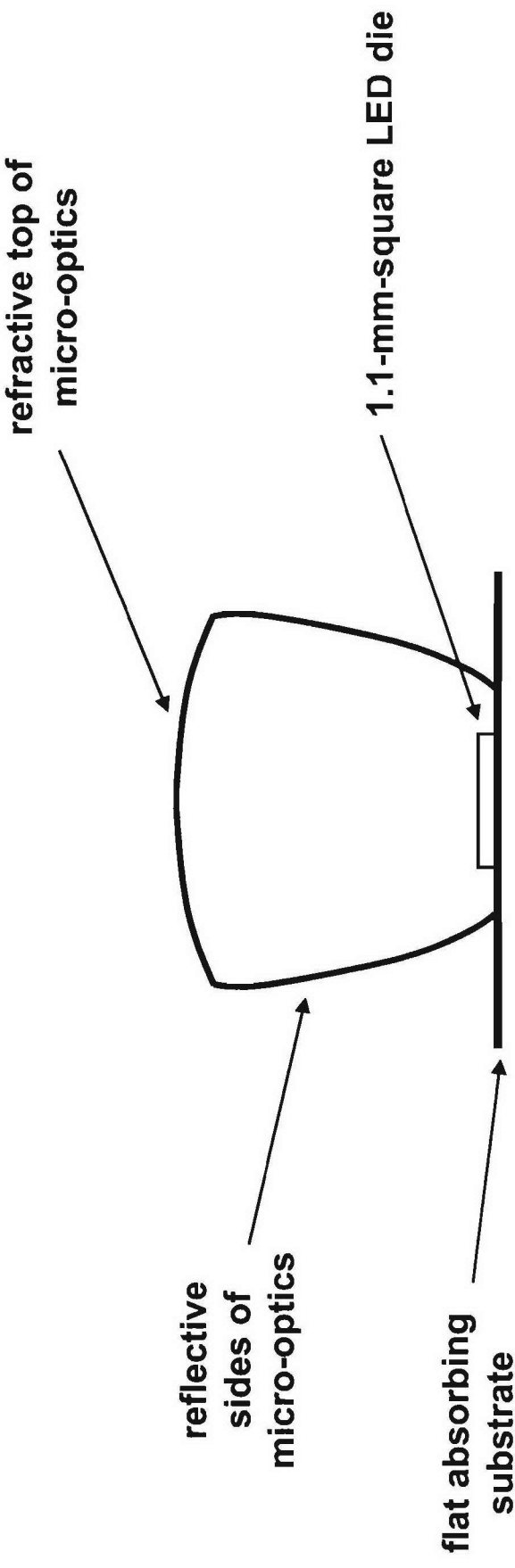
An Employee-Owned Company

- Target to which flux is to be transferred is 3-mm-diameter aperture, within half angle of 45° with respect to optical axis.

- Total target étendue: 11.10 mm<sup>2</sup>-sr.

## Micro-optics design approach

- Utilized the NonImaging COncentrator Synthesis (NICOS) code in its optimization mode to design the micro-optics.
- Maximum diameter of micro-optics: 3.0 mm.
- Half angle of output beam:  $45^\circ$ .
- Light source is assumed to be immersed in refractive medium of micro-optics.
- Designs utilize reflective sides and refractive top.
- Investigated both axisymmetric and non-axisymmetric designs.



## Optimized micro-optics designs



An Employee-Owned Company

### Five optimized designs were developed:

- Axisymmetric optics, with reflective coating and 0.2-mm source clearance.
- Axisymmetric optics, TIR reflective surface and 0.2-mm source clearance.
- Non-axisymmetric optics, with reflective coating and 0.2-mm source clearance.
- Non-axisymmetric optics, with reflective coating and 0.1-mm source clearance.
- Non-axisymmetric optics, with reflective coating and 0.0-mm source clearance.

**Axisymmetric micro-optics, with reflective coating  
and 0.2-mm source clearance**

## Optimized axisymmetric micro-optics, with reflective coating and 0.2-mm source clearance



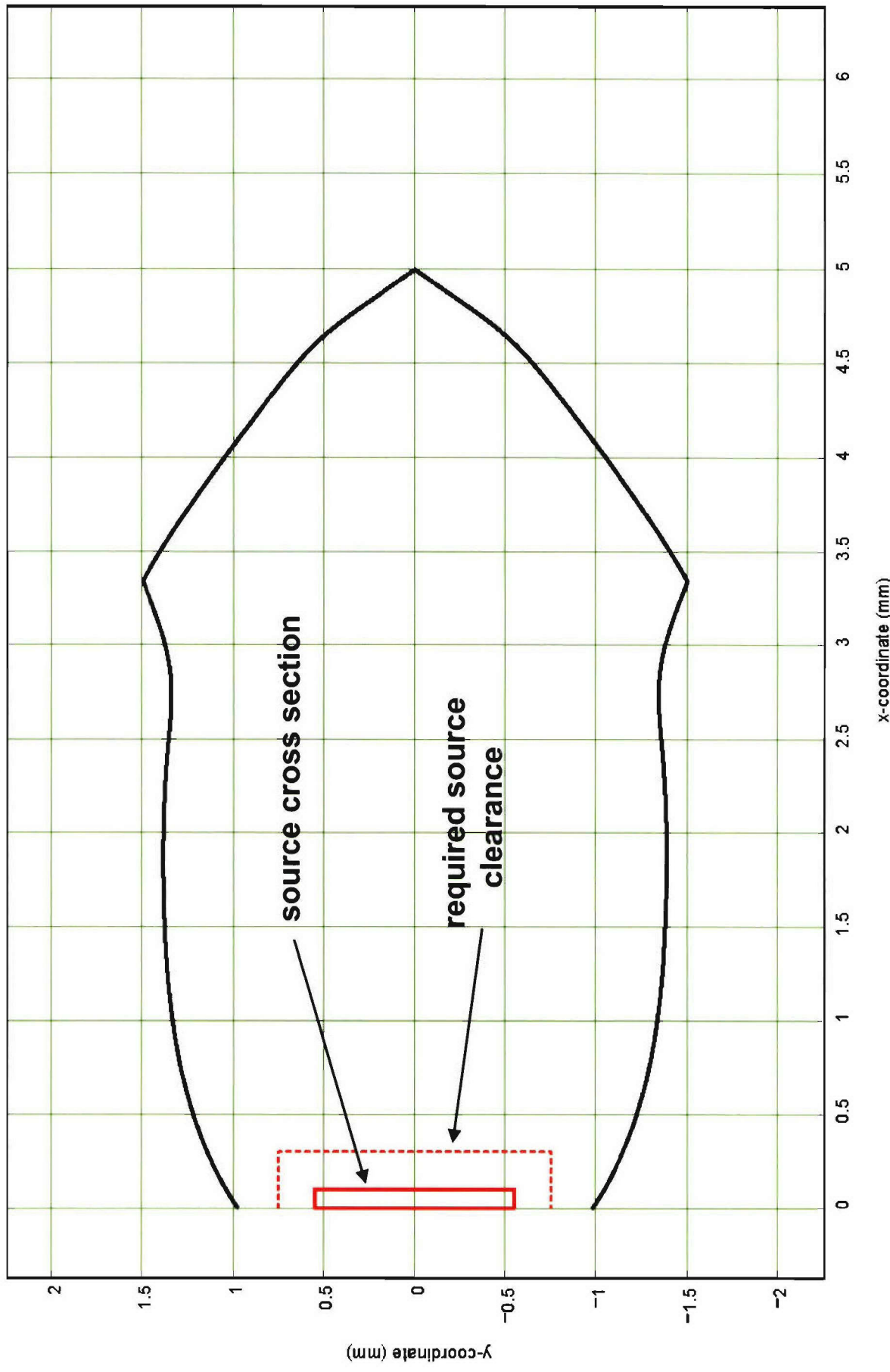
An Employee-Owned Company

- Design designation: C01.
- Minimum diameter of micro-optics: 1.9556 mm (provides 0.2-mm clearance relative to diagonal source dimension).
- Maximum diameter of micro-optics: 3.0 mm.
- Refractive index: 1.5.
- Optimized for reflective surface having 100% reflectance.
- Optimized for refractive surface having 100% transmittance.
- Length: 4.99 mm.
- Performance plots assume 100% reflectance for reflective surface and 100% transmittance for refractive surface.

## Cross section of design C01

Case = "C01"

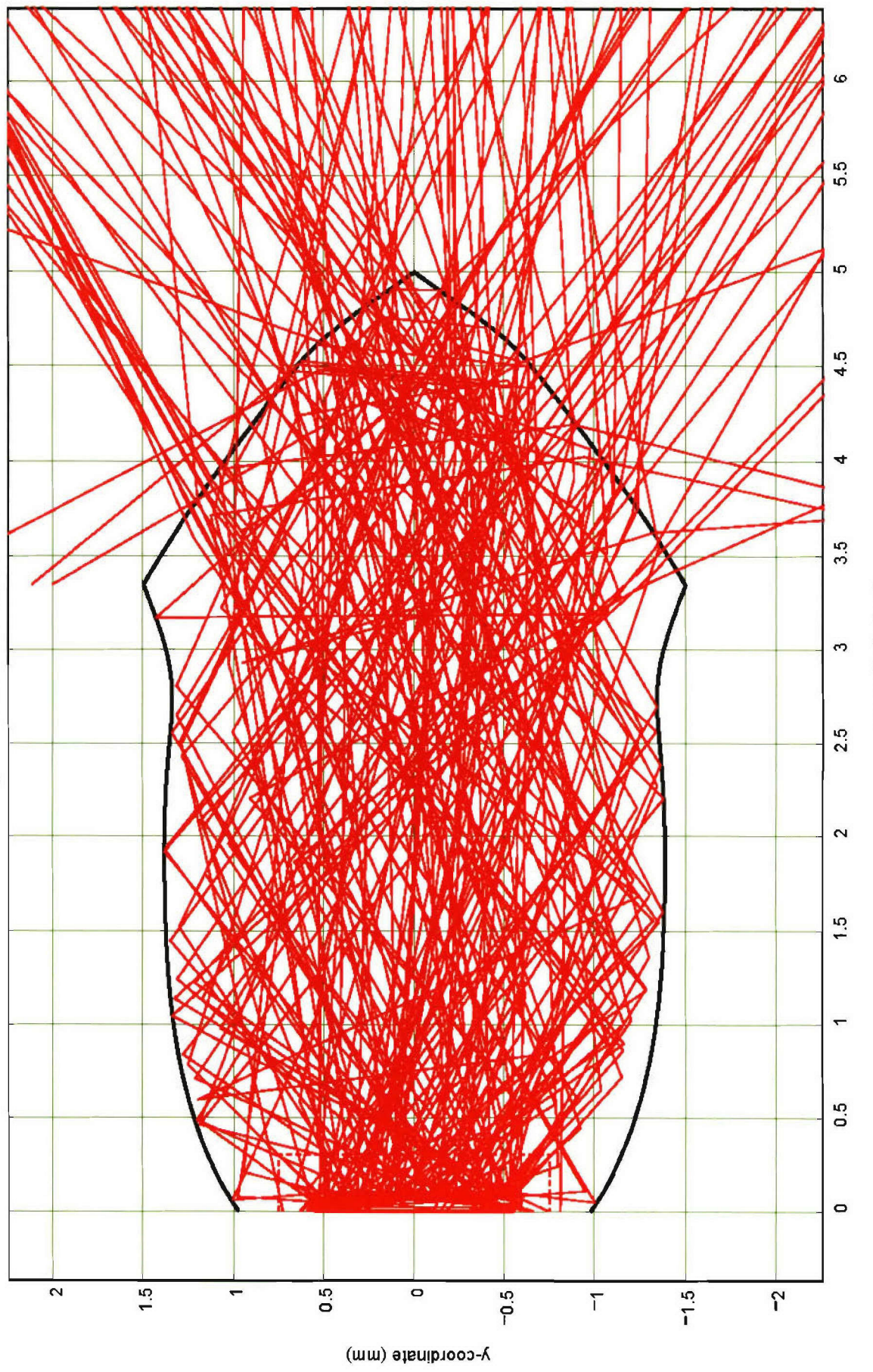
Optimized lens shape (x,y-plane)



## Cross section of design C01, with traced rays

Case = "C01"

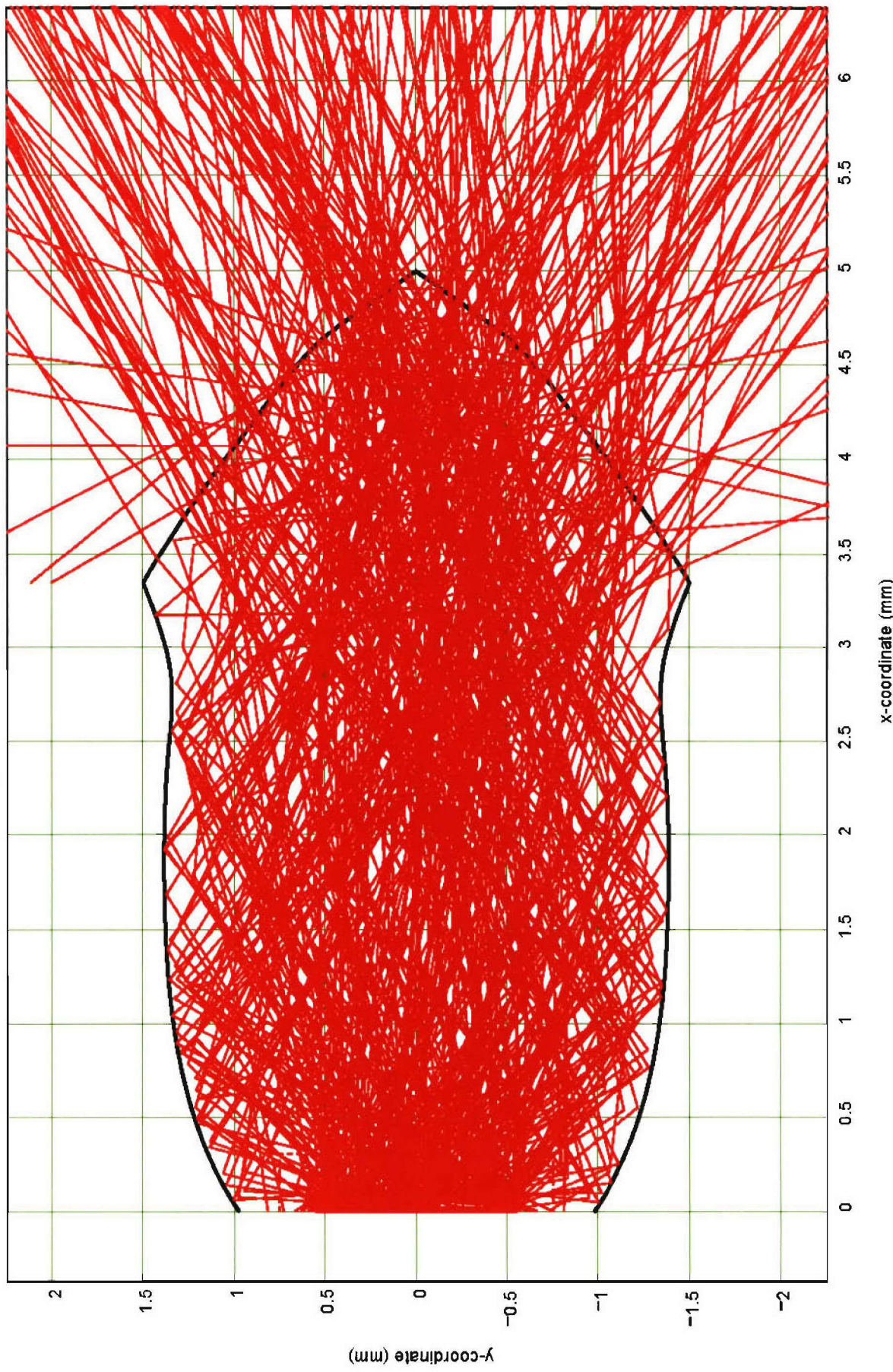
Optimized lens shape (x,y-plane)



# Cross section of design C01, with larger number of traced rays

Case = "C01"

Optimized lens shape (x,y-plane)



## Three-dimensional representation of design C01



An Employee-Owned Company

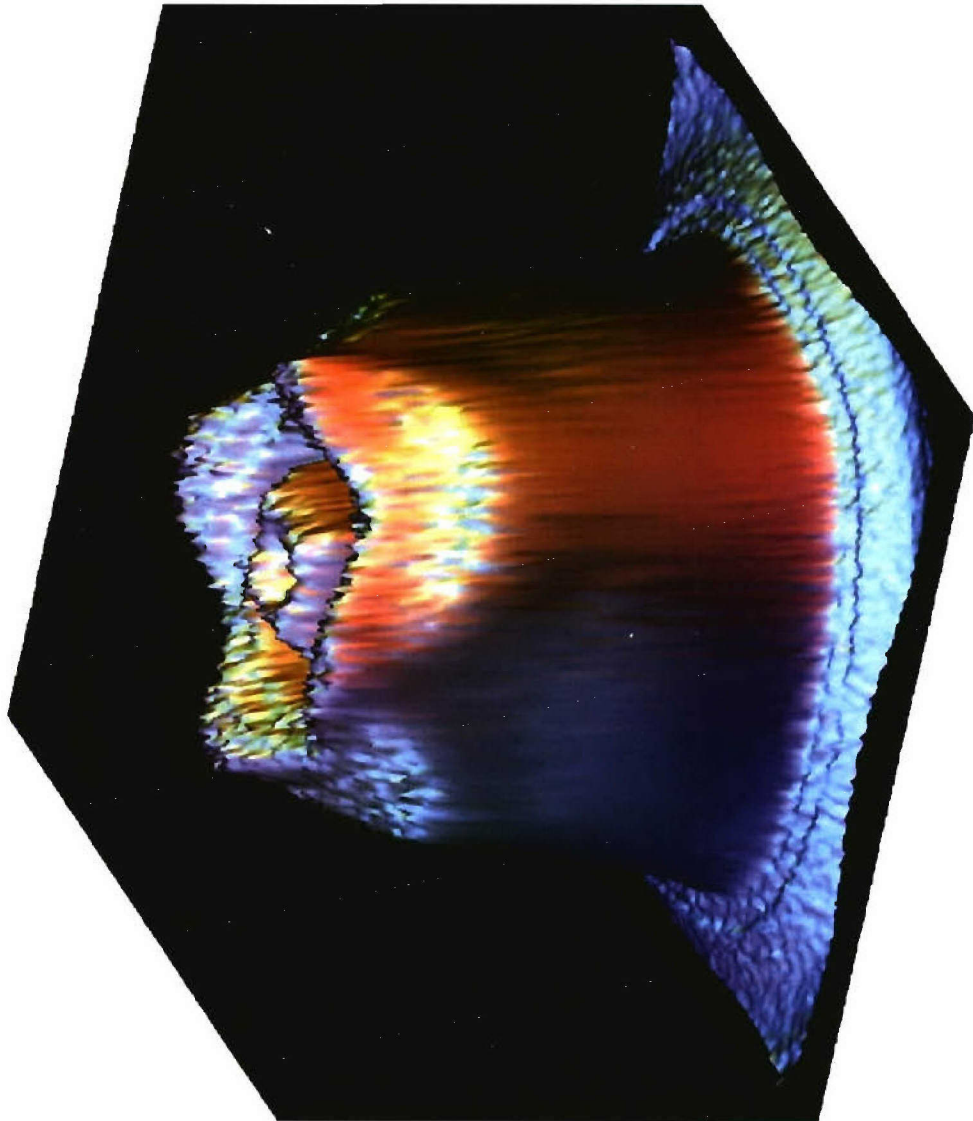


## Total source étendue versus available source étendue

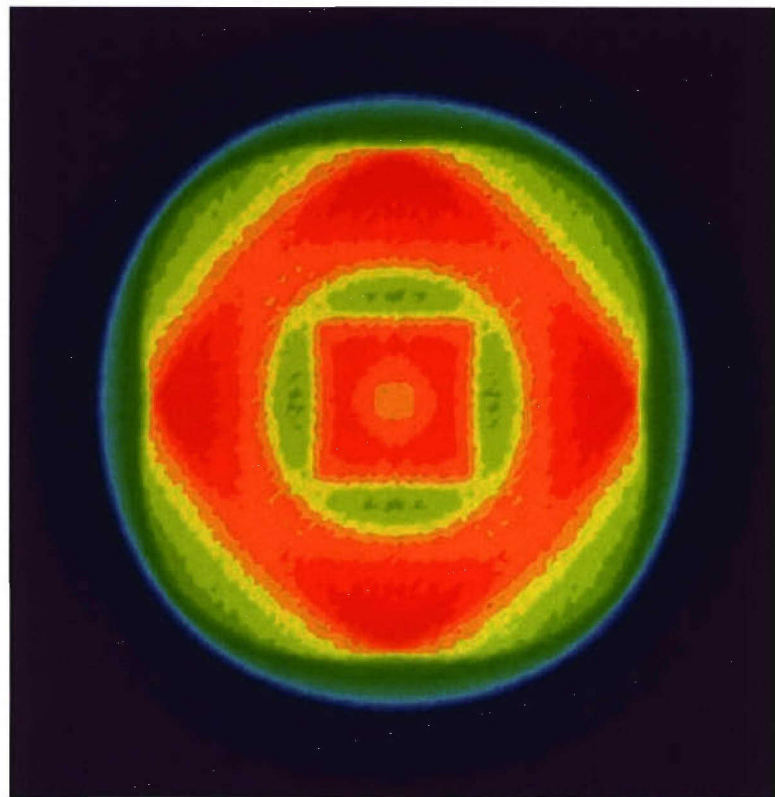
---

- Surface area of source:  $1.65 \text{ mm}^2$ .
- Projected solid angle of source:  $3.1416 \text{ sr}$ .
- Refractive index in which source is immersed: 1.50.
- Total source étendue:  $11.66 \text{ mm}^2\text{-sr}$ .
- Due to source-clearance requirements, 11.31% of source flux is directly absorbed by substrate, without being collected by micro-optics. So only 88.69% of source étendue is actually available.
  - Available source étendue:  $10.34 \text{ mm}^2\text{-sr}$ .

## Micro-optics design C01: intensity distribution

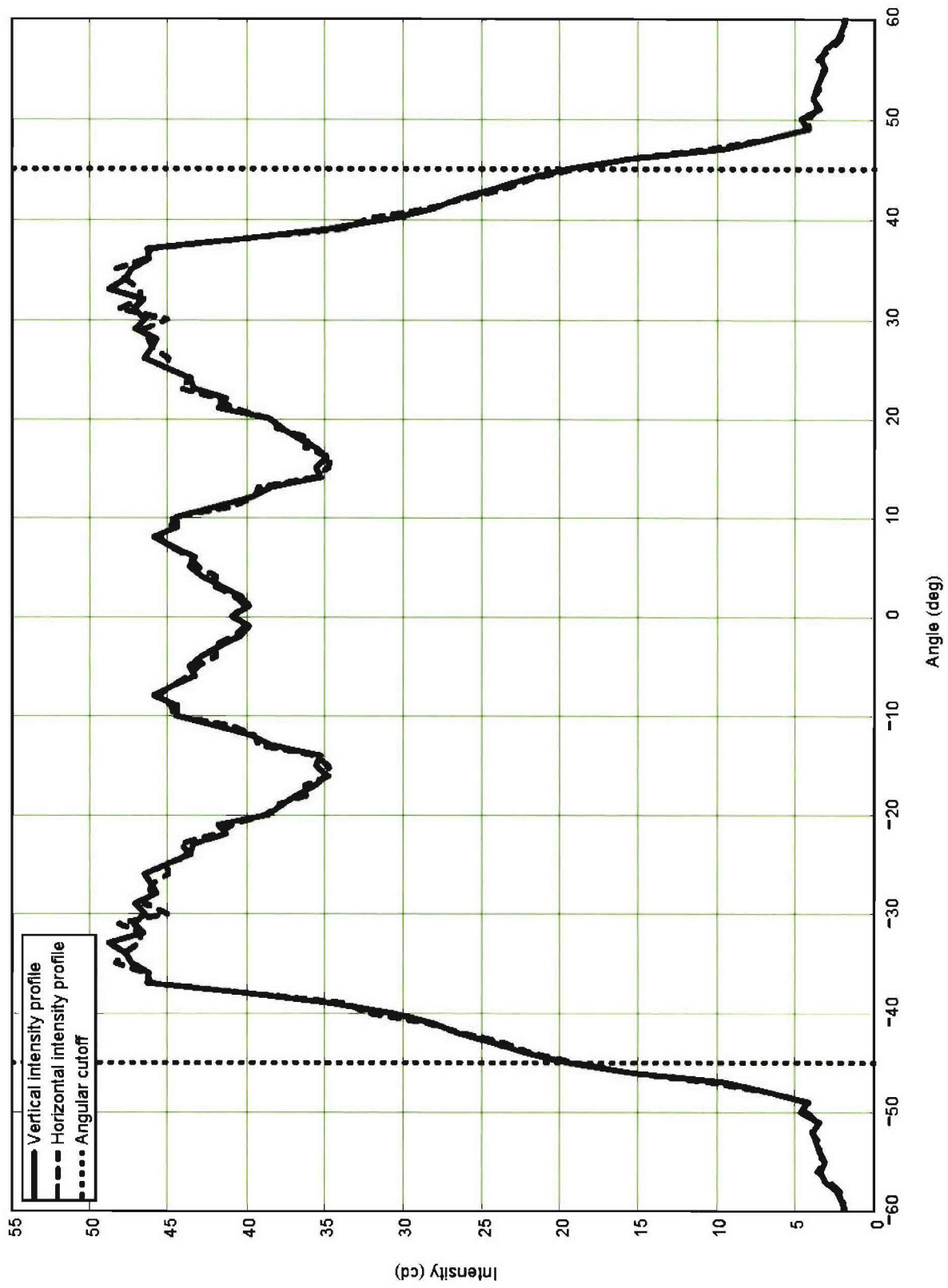


(surface plot)  
(pseudo-color contour plot)



# Micro-optics design C01: intensity profiles

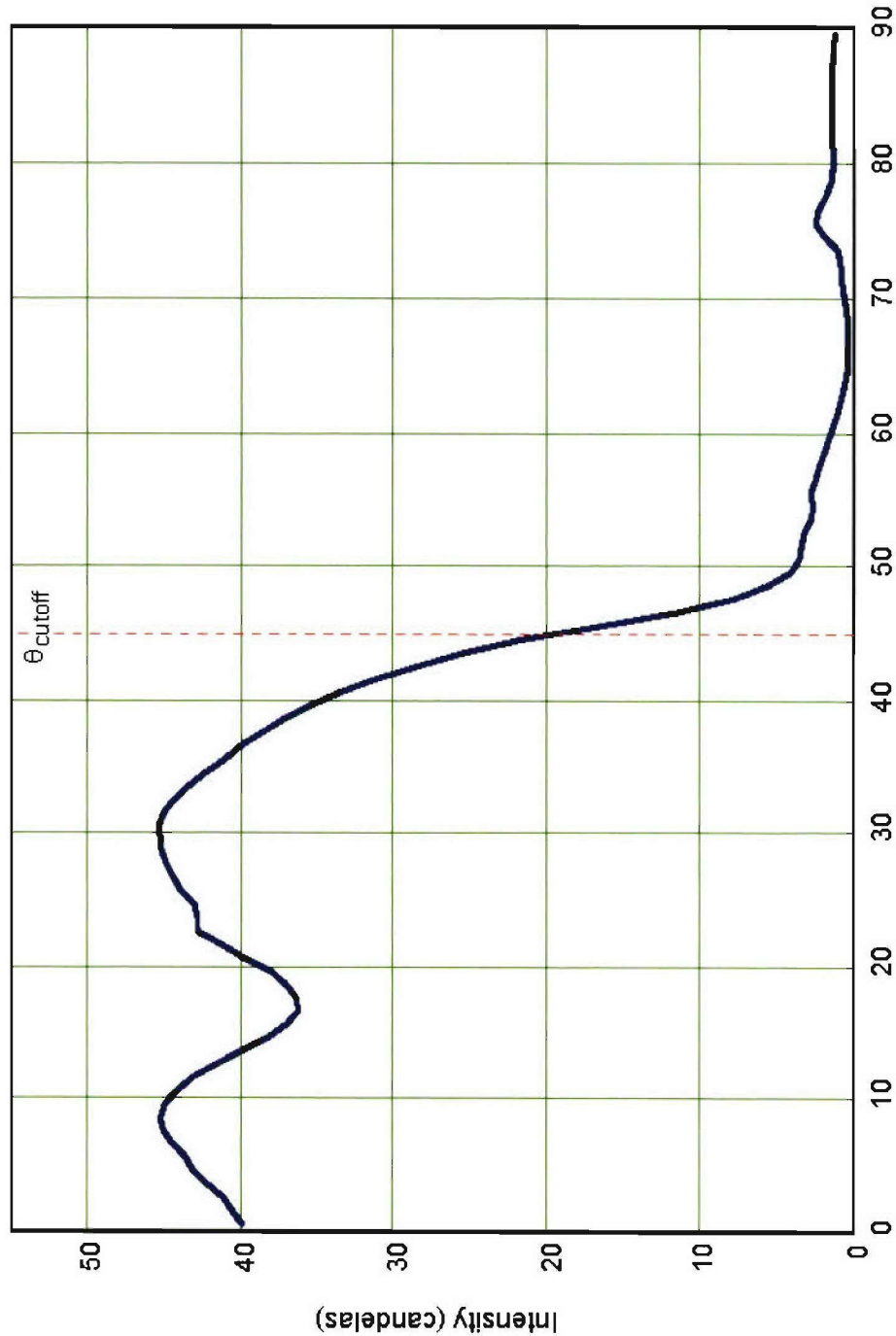
Case C01: Vertical and horizontal intensity profiles



## Micro-optics design C01: radial intensity distribution

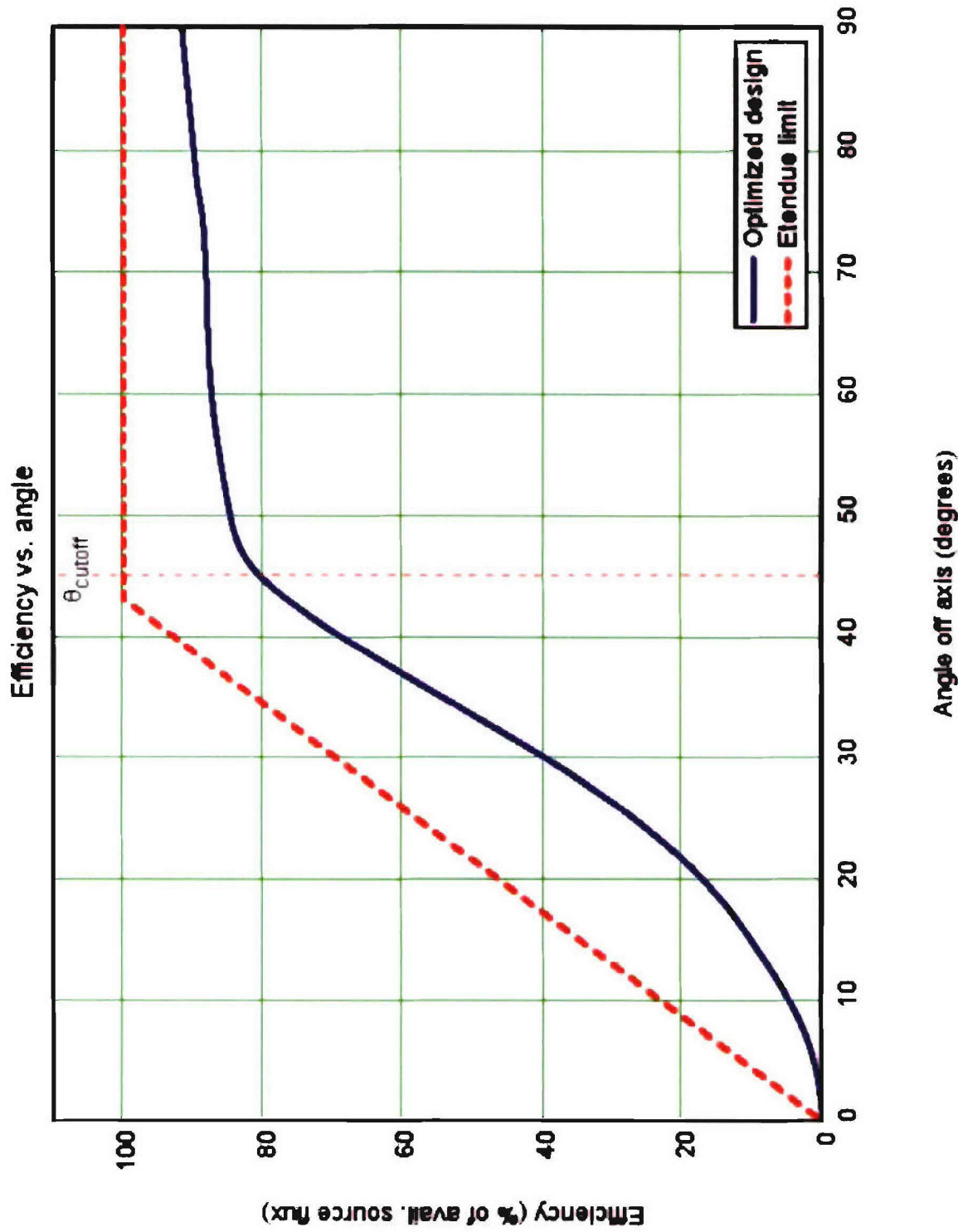
Case = "C01"

Intensity as a function of angle



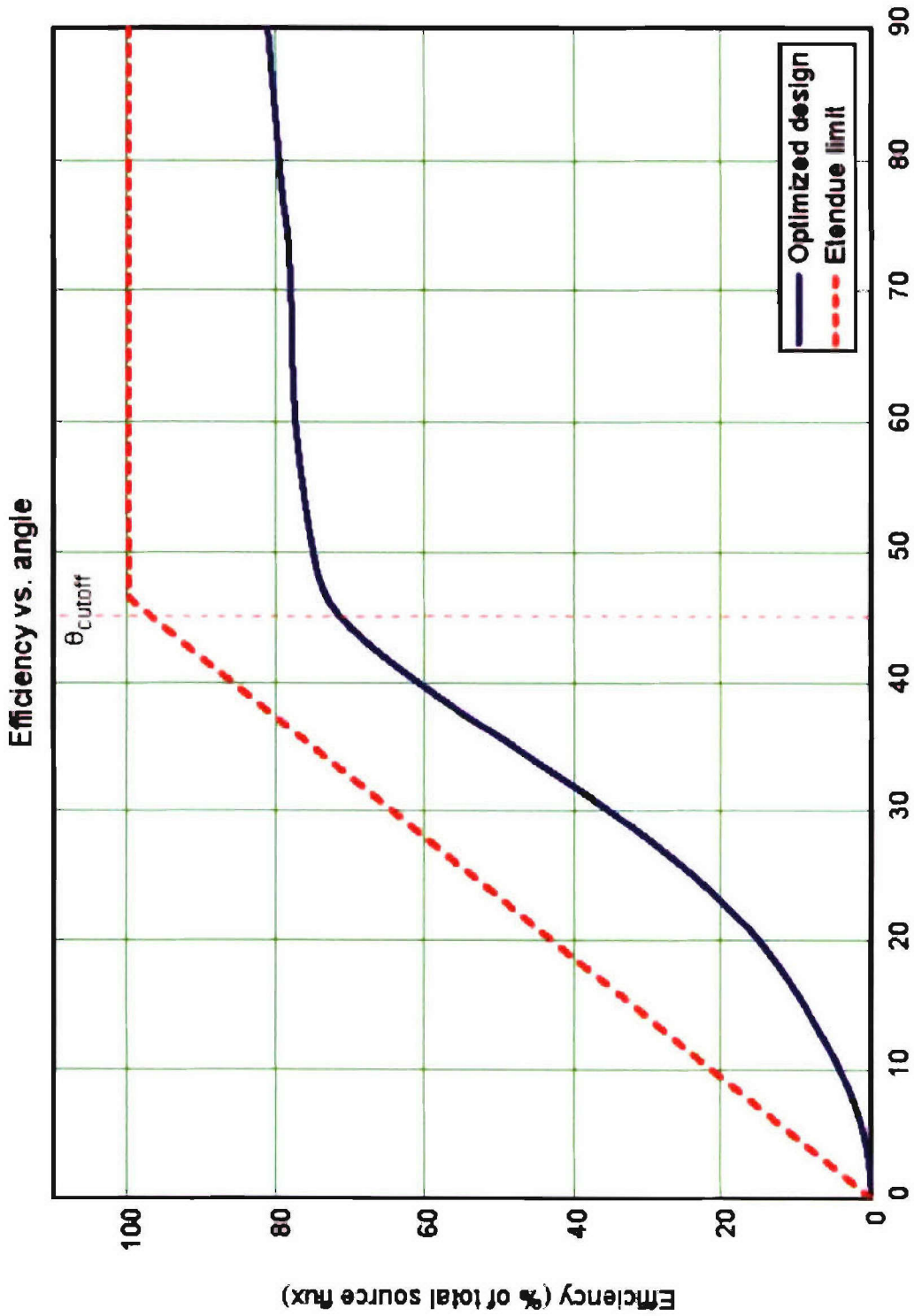
(intensity output averaged over annular angular bins as a function of angle off axis)

# Micro-optics design C01: renormalized efficiency versus angle



(efficiency as a percentage of available source étendue)

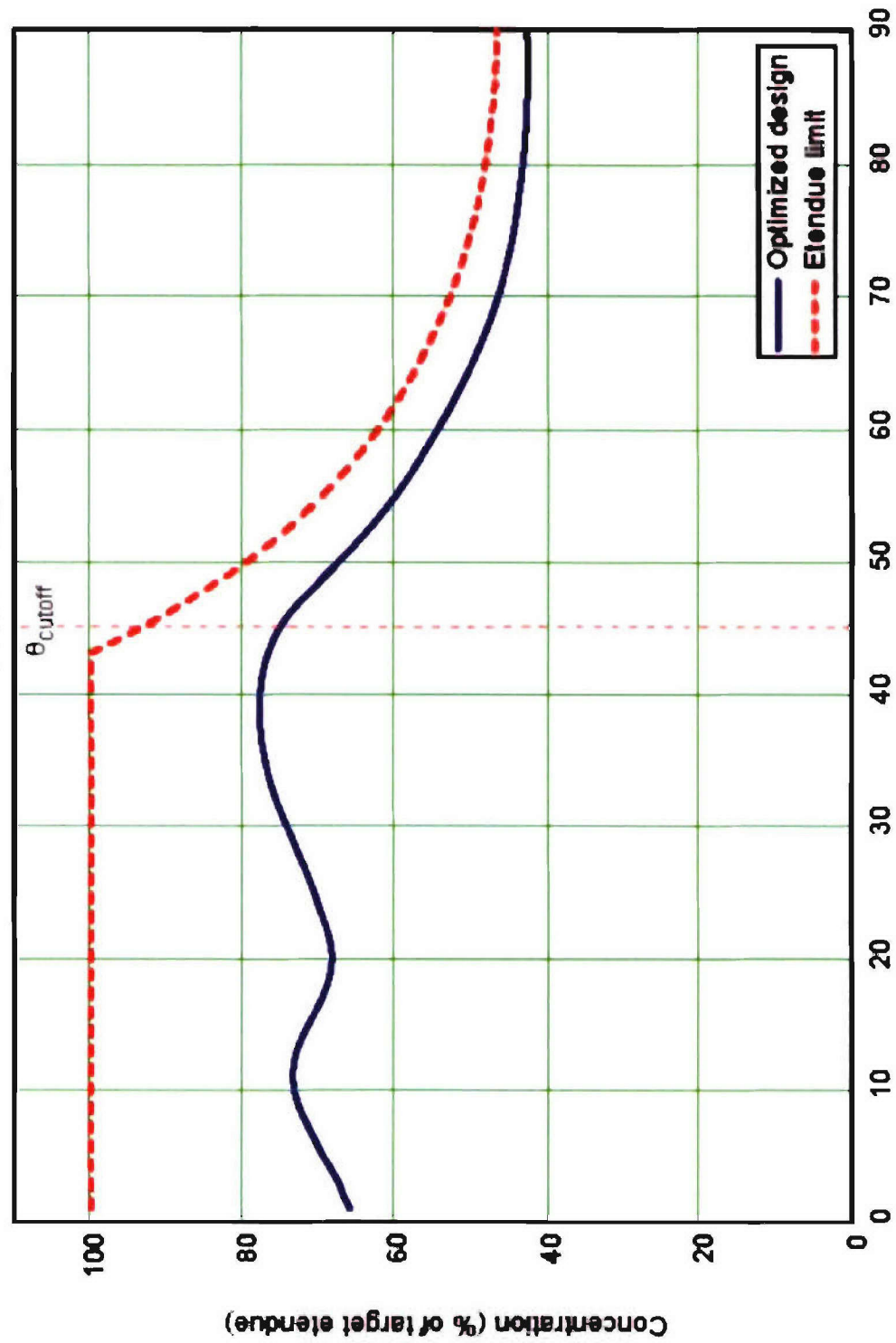
## Micro-optics design C01: total efficiency versus angle



(efficiency as a percentage of total source étendue)

## Micro-optics design C01: concentration versus angle

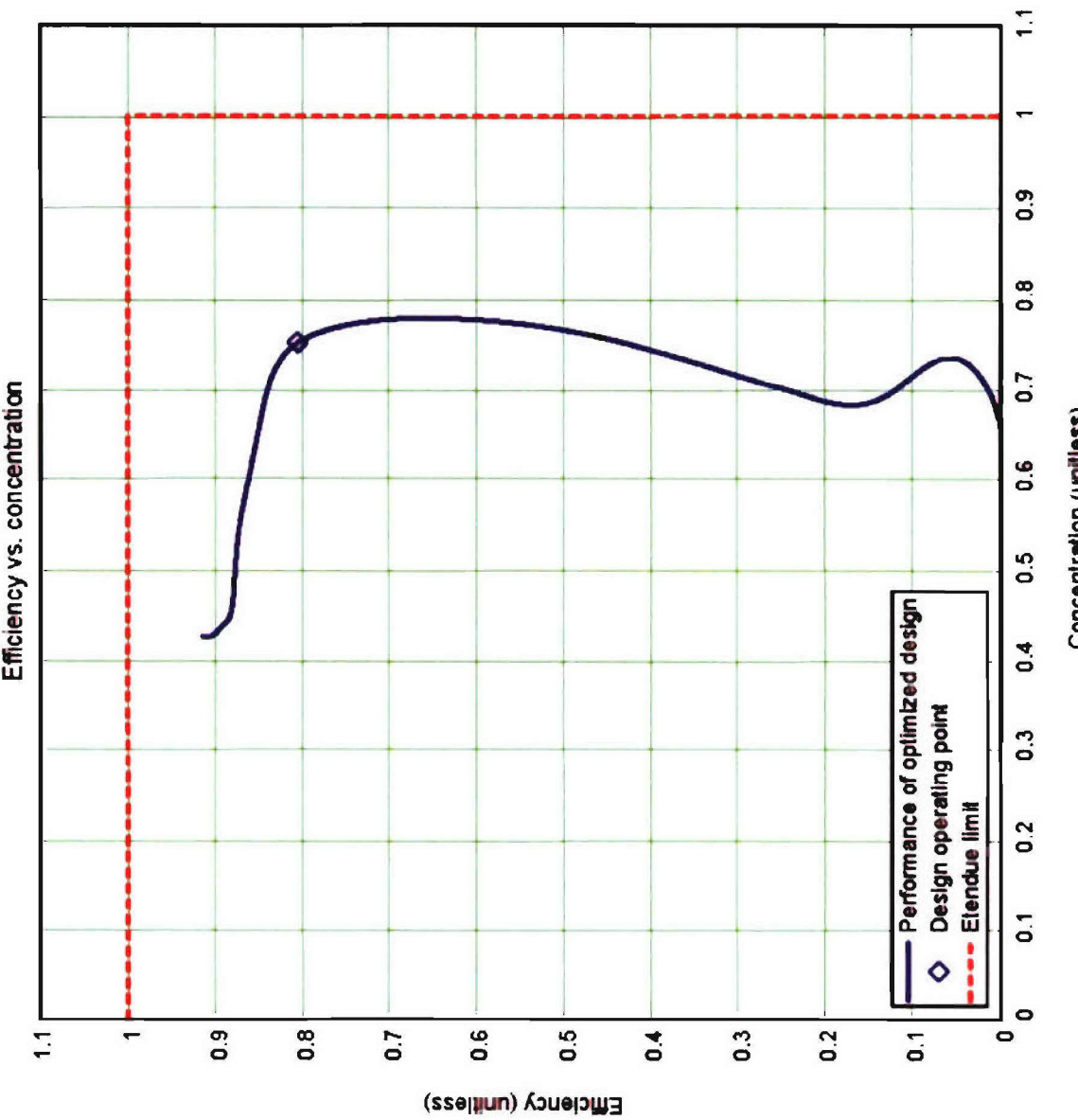
Concentration vs. angle



(étendue limit based on available source étendue)

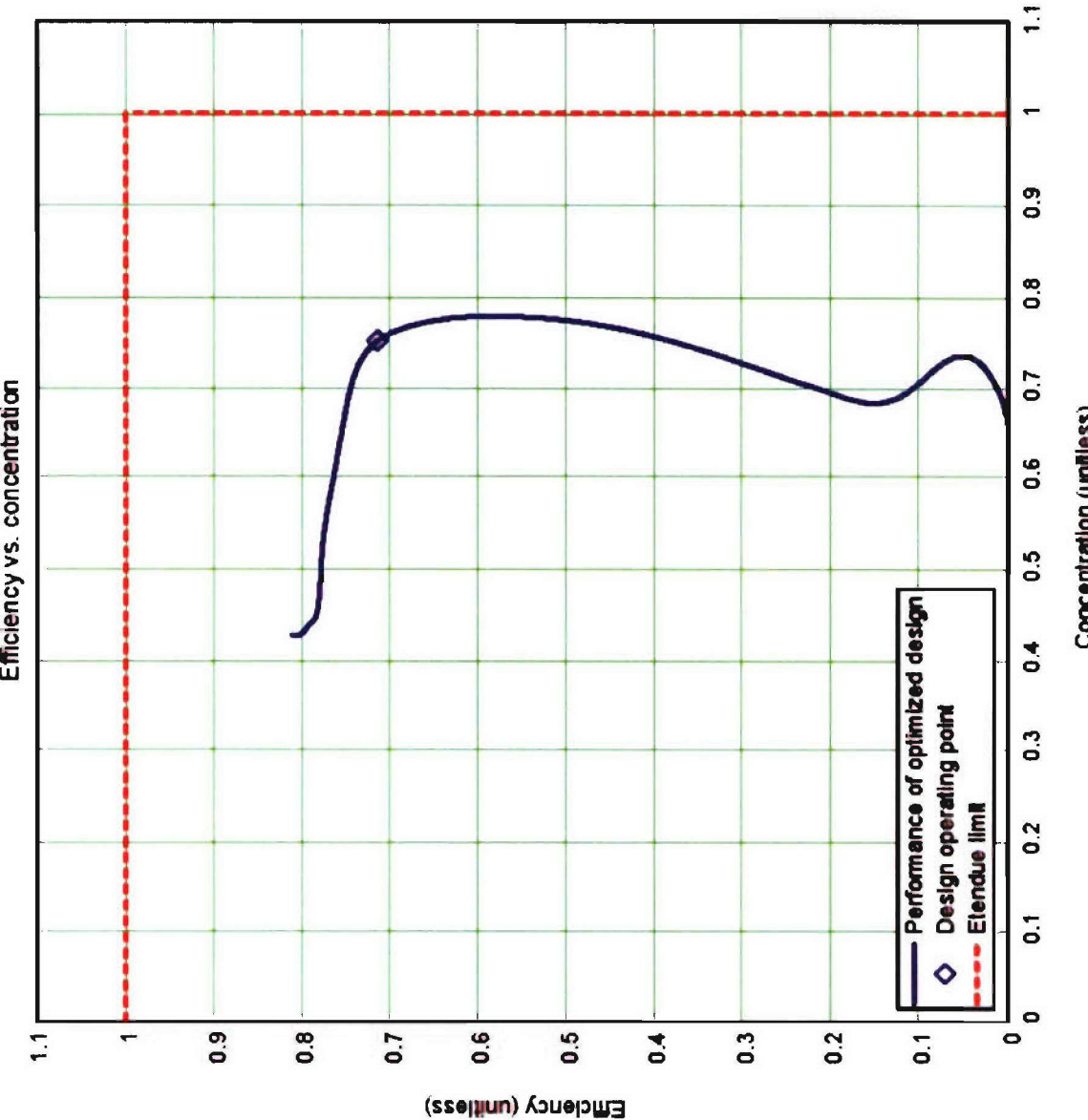
(étendue limit based on available source étendue)

## Micro-optics design C01: renorm. efficiency vs. concentration



(efficiency based on available source étendue)

# Micro-optics design C01: total efficiency versus concentration



(efficiency based on total source étendue)



**Axisymmetric micro-optics, with TIR reflective surface  
and 0.2-mm source clearance**

## Optimized axisymmetric micro-optics, with TIR reflective surface and 0.2-mm source clearance

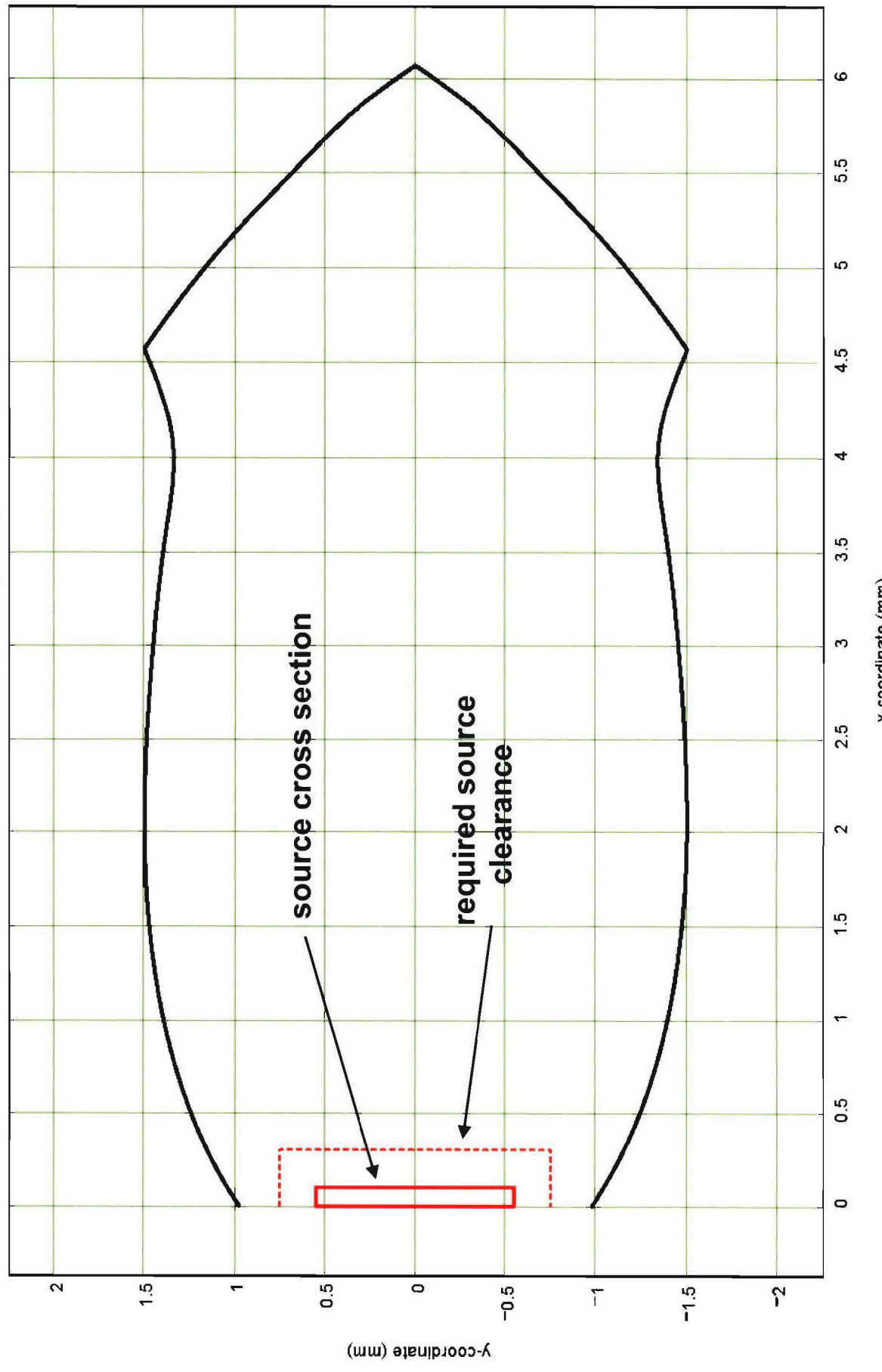


- Design designation: G01.
- Minimum diameter of micro-optics: 1.9556 mm (provides 0.2-mm clearance relative to diagonal source dimension).
- Maximum diameter of micro-optics: 3.0 mm.
- Refractive index: 1.5.
- Optimized for uncoated reflective surface utilizing total internal reflection (TIR).
- Optimized for refractive surface having 100% transmittance.
- Length: 6.06 mm.
- Performance plots assume uncoated (TIR) reflective surfaces and 100% transmittance for refractive surface.

## Cross section of design G01

Case = "G01"

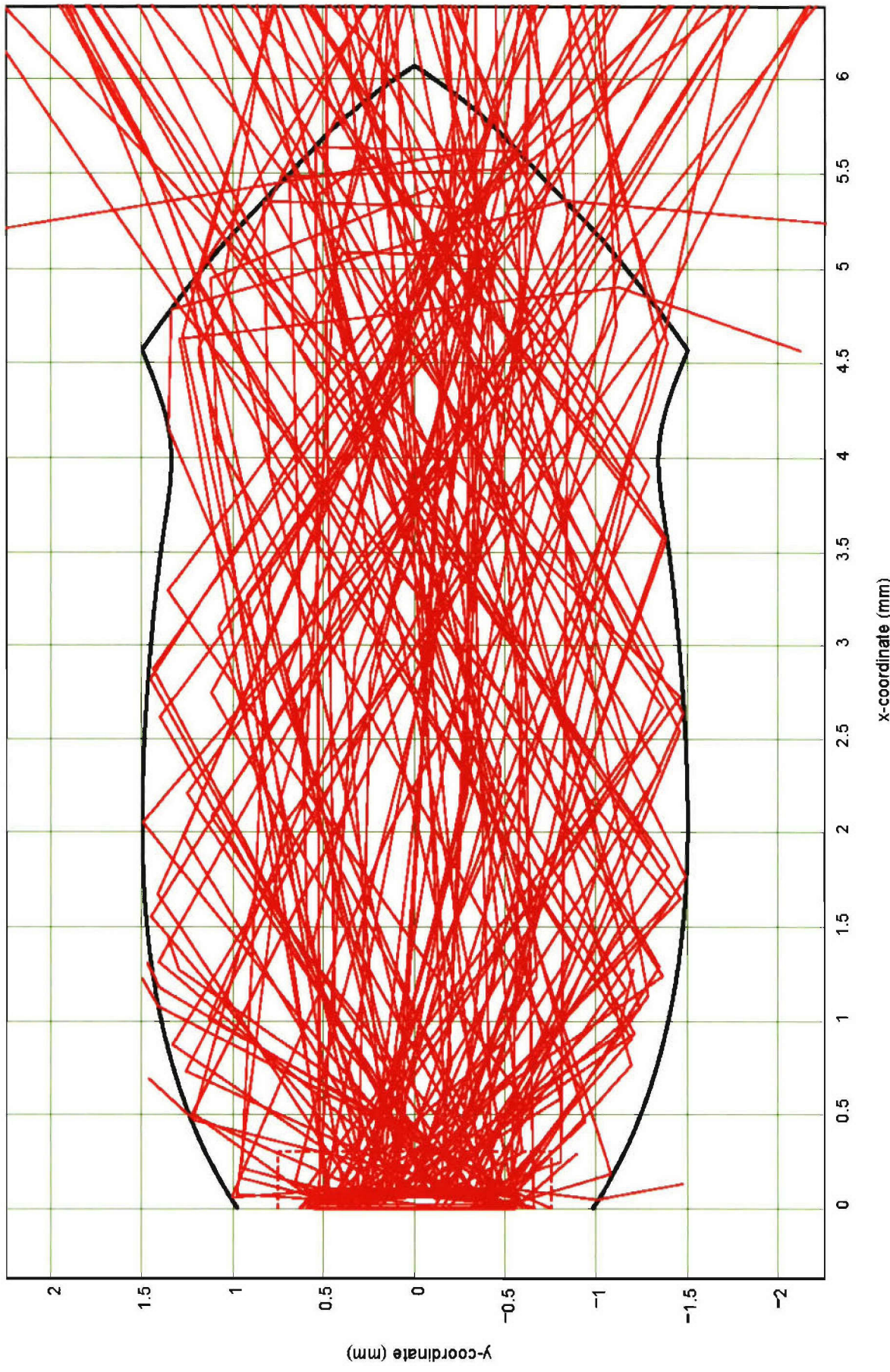
Optimized lens shape (x,y-plane)



## Cross section of design G01, with traced rays

Case = "G01"

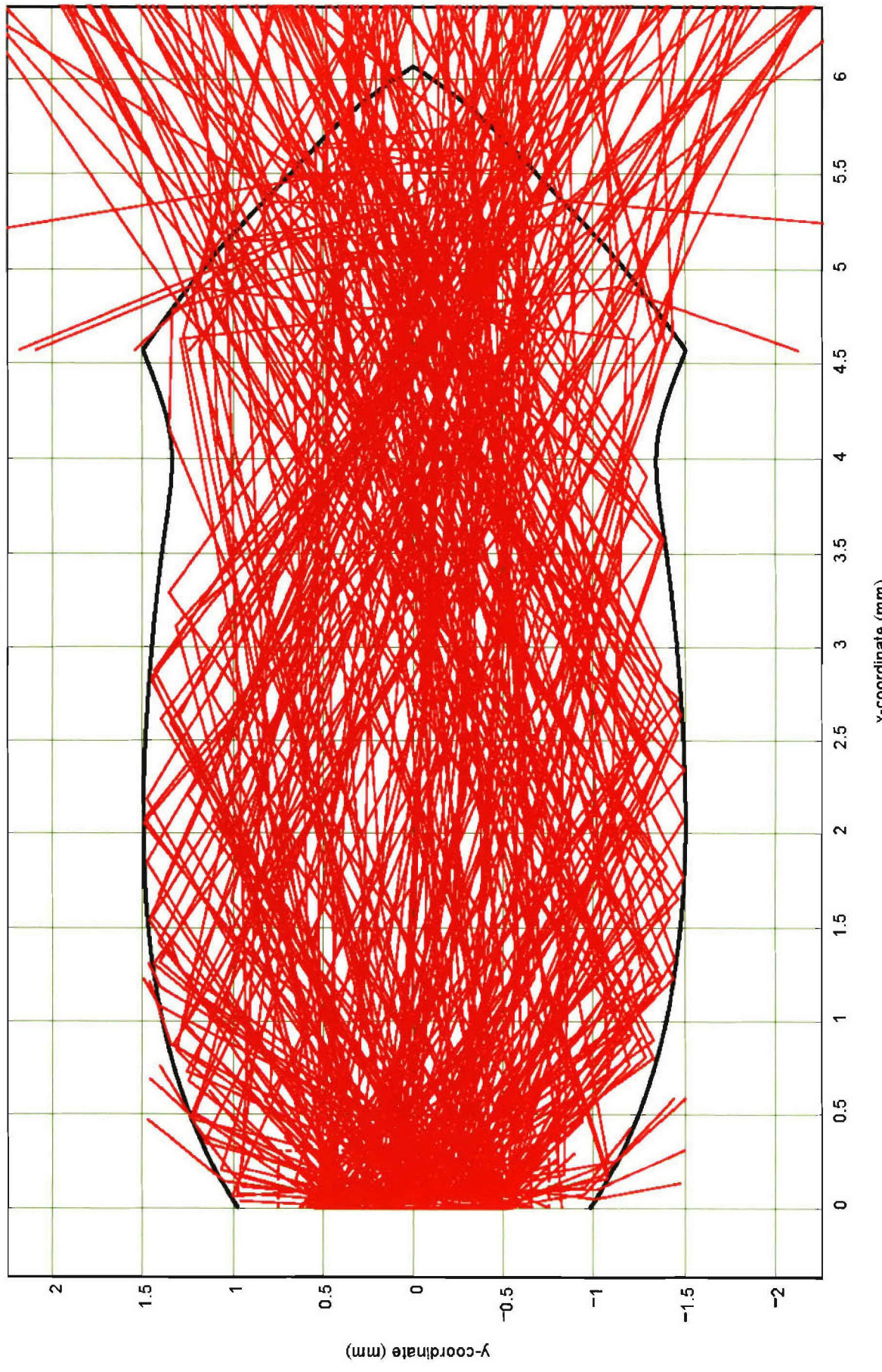
Optimized lens shape (x,y-plane)



## Cross section of design G01, with larger number of traced rays

Case = "G01"

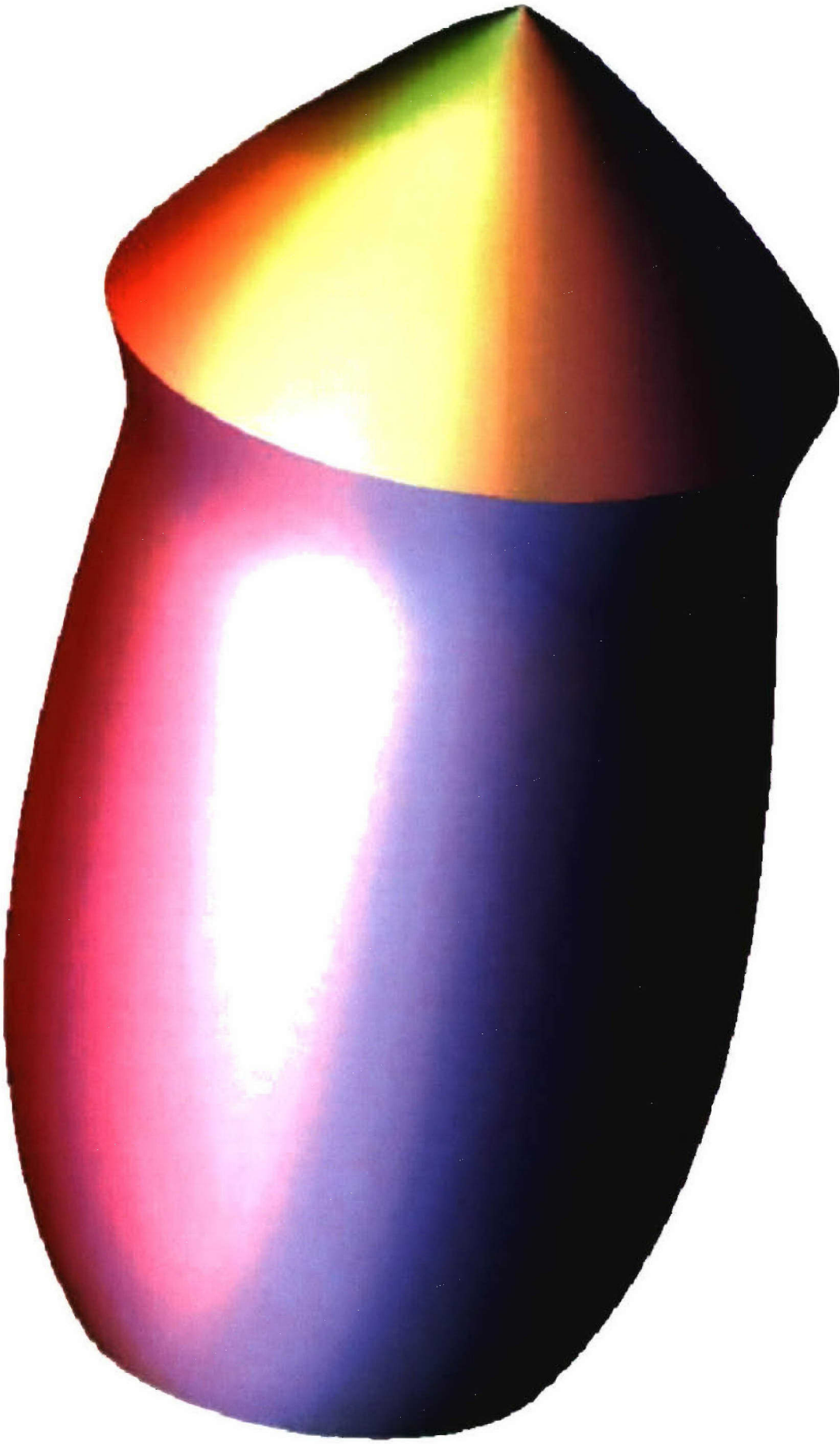
Optimized lens shape (x,y-plane)



## Three-dimensional representation of design G01



An Employee-Owned Company



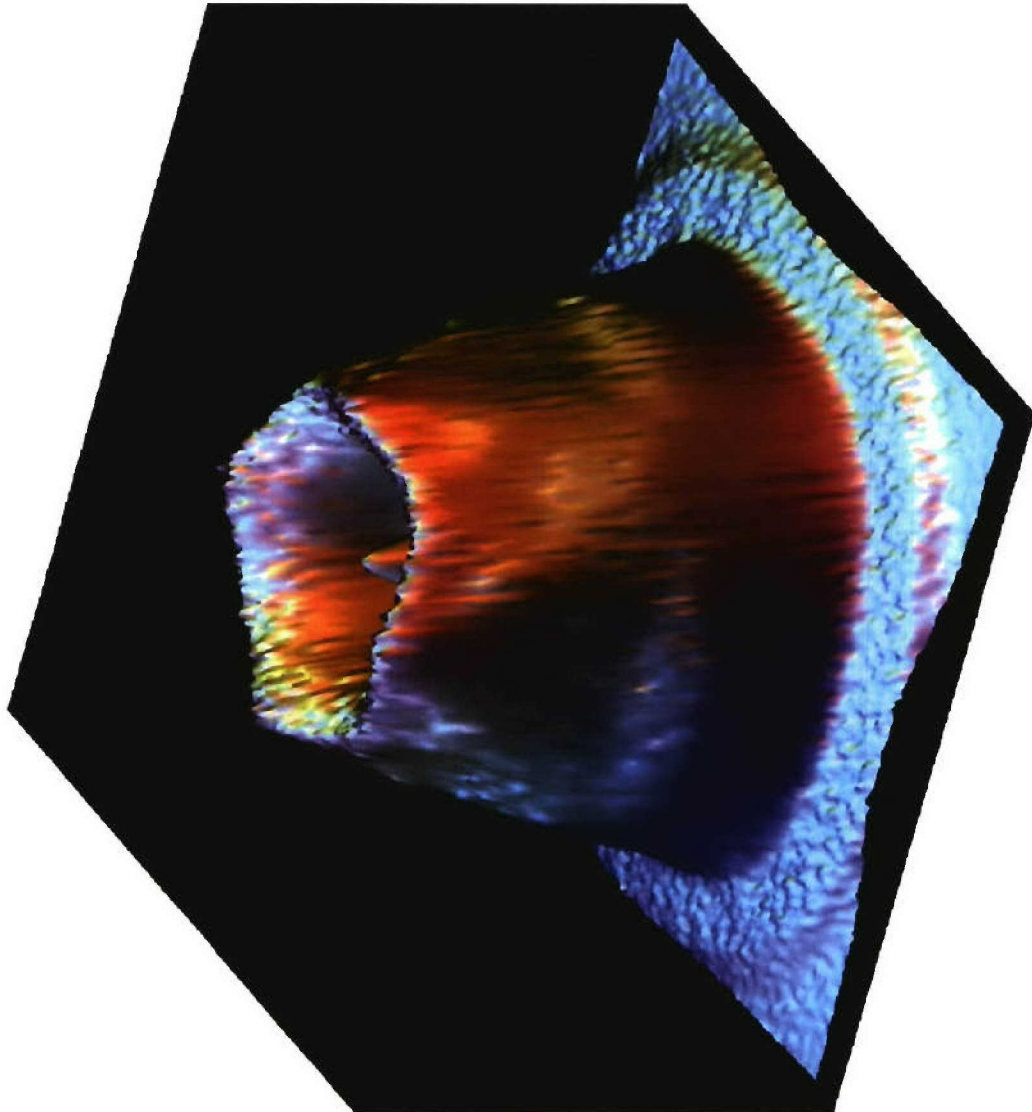
## Total source étendue versus available source étendue

- Surface area of source:  $1.65 \text{ mm}^2$ .
- Projected solid angle of source:  $3.1416 \text{ sr}$ .
- Refractive index in which source is immersed: **1.50**.
- Total source étendue:  $11.66 \text{ mm}^2\text{-sr}$ .
- Due to source-clearance requirements, 11.31% of source flux is directly absorbed by substrate, without being collected by micro-optics. So only 88.69% of source étendue is actually available.
- Available source étendue:  $10.34 \text{ mm}^2\text{-sr}$ .

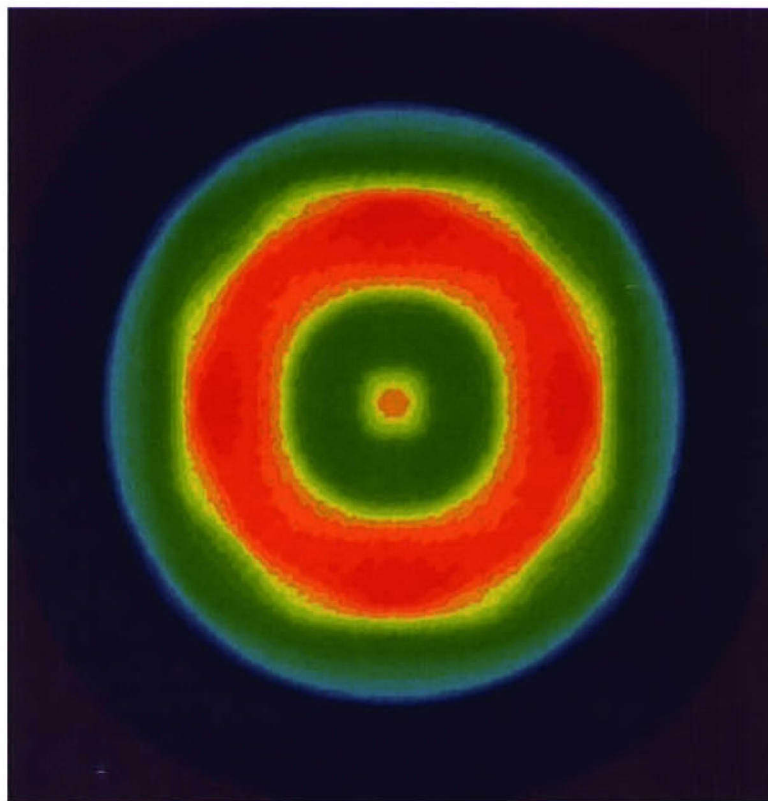
## Micro-optics design G01: intensity distribution



An Employee-Owned Company



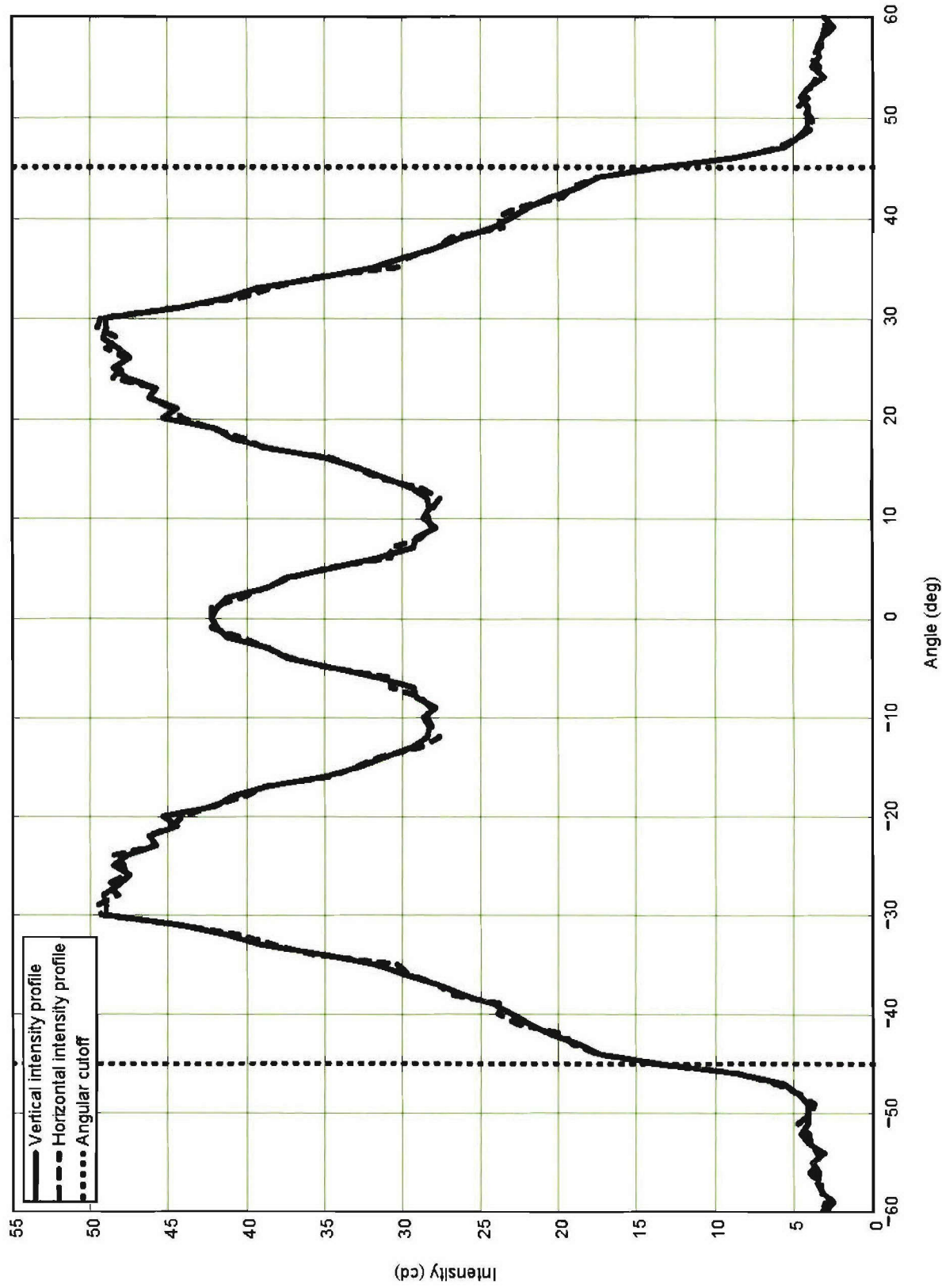
(surface plot)



(pseudo-color contour plot)

## Micro-optics design G01: intensity profiles

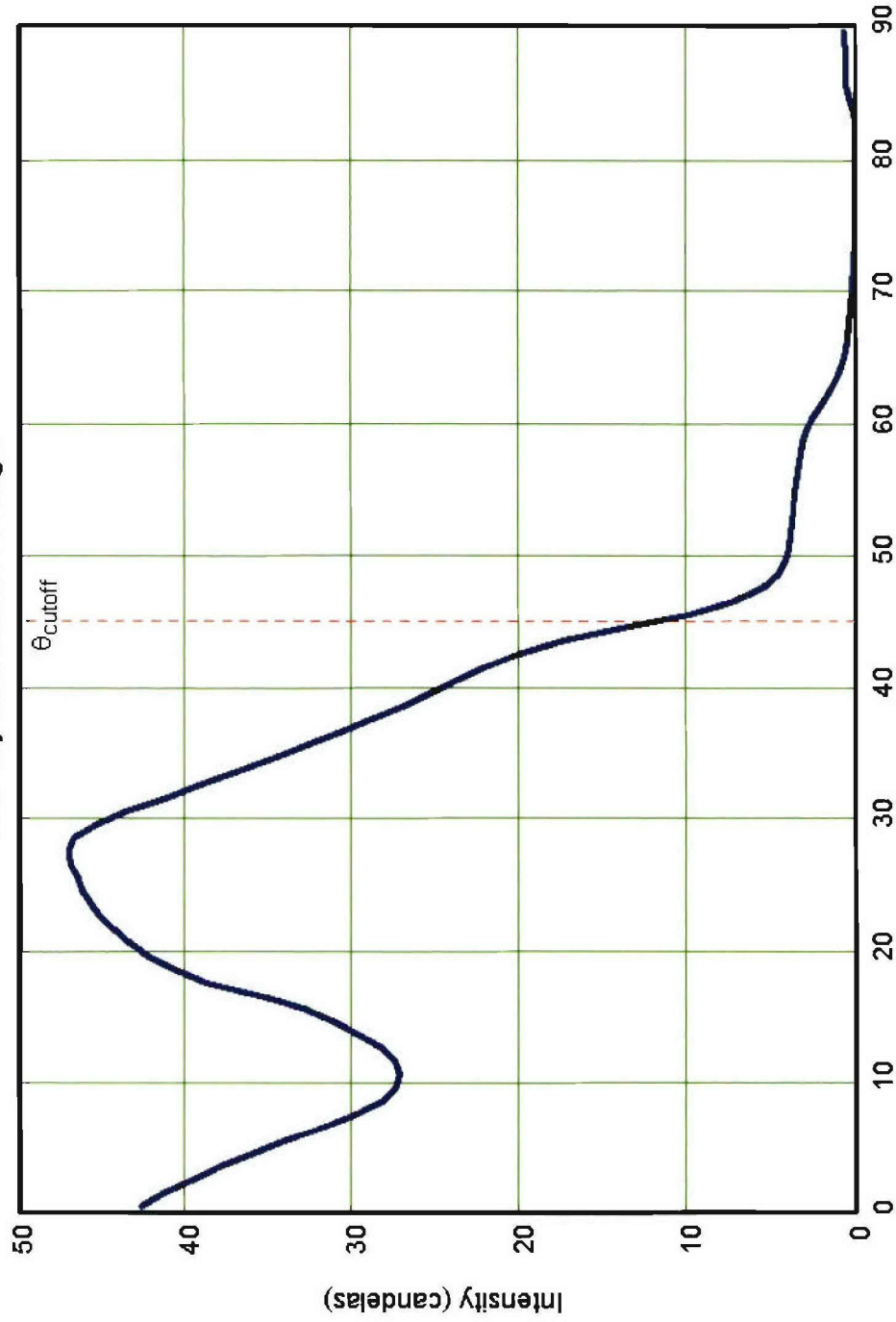
Case G01: Vertical and horizontal intensity profiles



# Micro-optics design G01: radial intensity distribution

Case = "G01"

Intensity as a function of angle

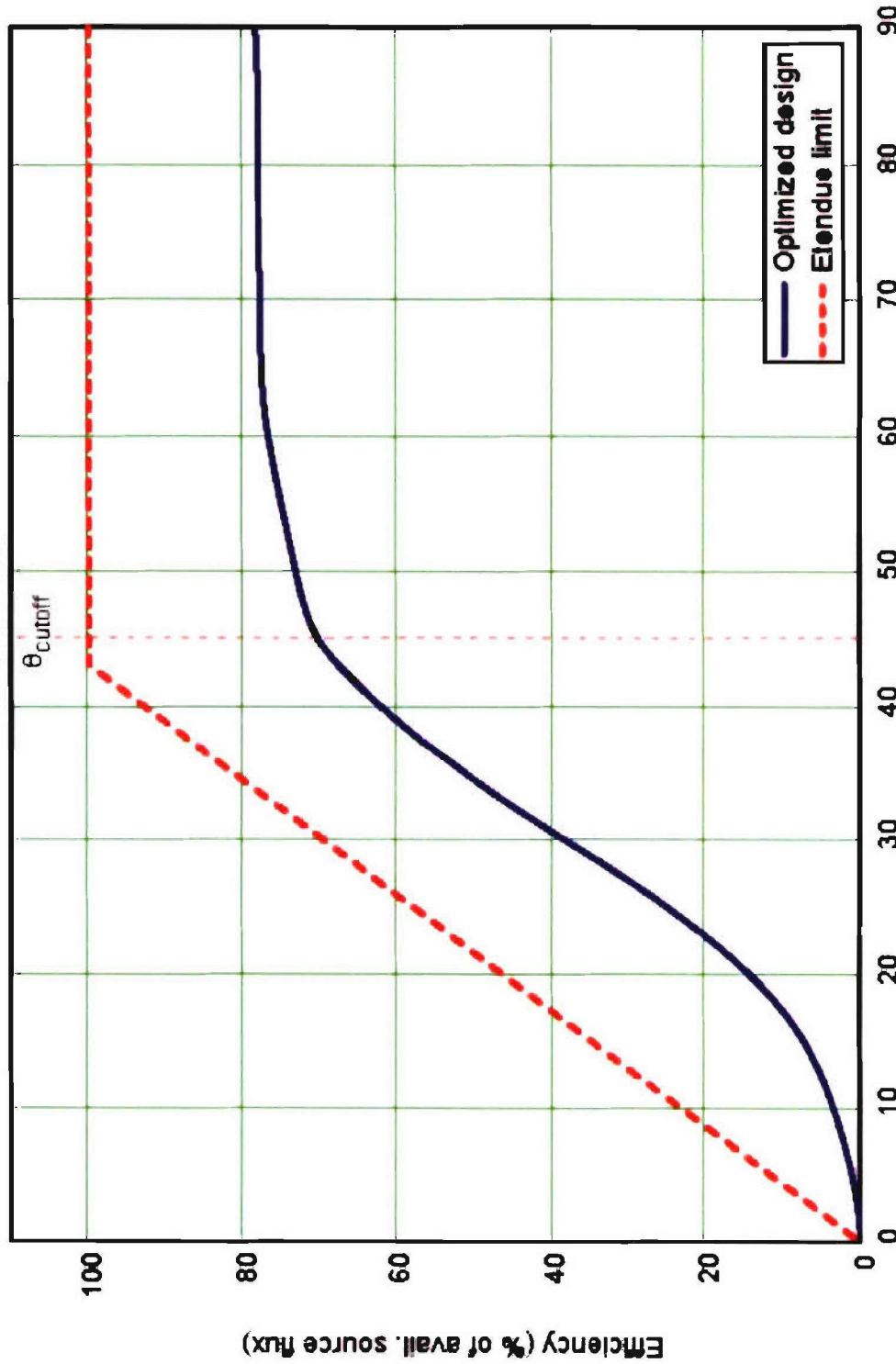


Intensity output averaged over annular angular bins as a function of angle off axis)

(intensity output averaged over annular angular bins as a function of angle off axis)

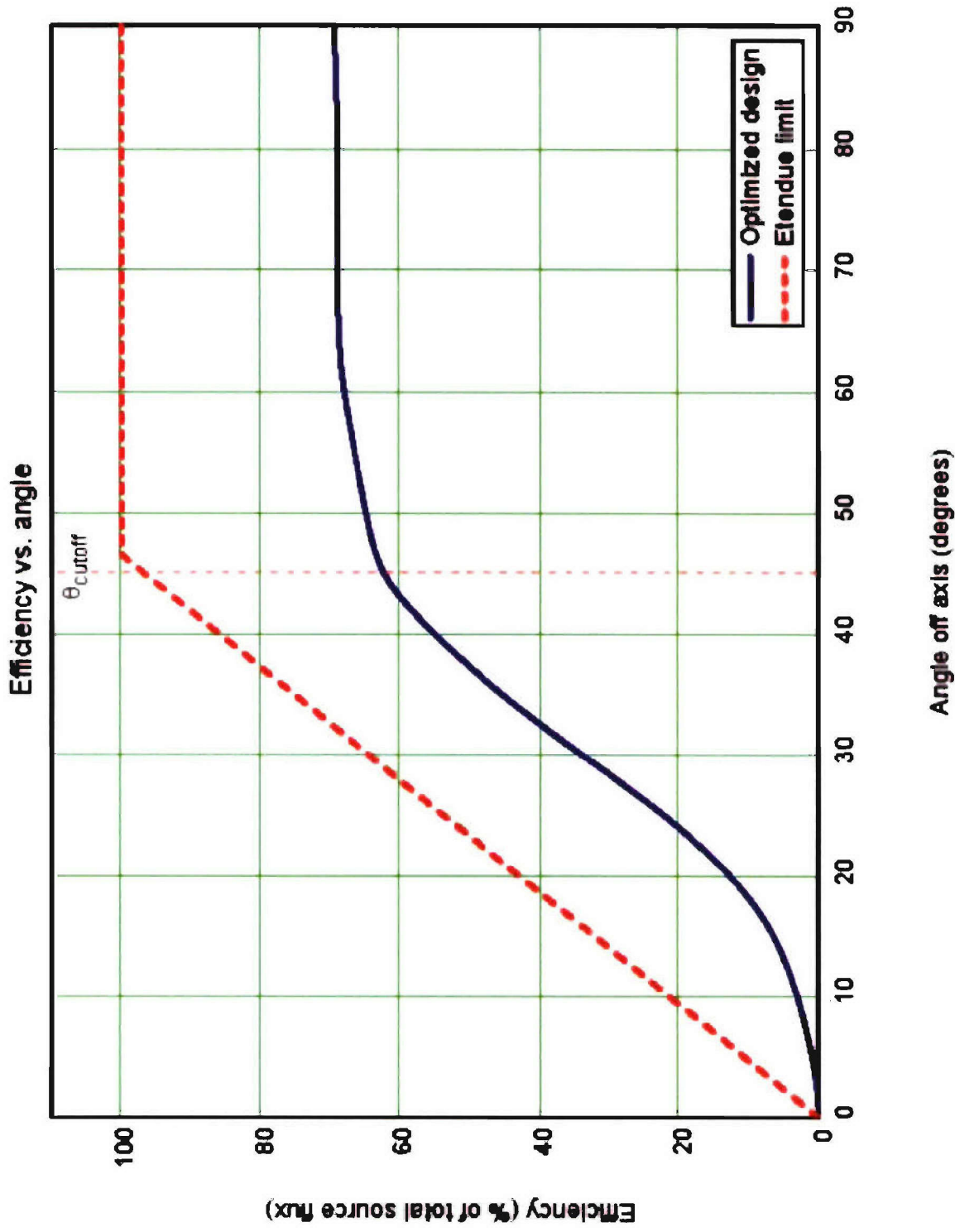
## Micro-optics design G01: renormalized efficiency versus angle

Efficiency vs. angle



(efficiency as a percentage of available source étendue)

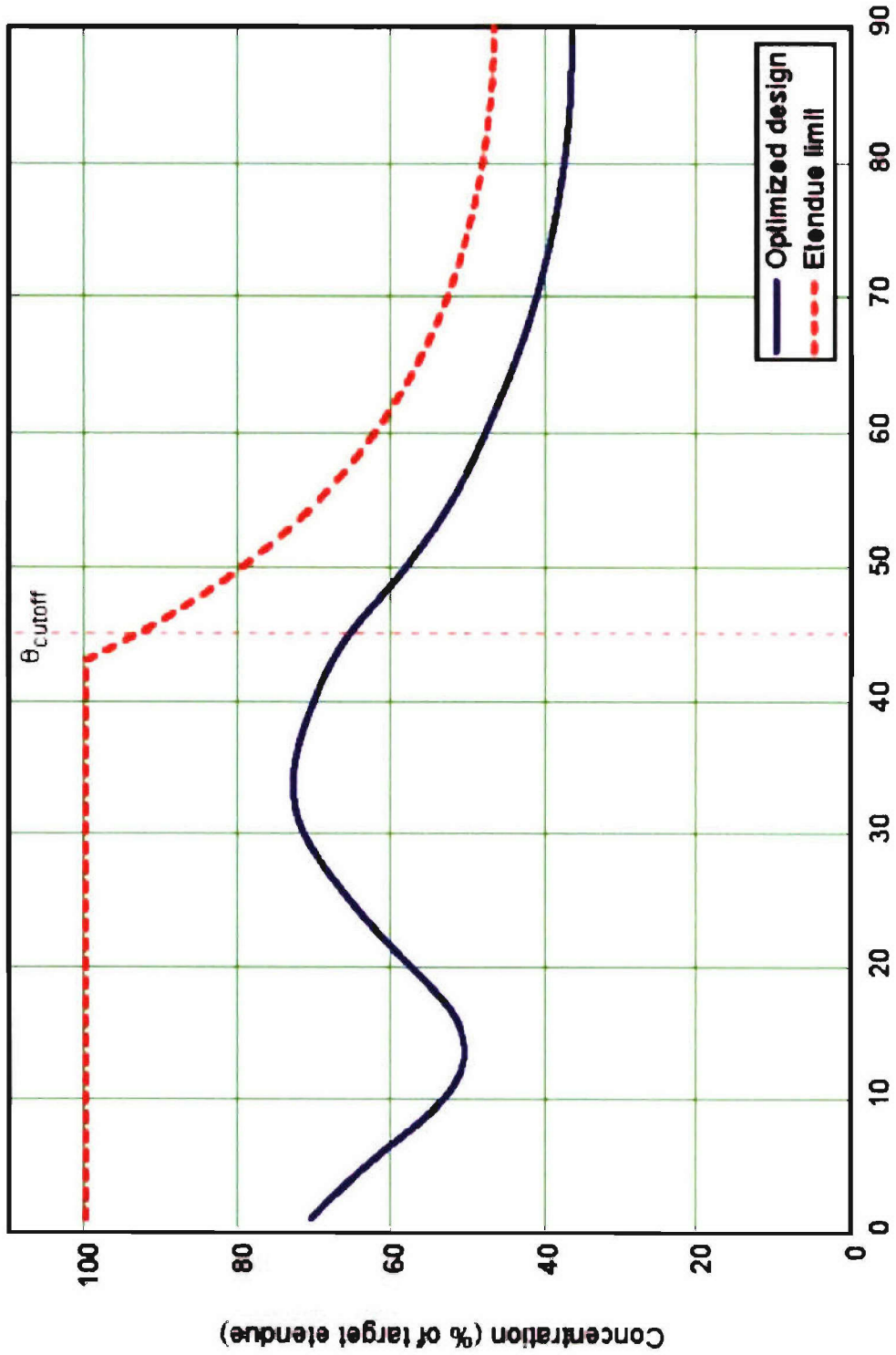
# Micro-optics design G01: total efficiency versus angle



(efficiency as a percentage of total source étendue)

## Micro-optics design G01: concentration versus angle

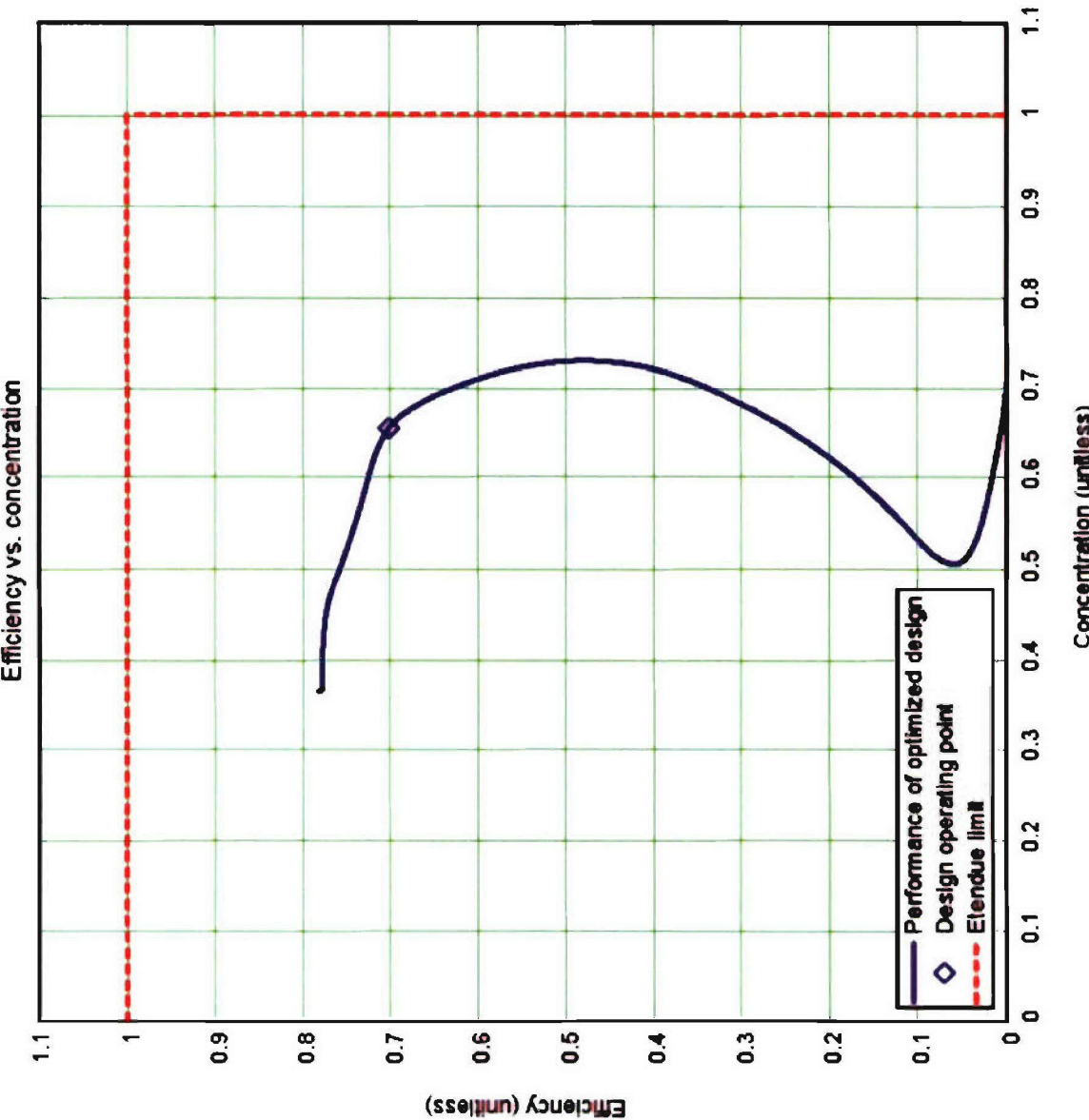
Concentration vs. angle



Angle off axis (degrees)

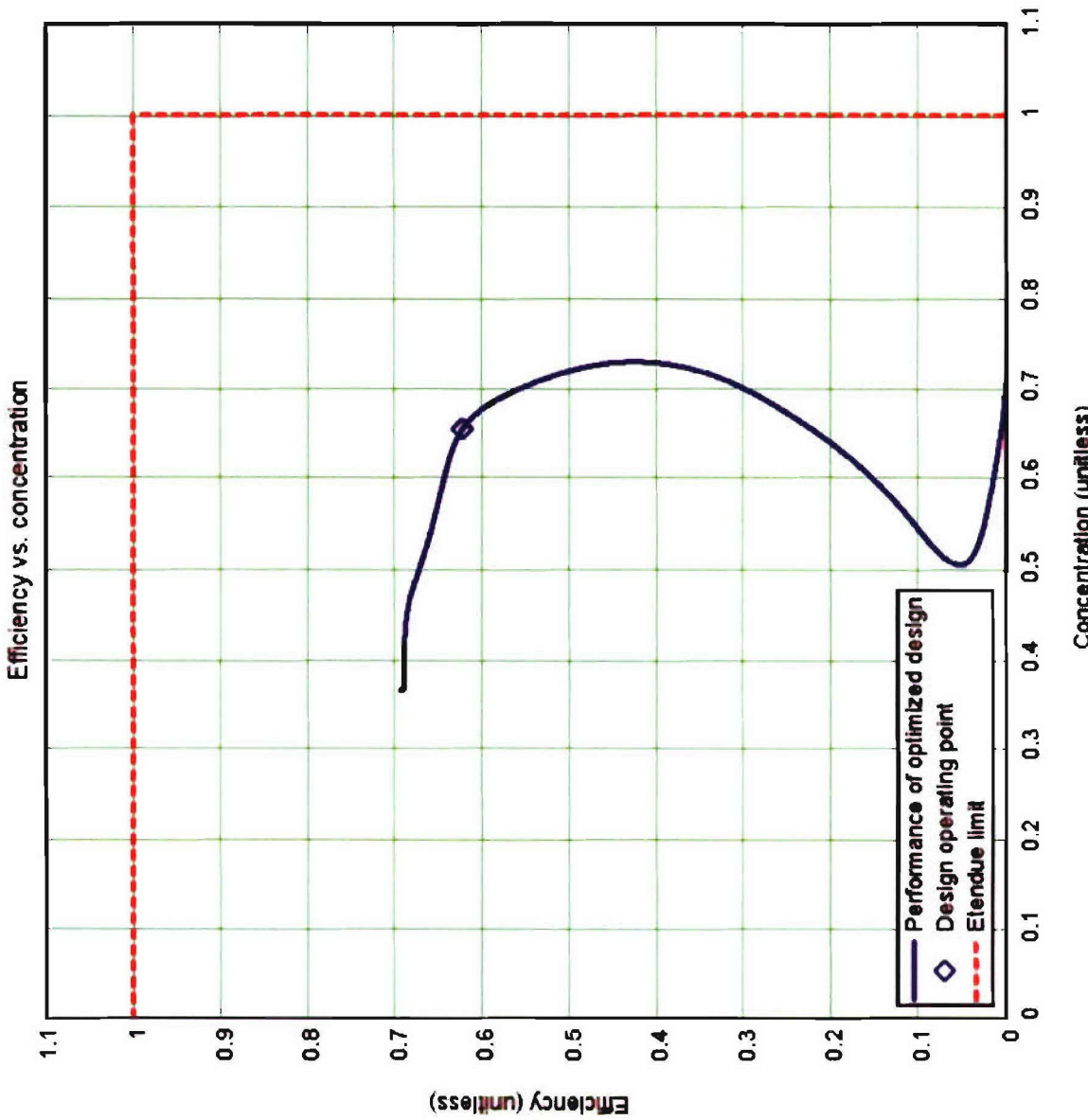
(étendue limit based on available source étendue)

## Micro-optics design G01: renorm. efficiency vs. concentration



(efficiency based on available source étendue)

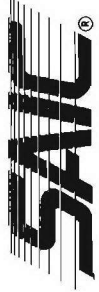
## Micro-optics design G01: total efficiency versus concentration



(efficiency based on total source étendue)

**Non-axisymmetric micro-optics, with reflective coating  
and 0.2-mm source clearance**

## Optimized non-axisymmetric micro-optics, with reflective coating and 0.2-mm source clearance

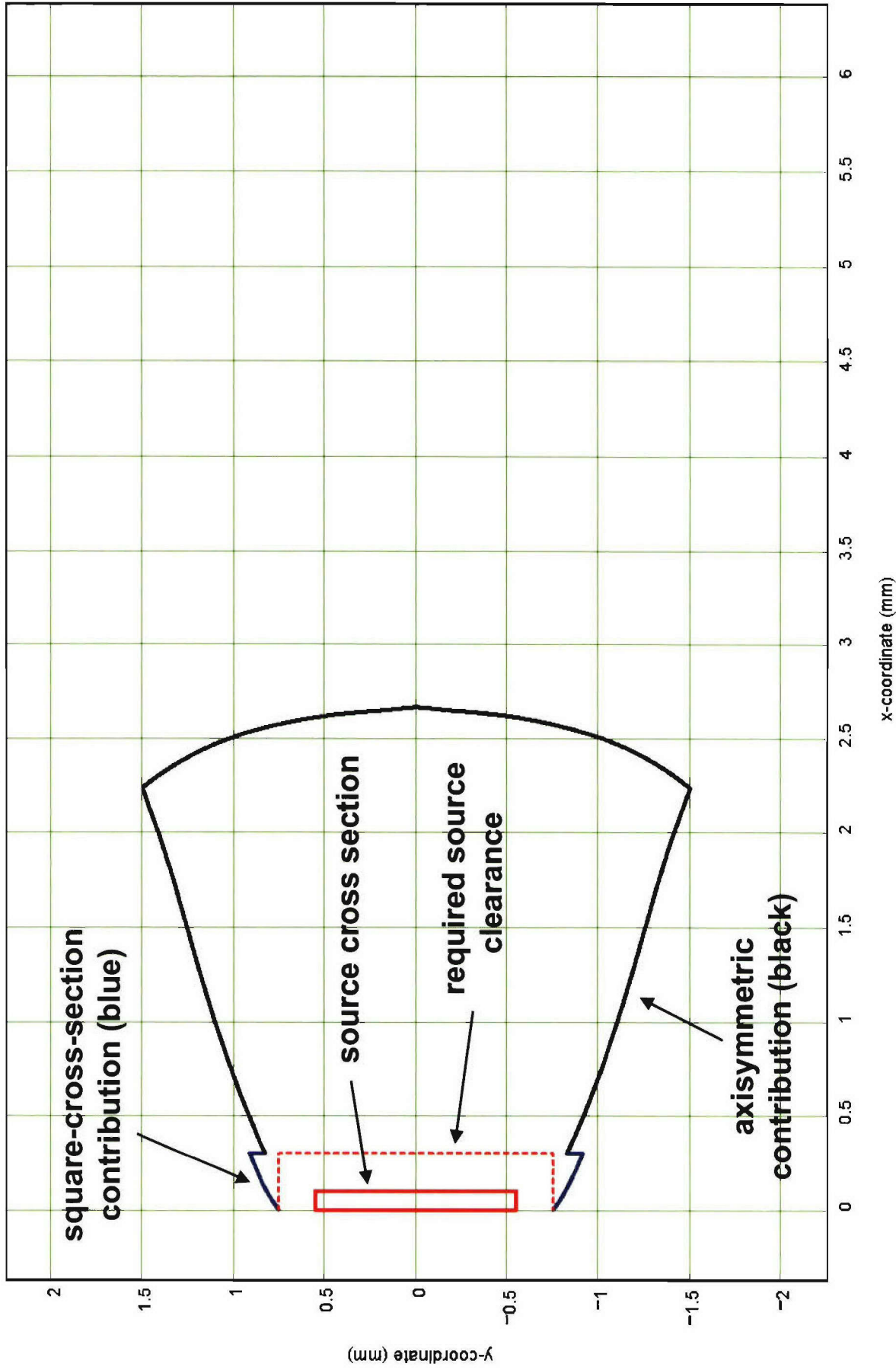


- Design designation: H03.
- Shape of reflective section of micro-optics combines square-cross-section and axisymmetric contributions.
- Refractive surface is axisymmetric
- No optical surface is allowed to approach closer than 0.2 mm from surface of LED light source.
- Maximum diameter of micro-optics: 3.0 mm.
- Refractive index: 1.51.
- Optimized for reflective surface having 95% reflectance.
- Optimized for refractive surface having 100% transmittance.
- Length: 2.66 mm.
- Performance plots assume 100% reflectance for reflective surface and 100% transmittance for refractive surface.

## Cross section of design H03

Case = "H03"

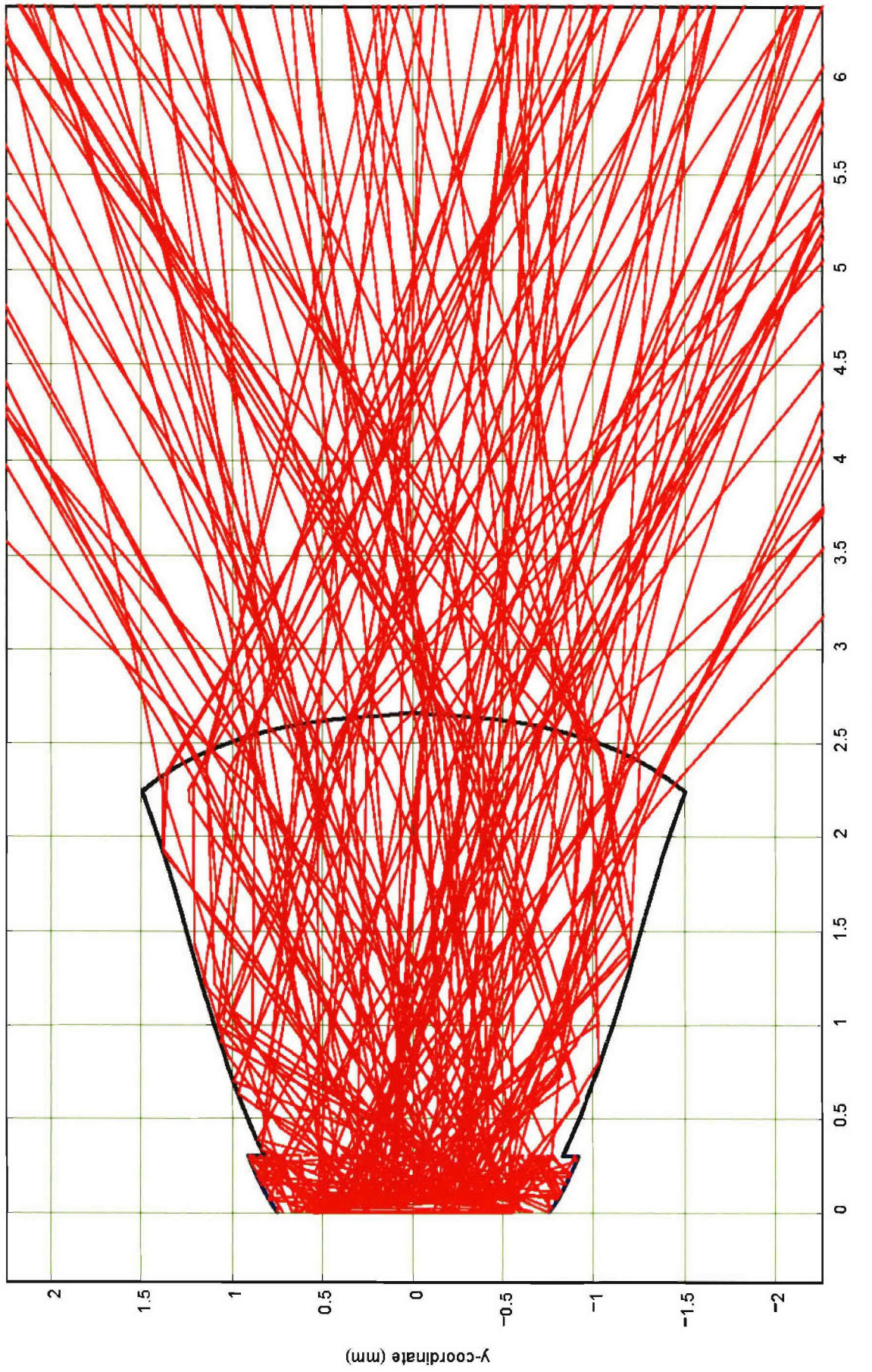
Optimized lens shape (x,y-plane)



## Cross section of design H03, with traced rays

Case = "H03"

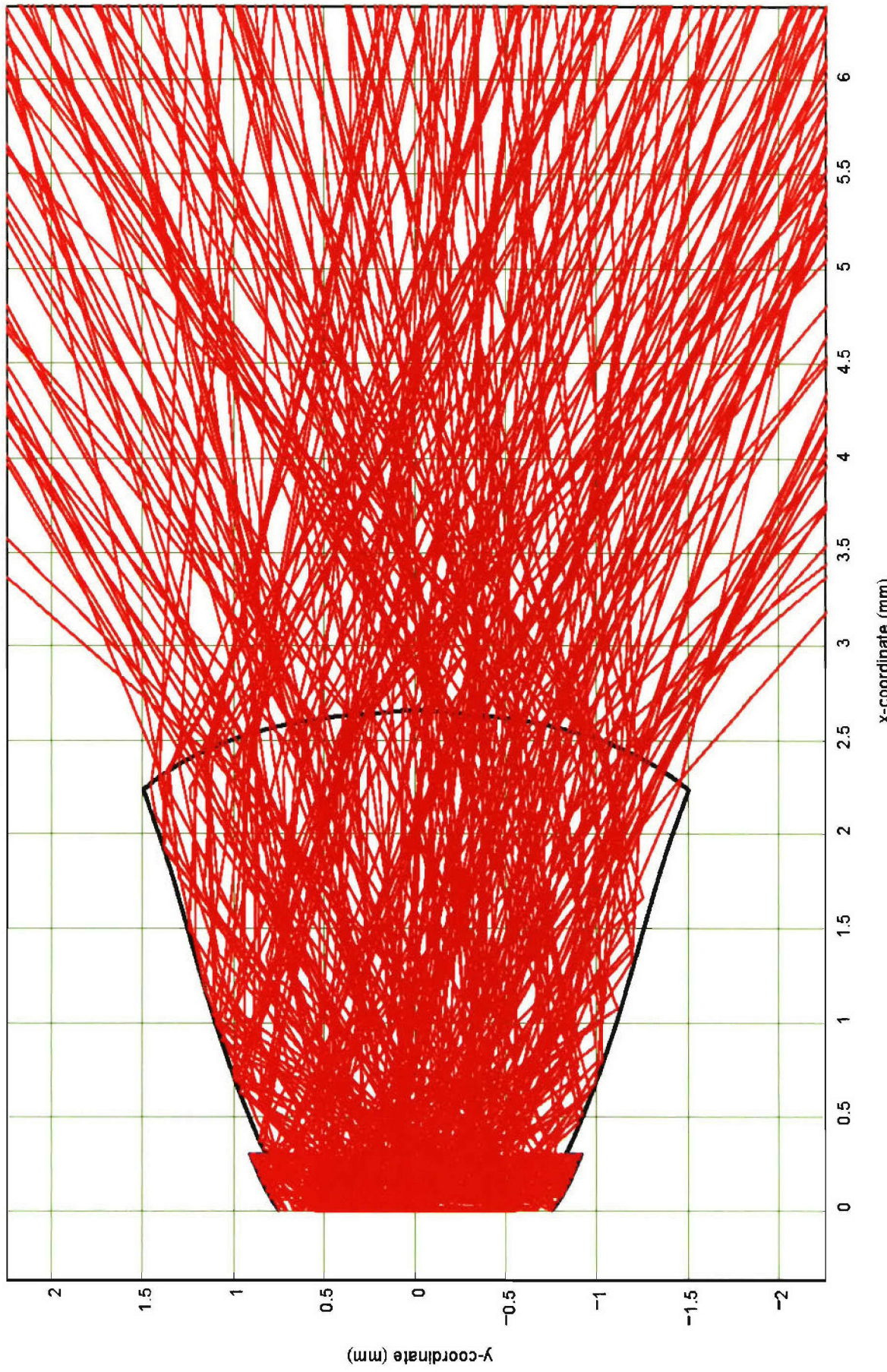
Optimized lens shape (x,y-plane)



# Cross section of design H03, with larger number of traced rays

Case = "H03"

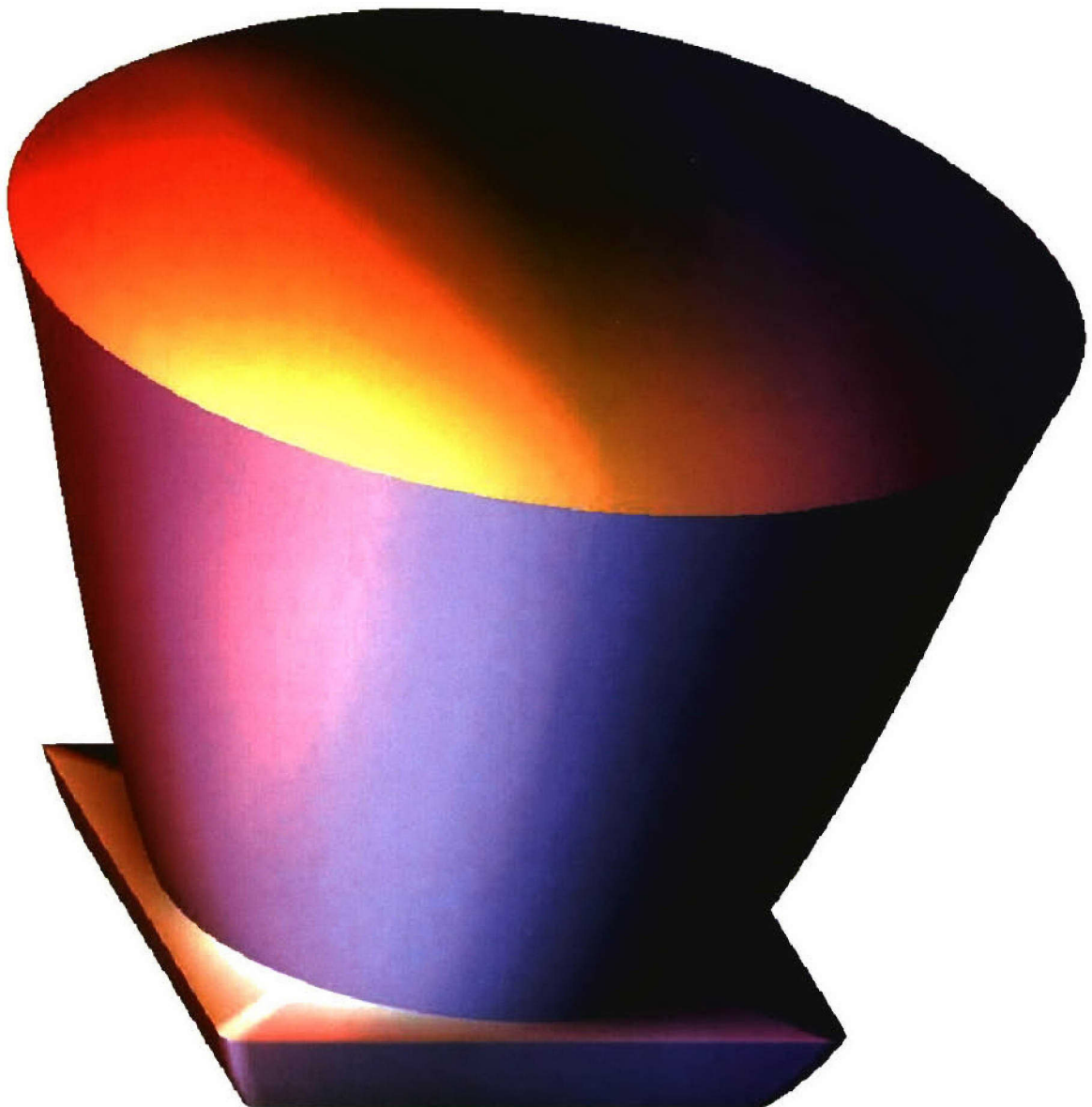
Optimized lens shape (x,y-plane)



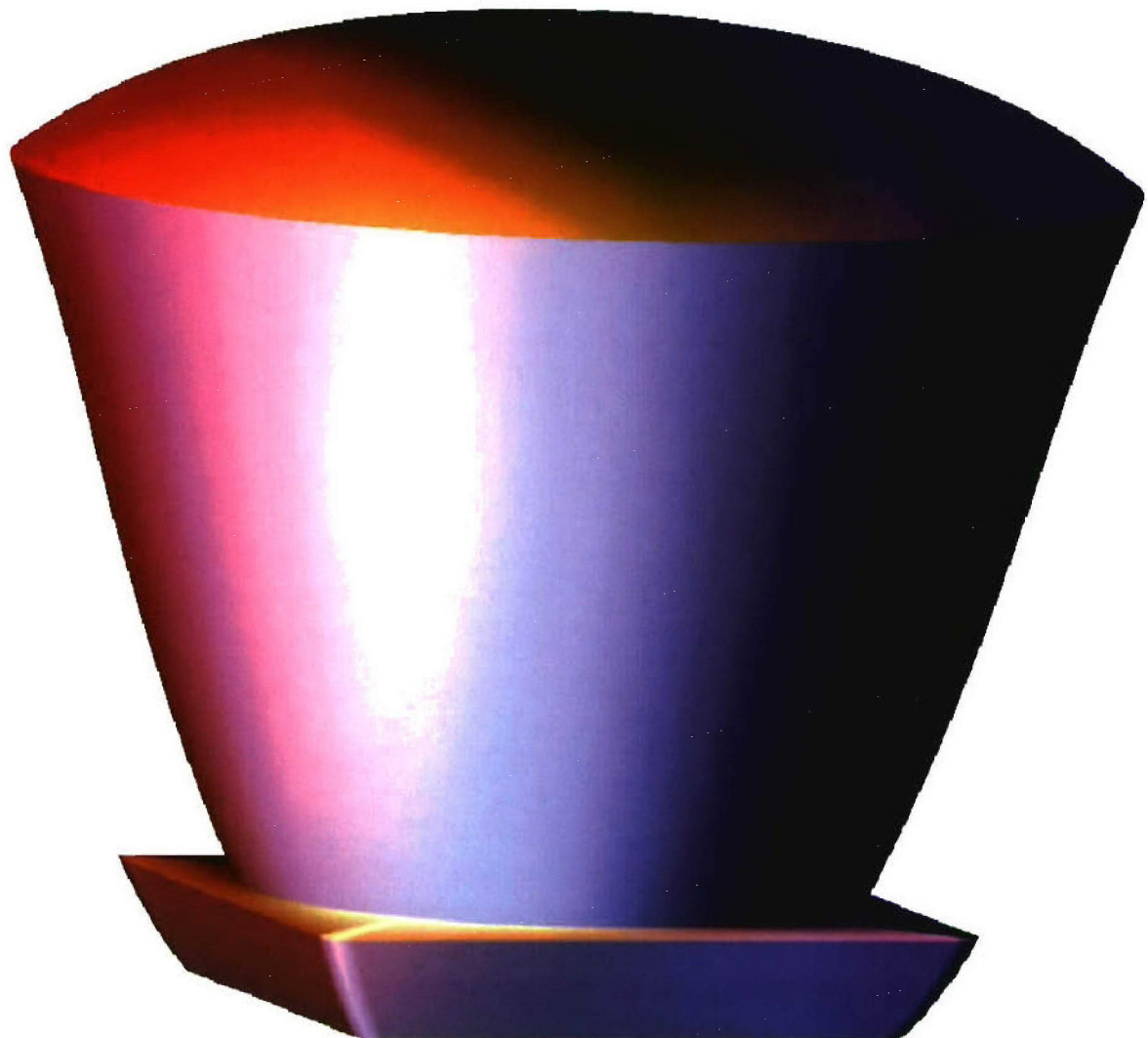
## Three-dimensional representation of design H03



An Employee-Owned Company



## Three-dimensional representation of design H03 (different view)

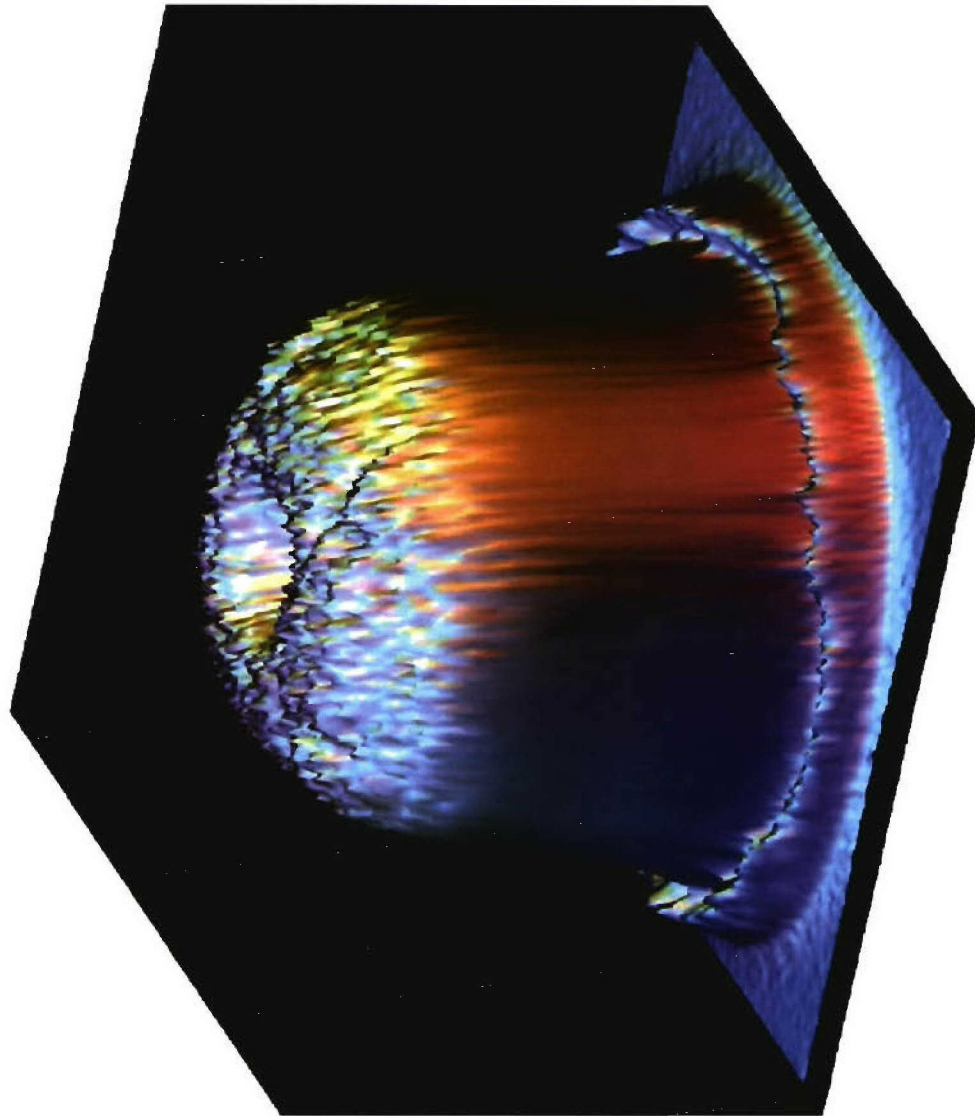


## Total source étendue versus available source étendue

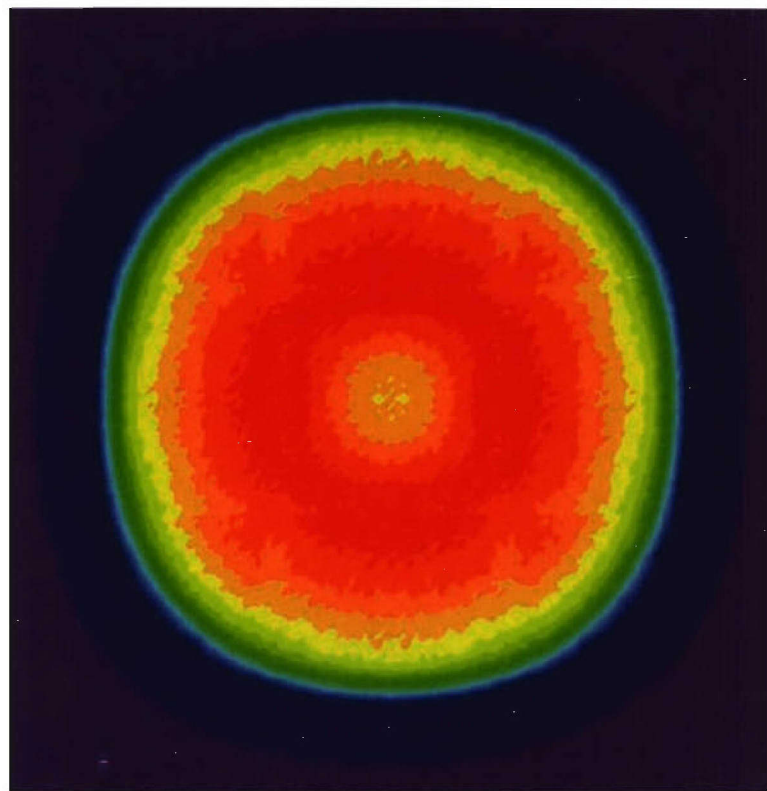


- Surface area of source:  $1.65 \text{ mm}^2$ .
- Projected solid angle of source:  $3.1416 \text{ sr}$ .
- Refractive index in which source is immersed: 1.51.
- Total source étendue:  $11.82 \text{ mm}^2\text{-sr}$ .
- Due to source-clearance requirements, 10.16% of source flux is directly absorbed by substrate, without being collected by micro-optics. So only 89.84% of source étendue is actually available.
- Available source étendue:  $10.62 \text{ mm}^2\text{-sr}$ .

## Micro-optics design H03: intensity distribution



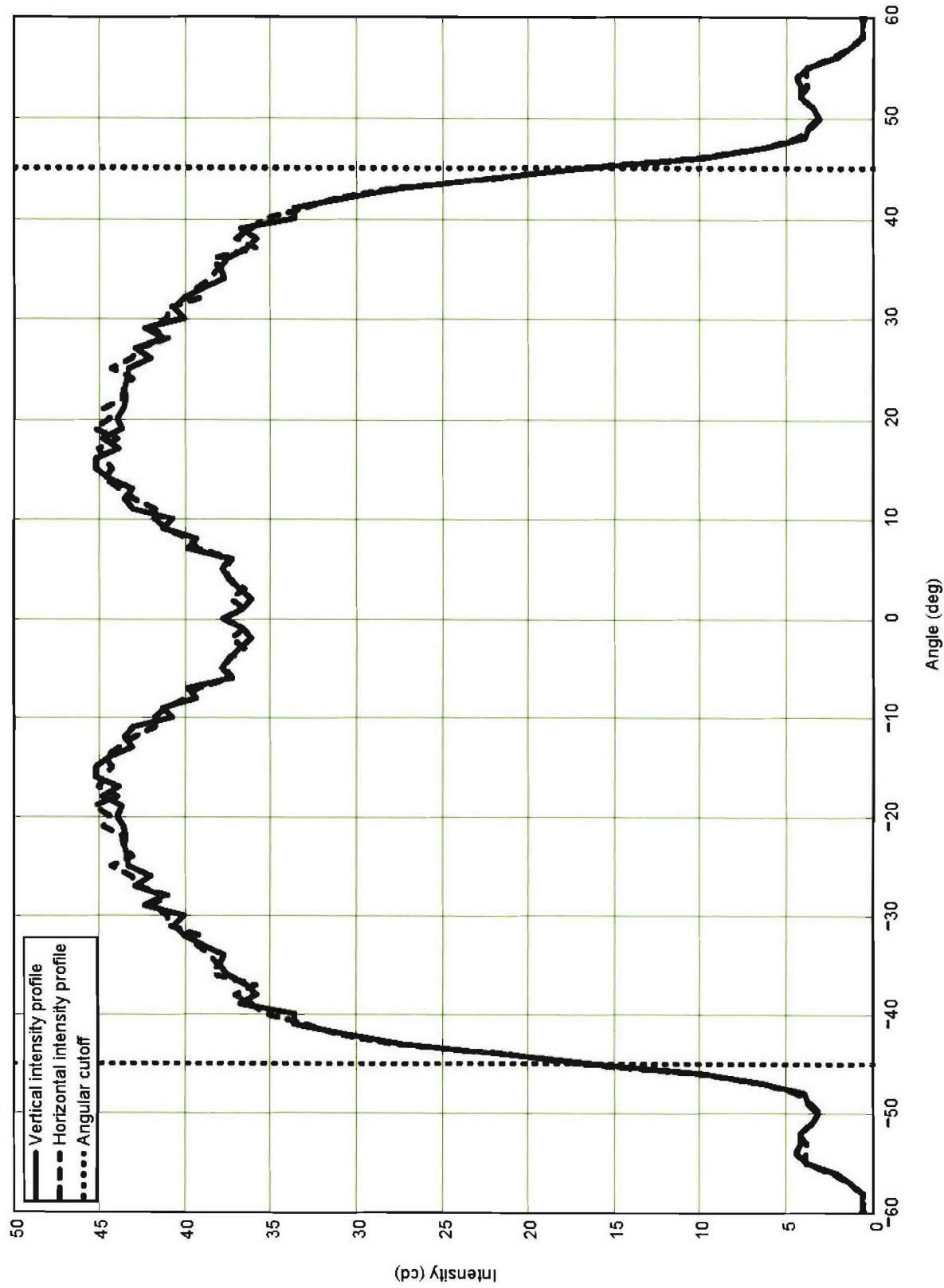
(pseudo-color contour plot)



(surface plot)

## Micro-optics design H03: intensity profiles

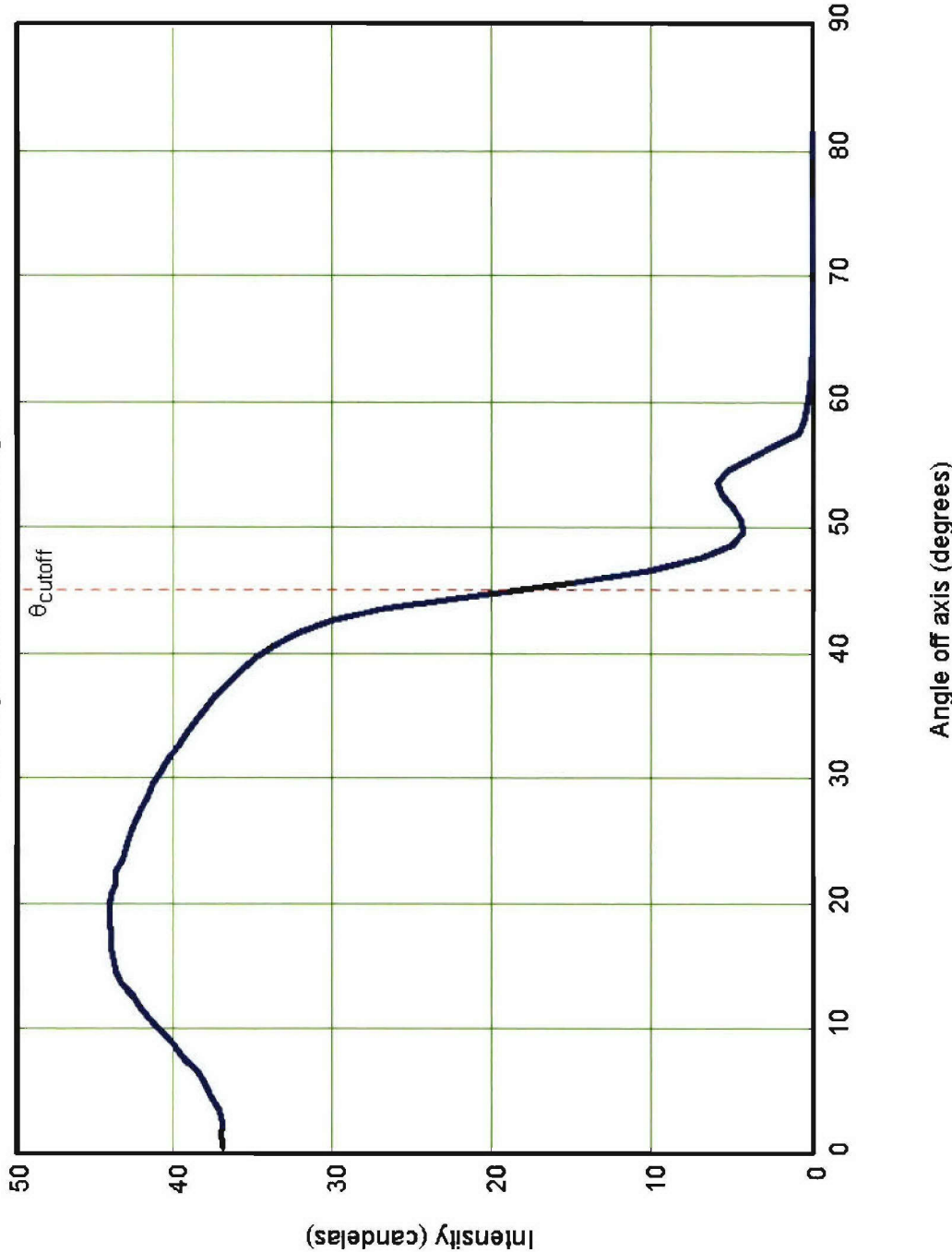
Case H03: Vertical and horizontal intensity profiles



## Micro-optics design H03: radial intensity distribution

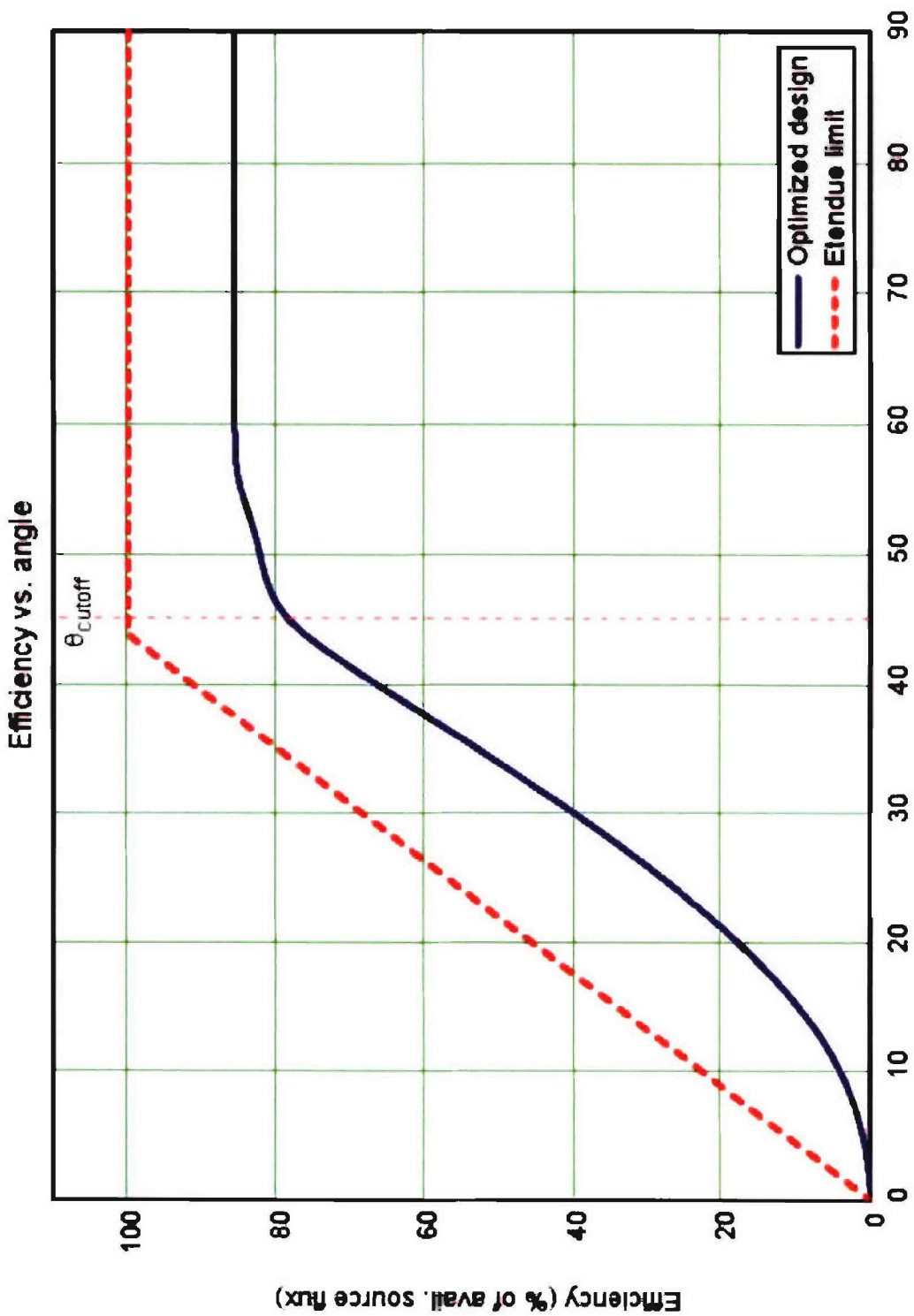
Case = "H03"

Intensity as a function of angle



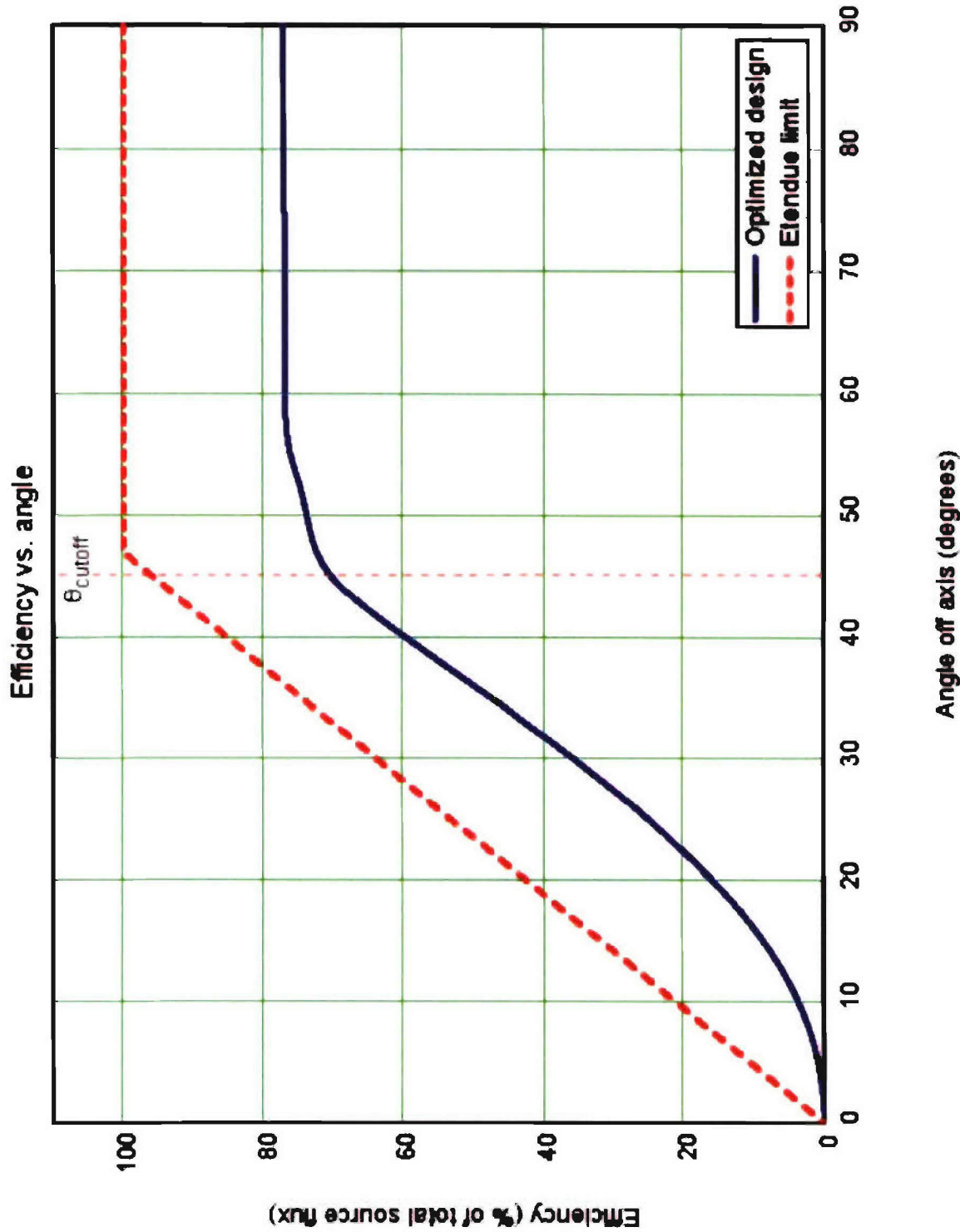
(intensity output averaged over annular angular bins as a function of angle off axis)

## Micro-optics design H03: renormalized efficiency versus angle



(efficiency as a percentage of available source étendue)

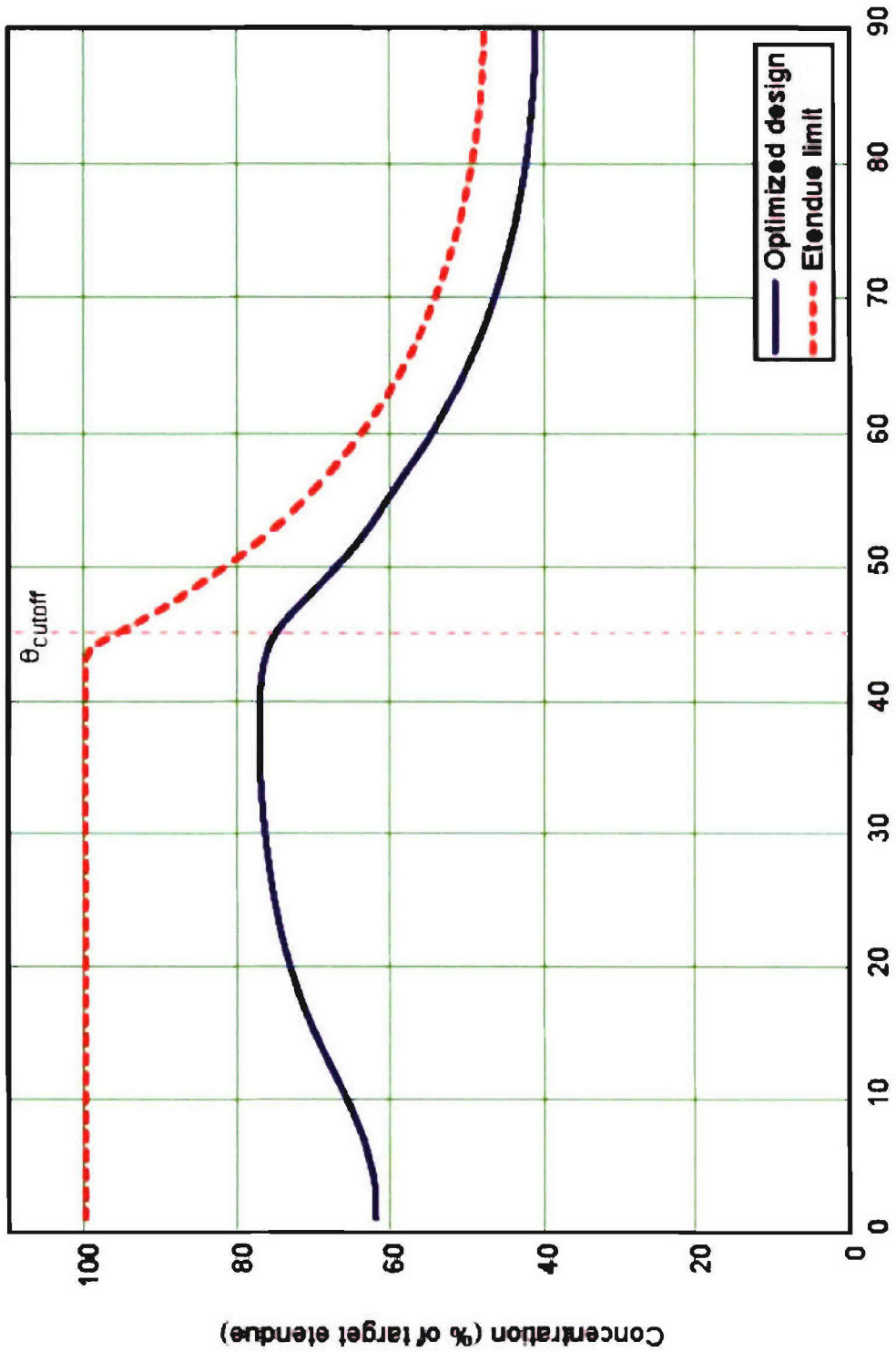
## Micro-optics design H03: total efficiency versus angle



(efficiency as a percentage of total source étendue)

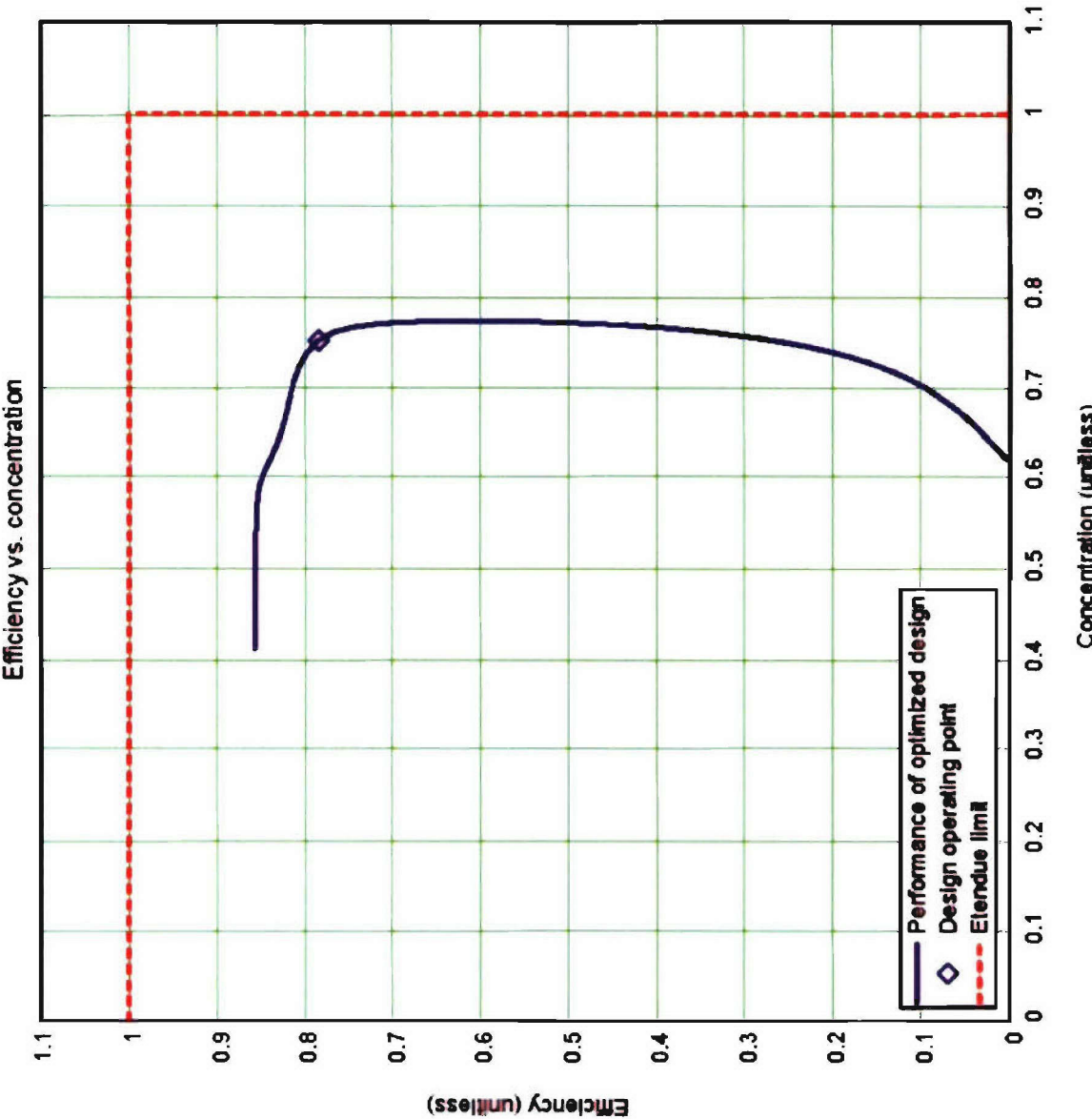
## Micro-optics design H03: concentration versus angle

Concentration vs. angle



(étendue limit based on available source étendue)

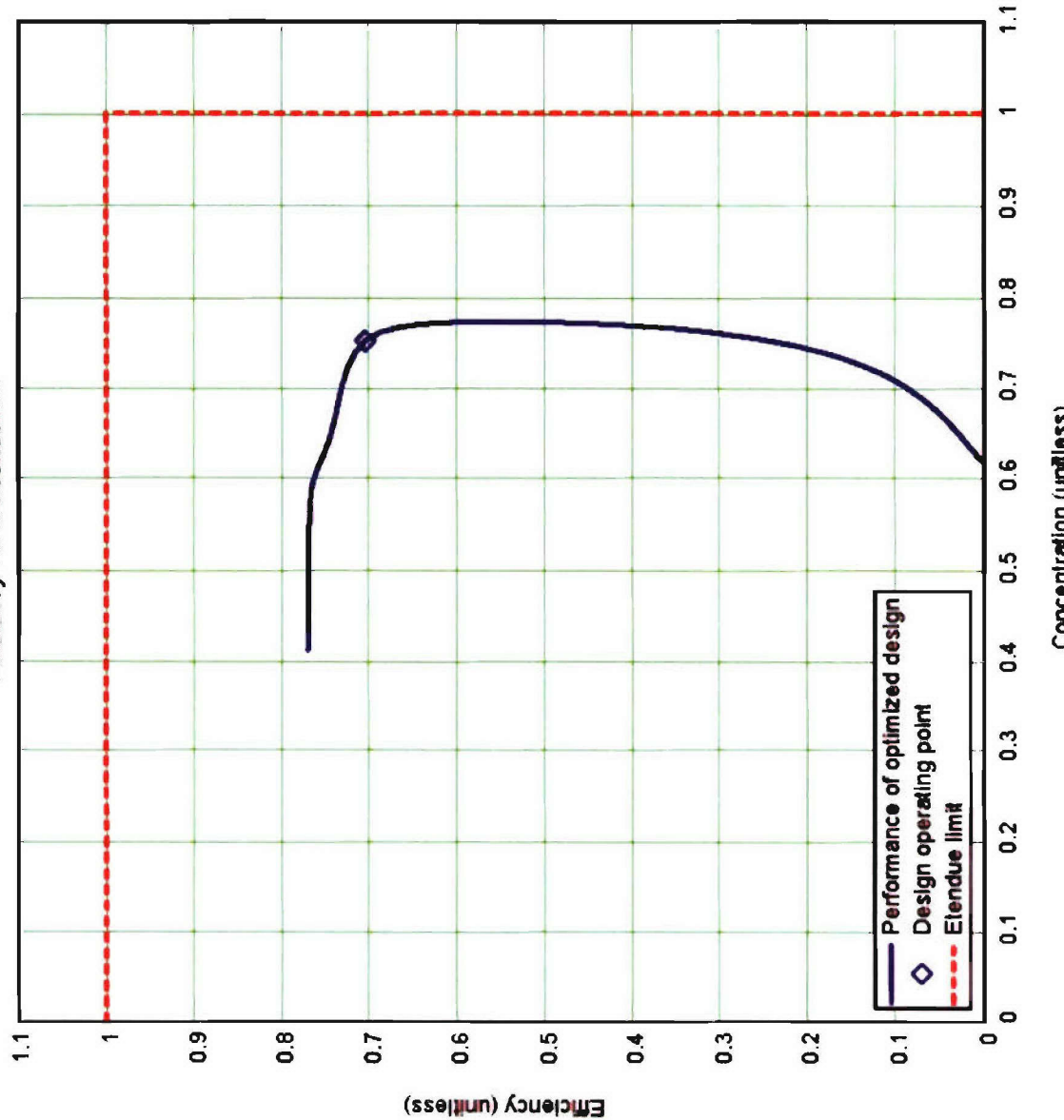
# Micro-optics design H03: renorm. efficiency vs. concentration



(efficiency based on available source étendue)

## Micro-optics design H03: total efficiency versus concentration

Efficiency vs. concentration



(efficiency based on total source étendue)

**Non-axisymmetric micro-optics, with reflective coating  
and 0.1-mm source clearance**

## Optimized non-axisymmetric micro-optics, with reflective coating and 0.1-mm source clearance



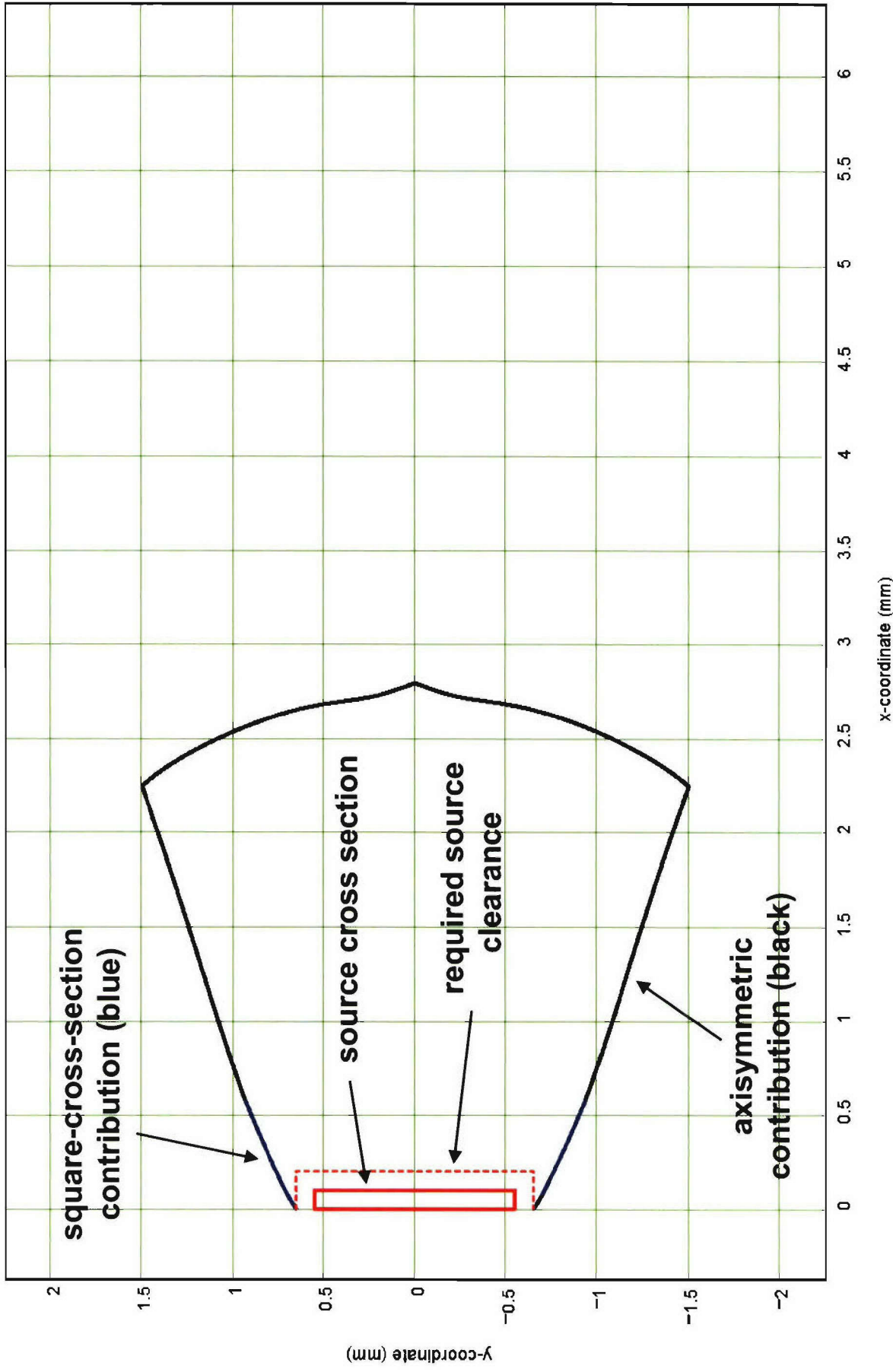
An Employee-Owned Company

- Design designation: R02.
- Shape of reflective section of micro-optics combines square-cross-section and axisymmetric contributions.
- Refractive surface is axisymmetric
- No optical surface is allowed to approach closer than 0.1 mm from surface of LED light source.
- Maximum diameter of micro-optics: 3.0 mm.
- Refractive index: 1.51.
- Optimized for reflective surface having 95% reflectance.
- Optimized for refractive surface having 100% transmittance.
- Length: 2.79 mm.
- Performance plots assume 100% reflectance for reflective surface and 100% transmittance for refractive surface.

# Cross section of design R02

Case = "R02"

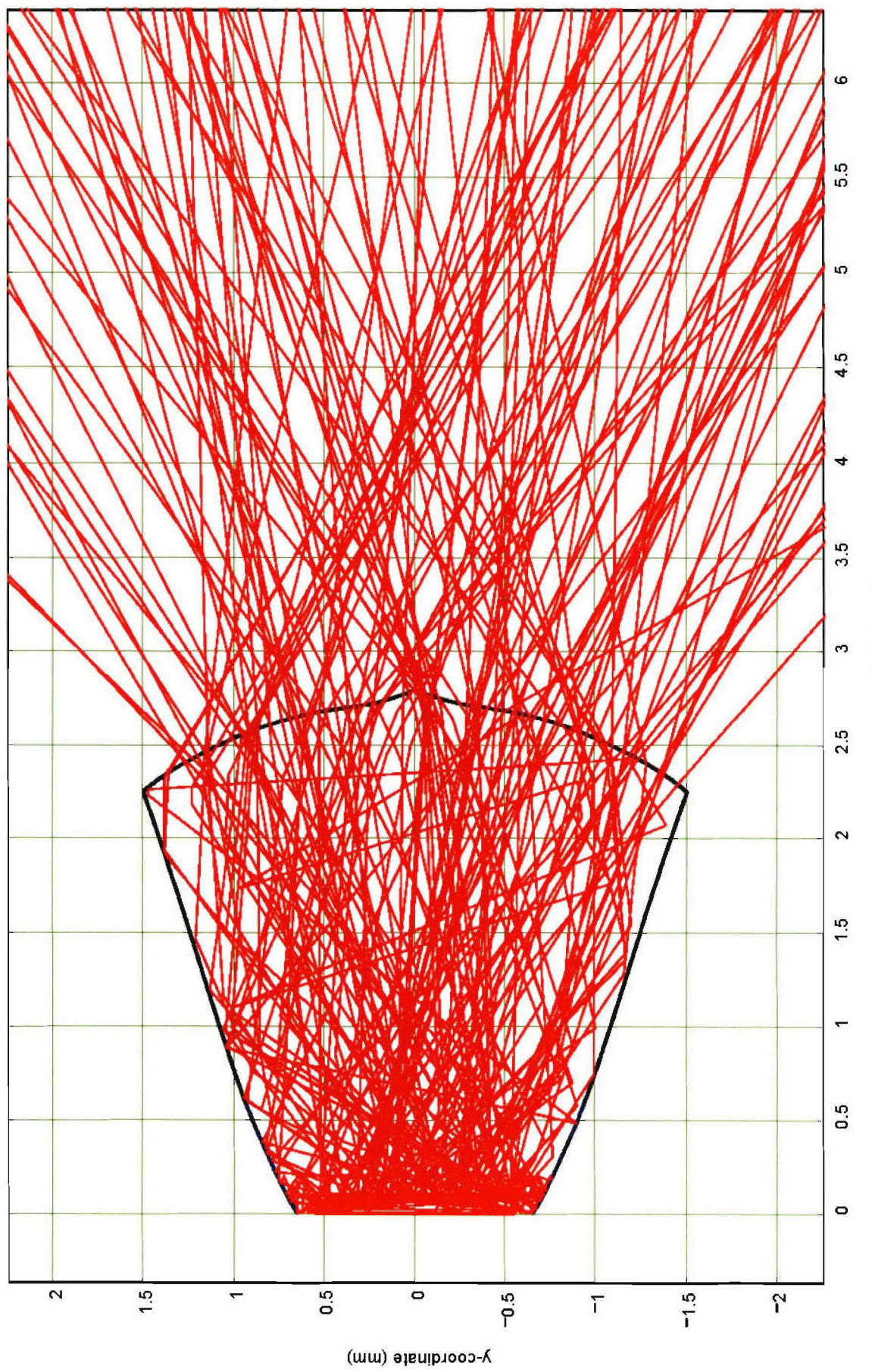
Optimized lens shape (x,y-plane)



## Cross section of design R02, with traced rays

Case = "R02"

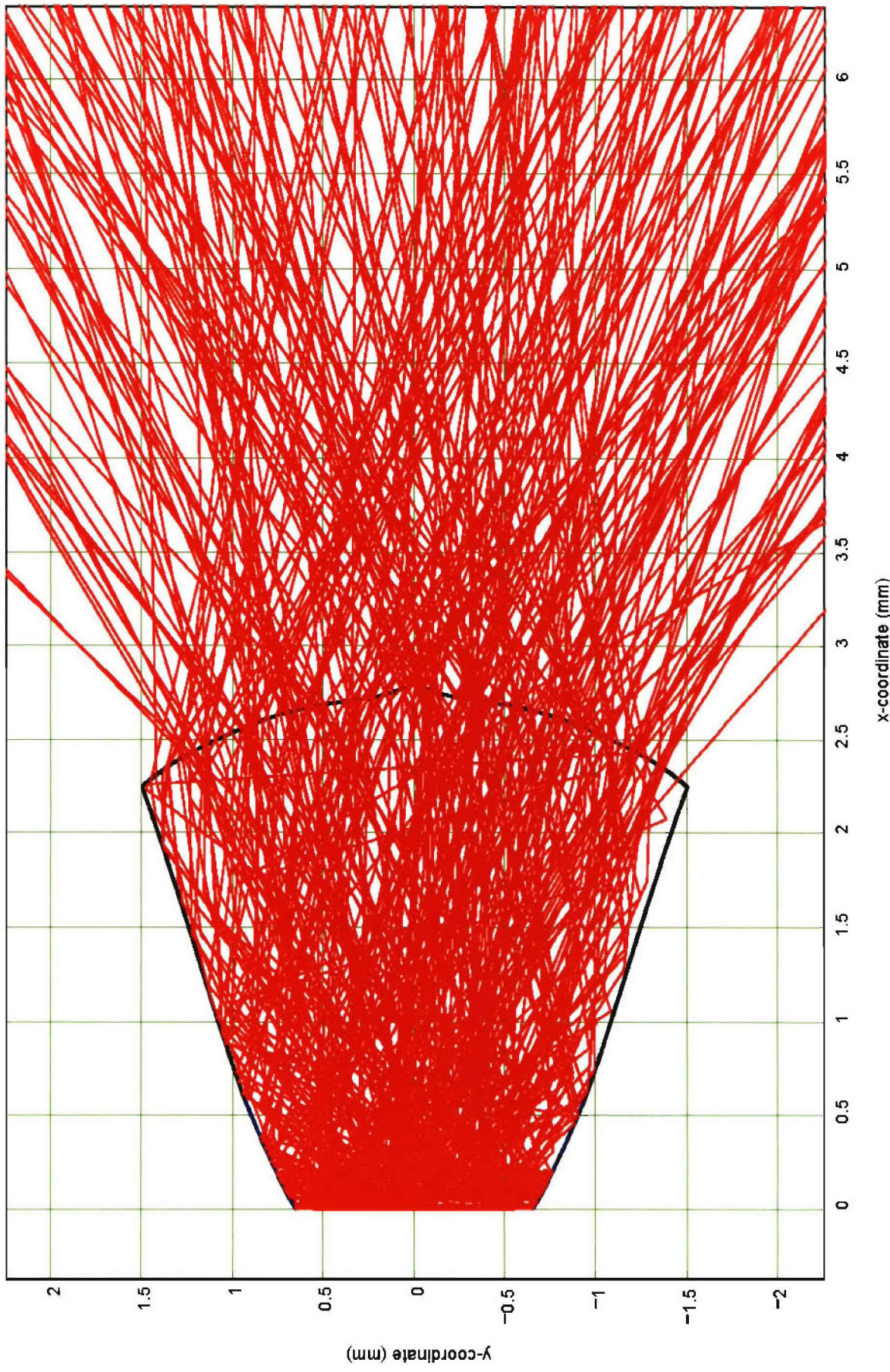
Optimized lens shape (x,y plane)



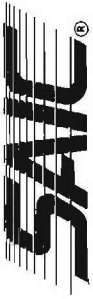
## Cross section of design R02, with larger number of traced rays

Case = "R02"

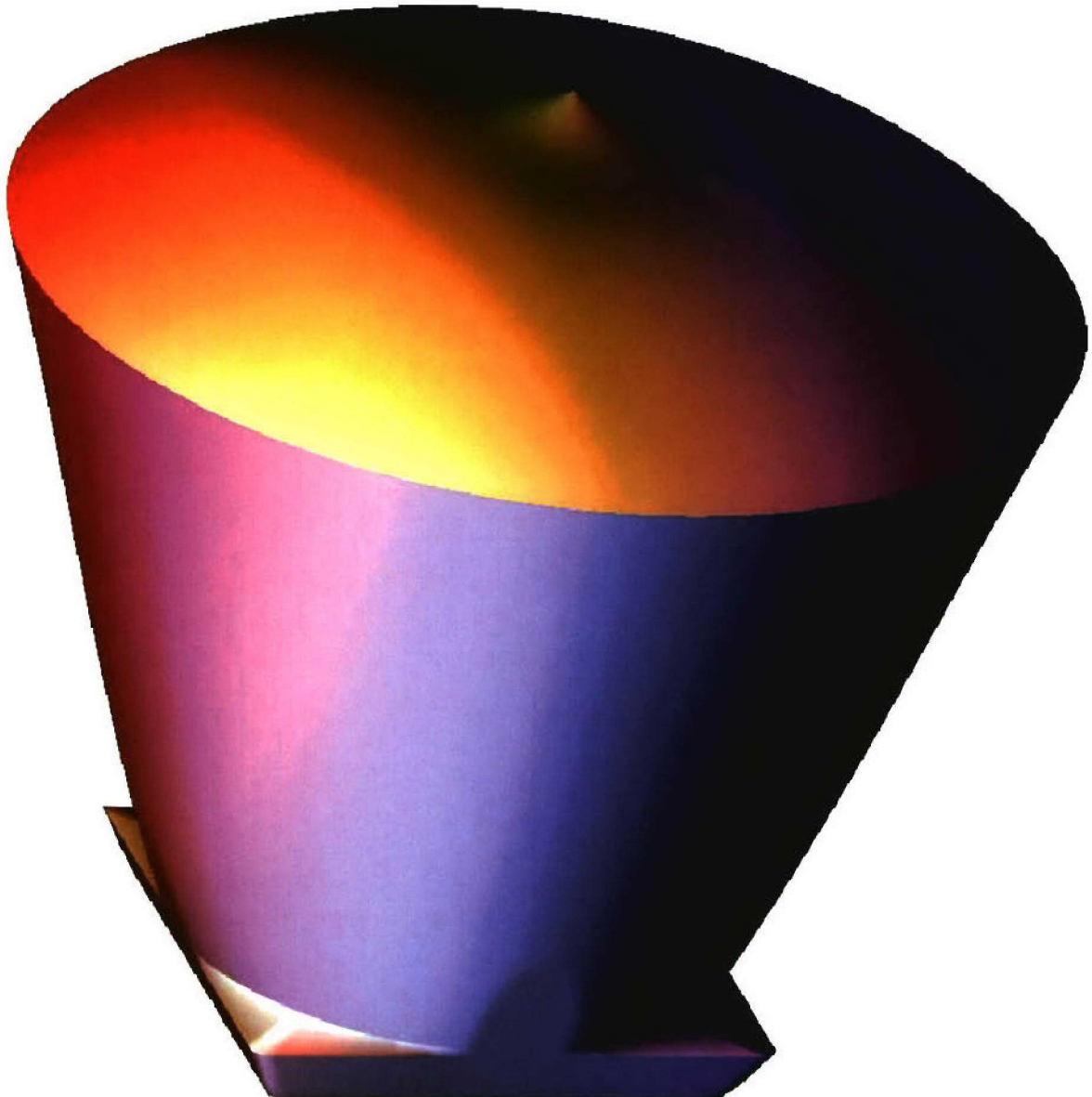
Optimized lens shape (x,y-plane)



## Three-dimensional representation of design R02



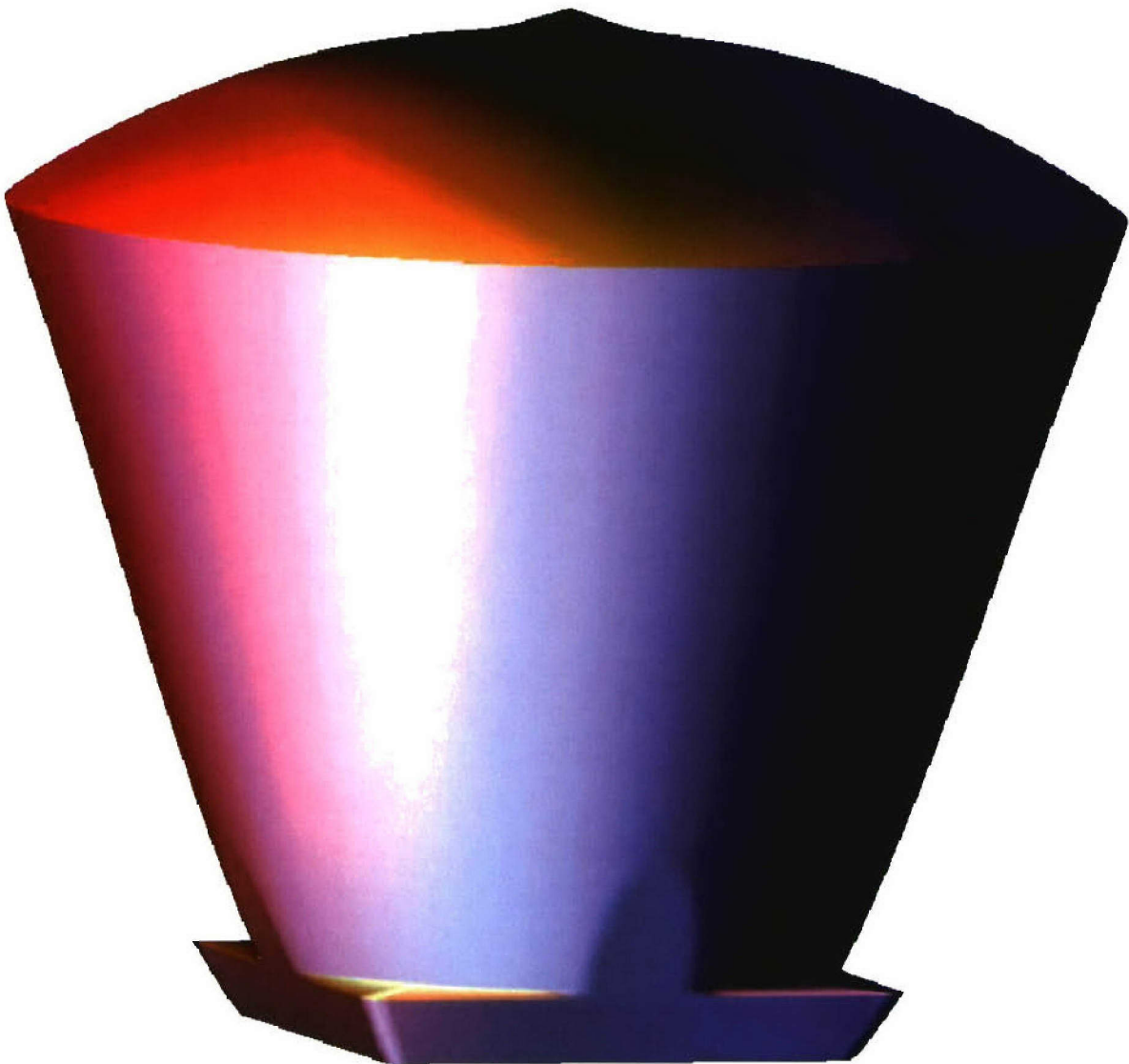
An Employee-Owned Company



## Three-dimensional representation of design R02 (different view)



*An Employee-Owned Company*



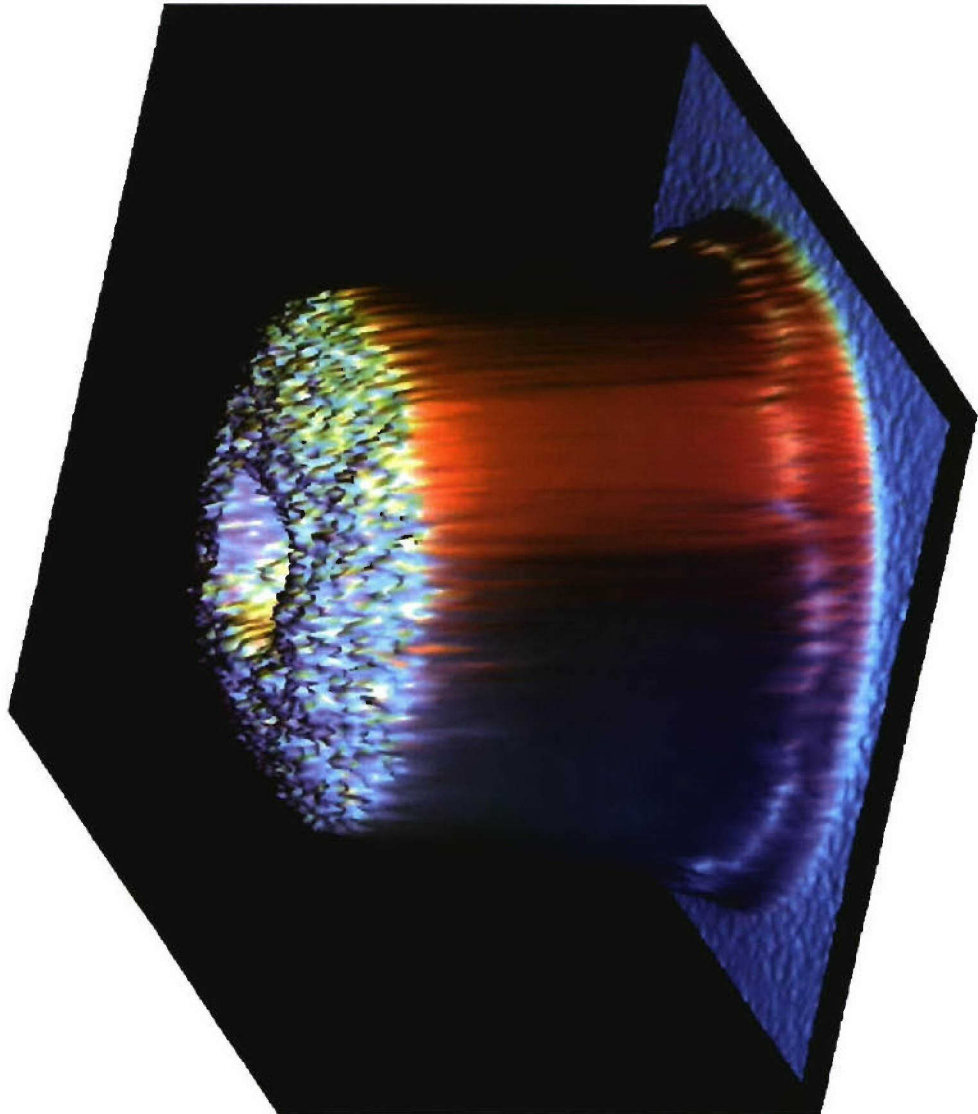
## Total source étendue versus available source étendue



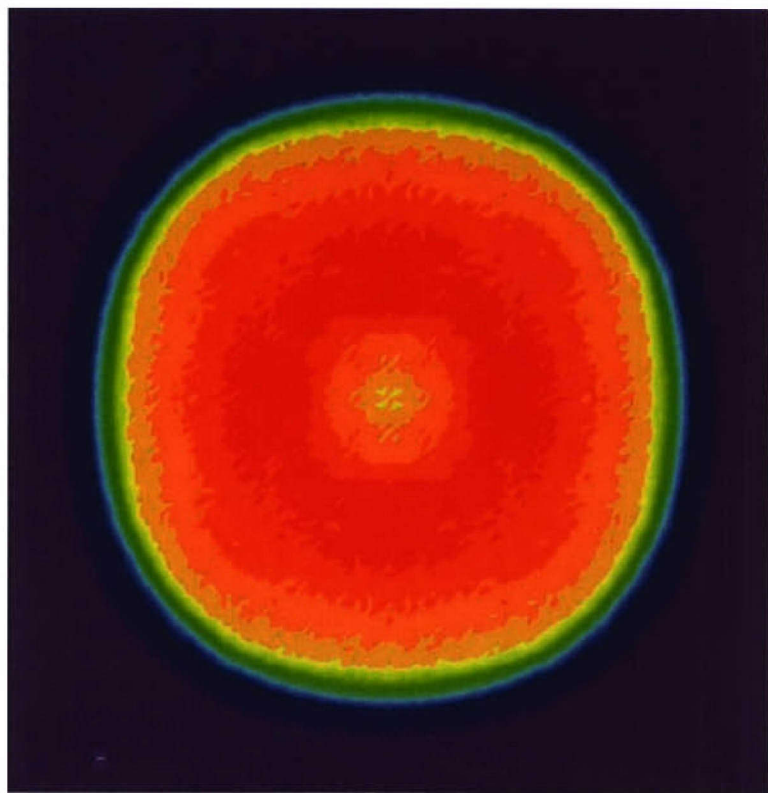
An Employee-Owned Company

- Surface area of source:  $1.65 \text{ mm}^2$ .
- Projected solid angle of source:  $3.1416 \text{ sr}$ .
- Refractive index in which source is immersed: 1.51.
- Total source étendue:  $11.82 \text{ mm}^2\text{-sr}$ .
- Due to source-clearance requirements, 7.78% of source flux is directly absorbed by substrate, without being collected by micro-optics. So only 92.22% of source étendue is actually available.
- Available source étendue:  $10.90 \text{ mm}^2\text{-sr}$ .

## Micro-optics design R02: intensity distribution



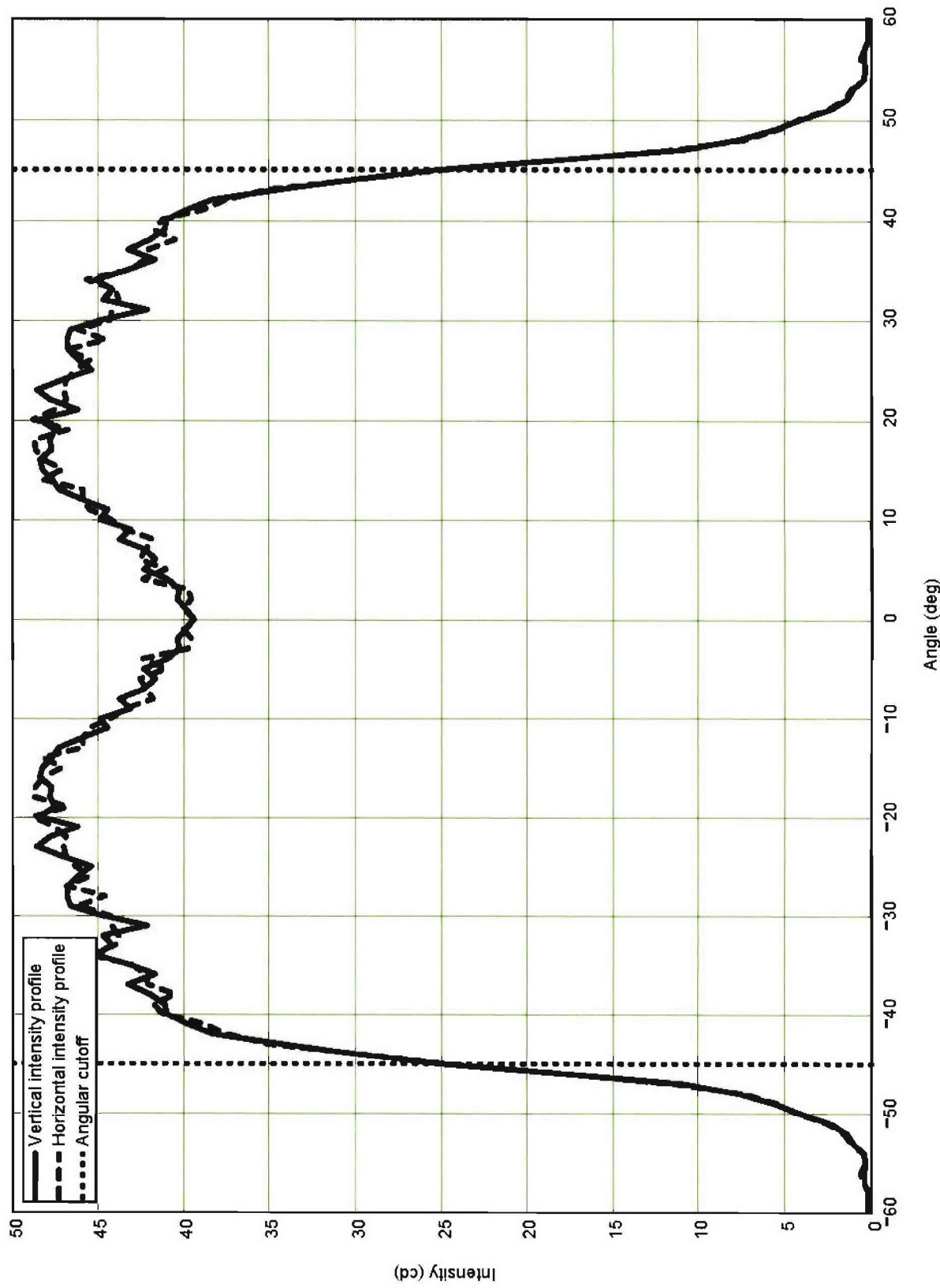
(surface plot)



(pseudo-color contour plot)

## Micro-optics design R02: intensity profiles

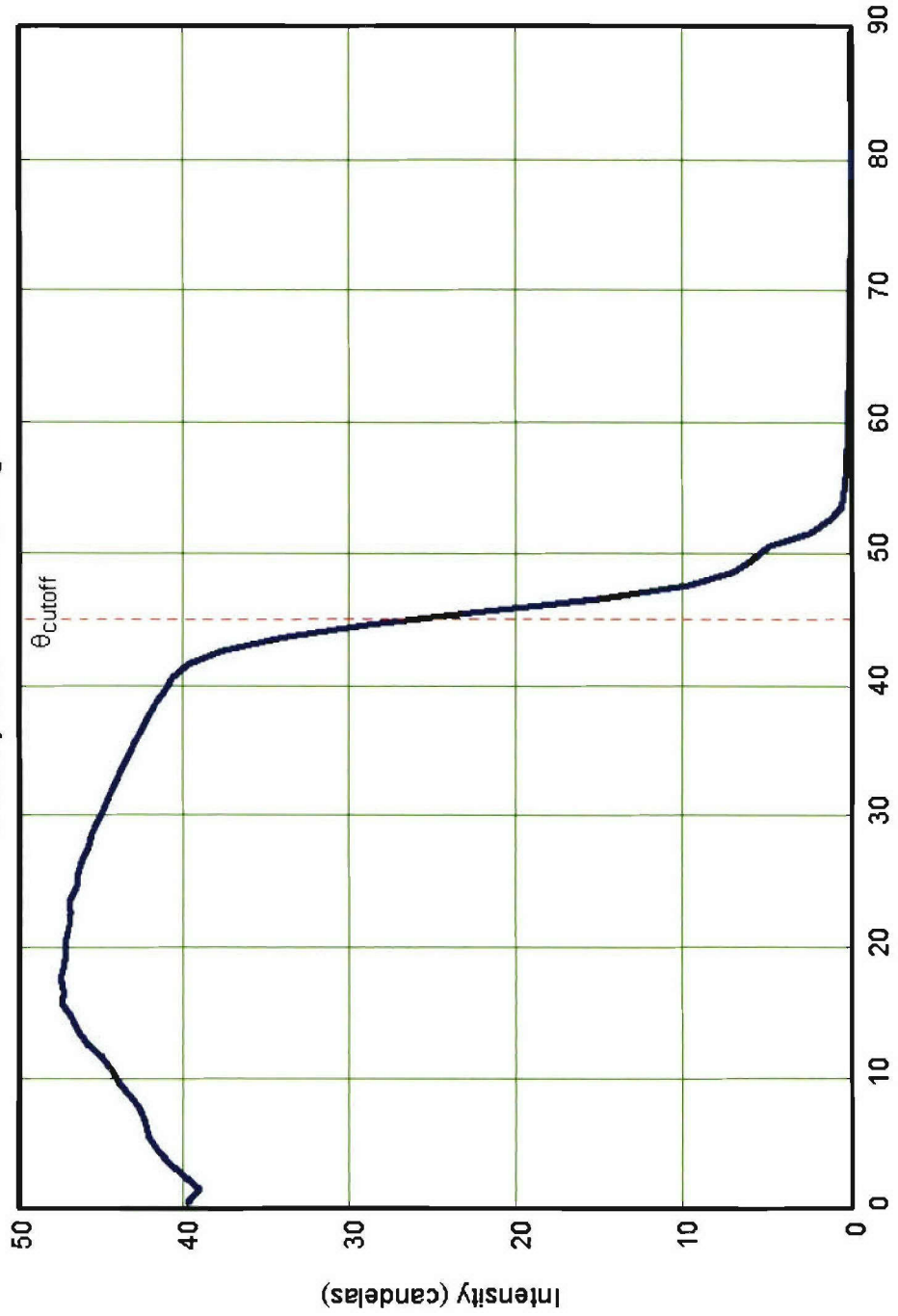
Case R02: Vertical and horizontal intensity profiles



## Micro-optics design R02: radial intensity distribution

Case = "R02"

Intensity as a function of angle

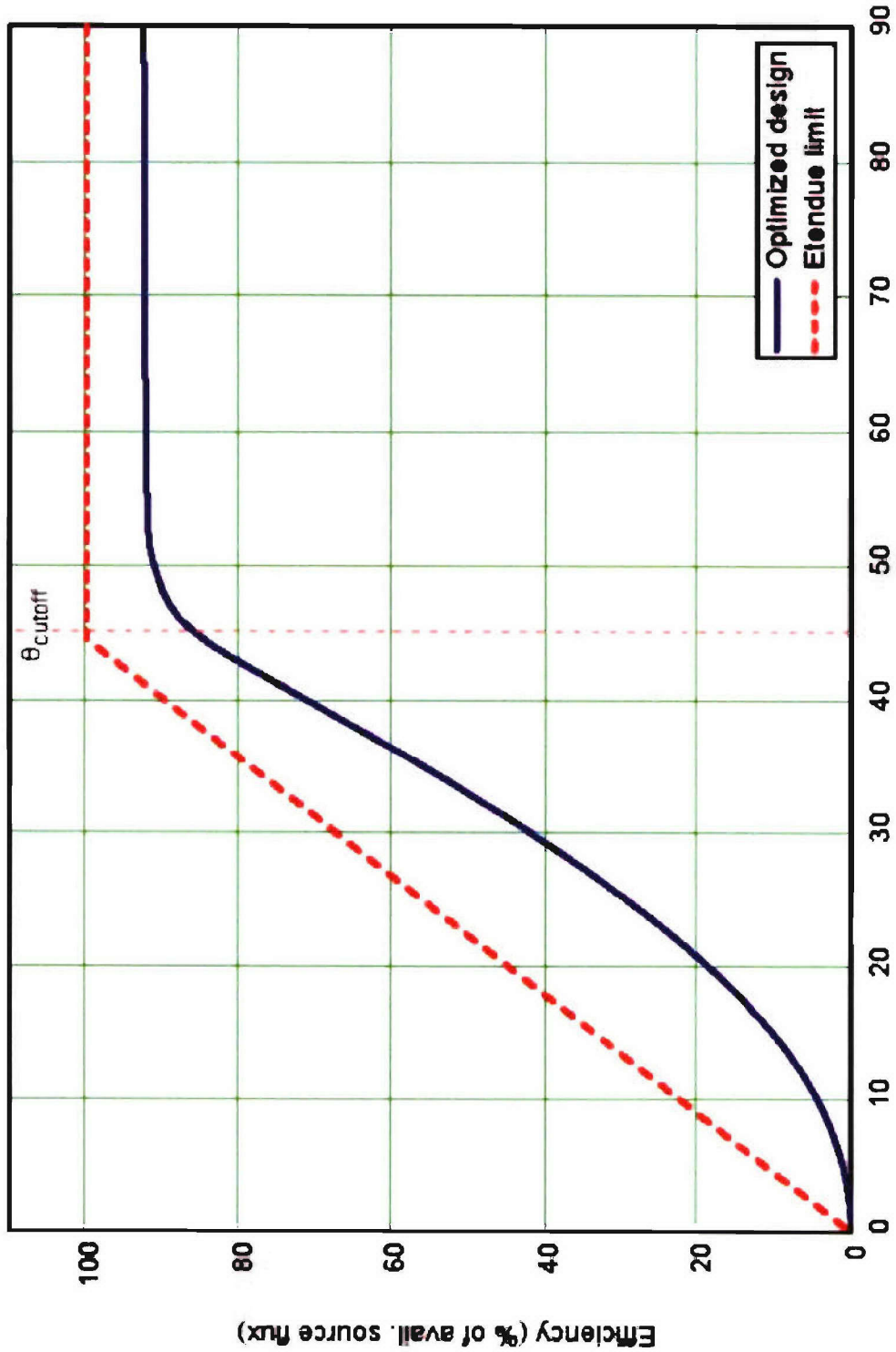


Angle off axis (degrees)

intensity output averaged over annular angular bins as a function of angle off axis)

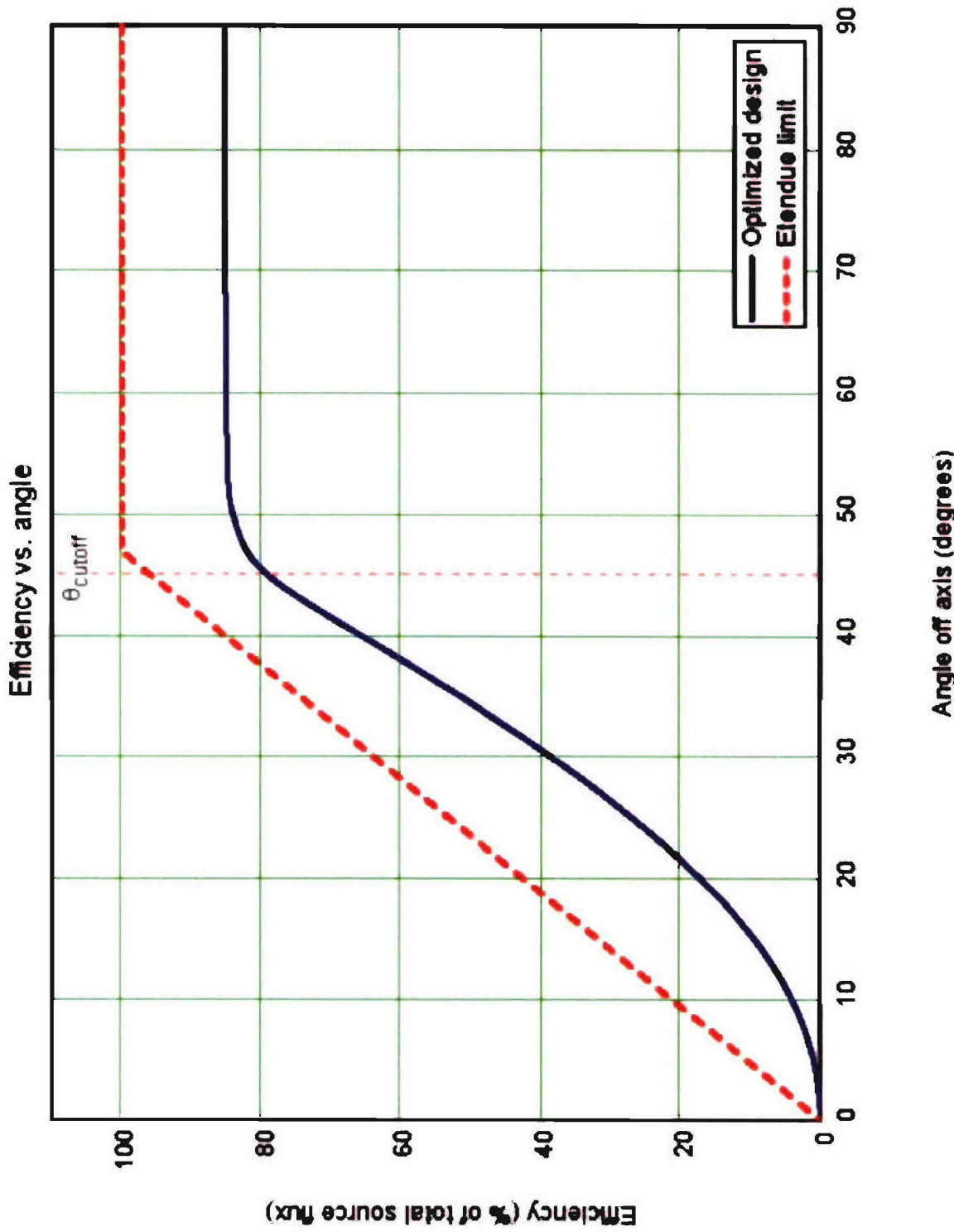
## Micro-optics design R02: renormalized efficiency versus angle

Efficiency vs. angle



(efficiency as a percentage of available source étendue)

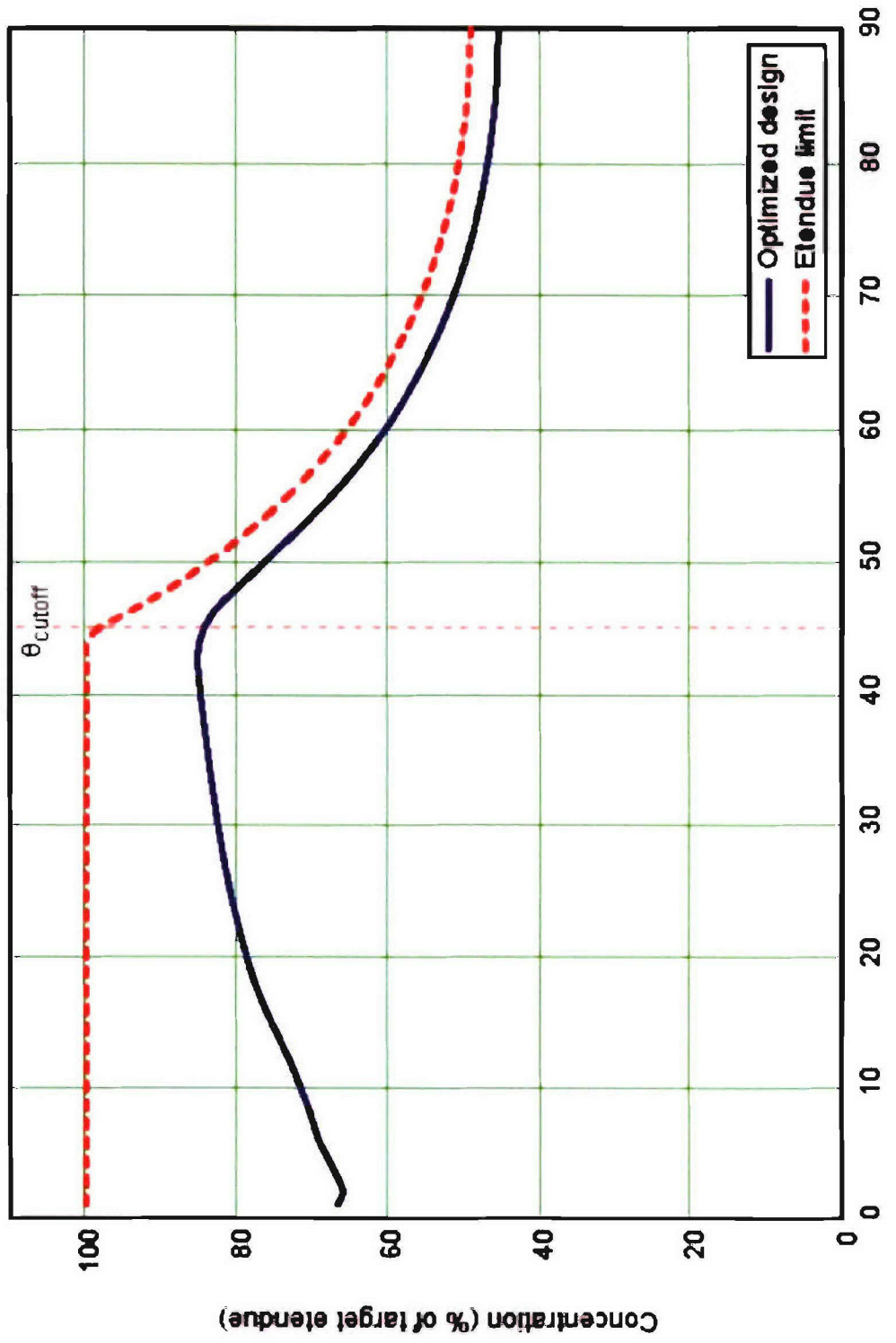
# Micro-optics design R02: total efficiency versus angle



(efficiency as a percentage of total source étendue)

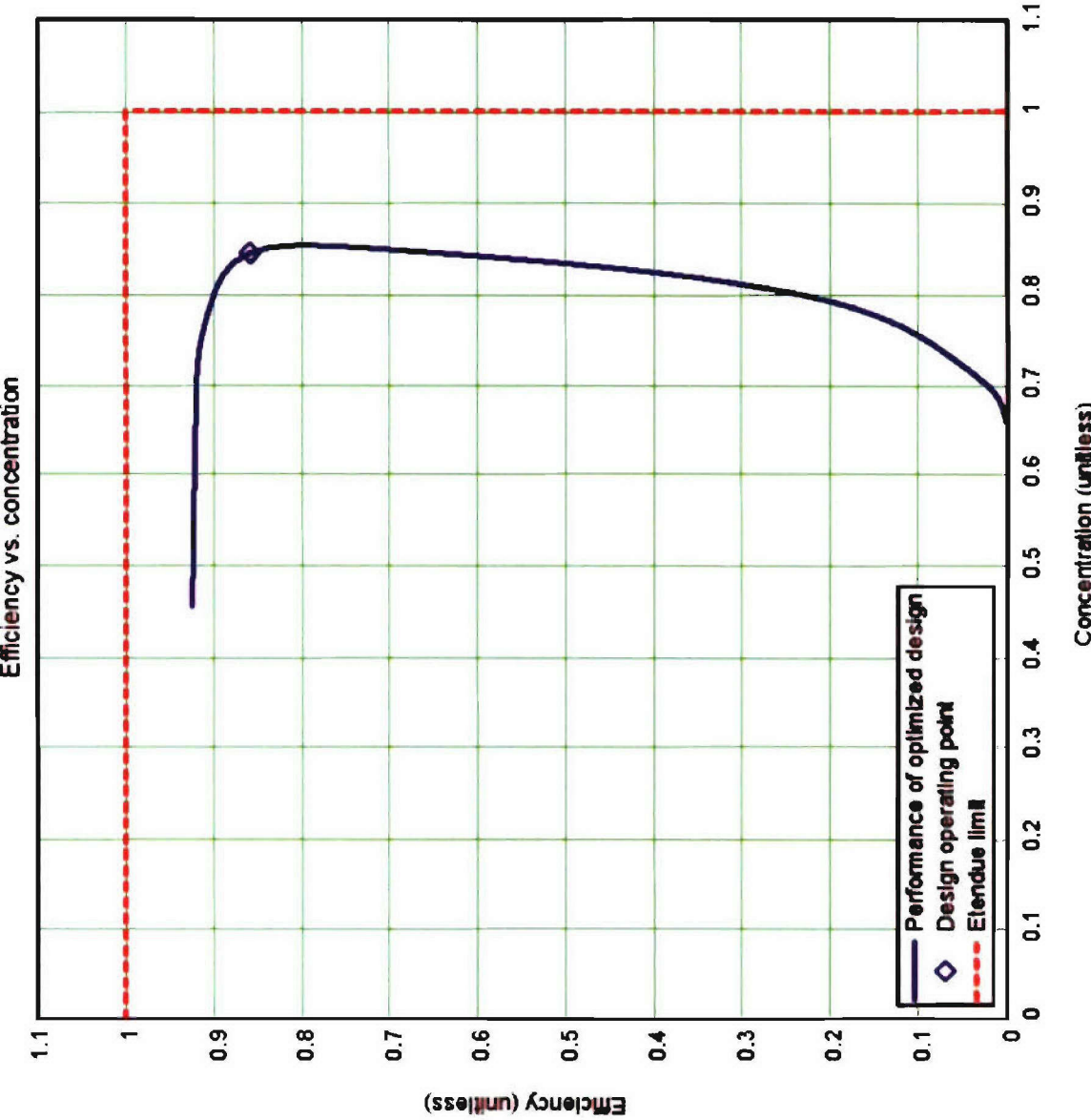
## Micro-optics design R02: concentration versus angle

Concentration vs. angle



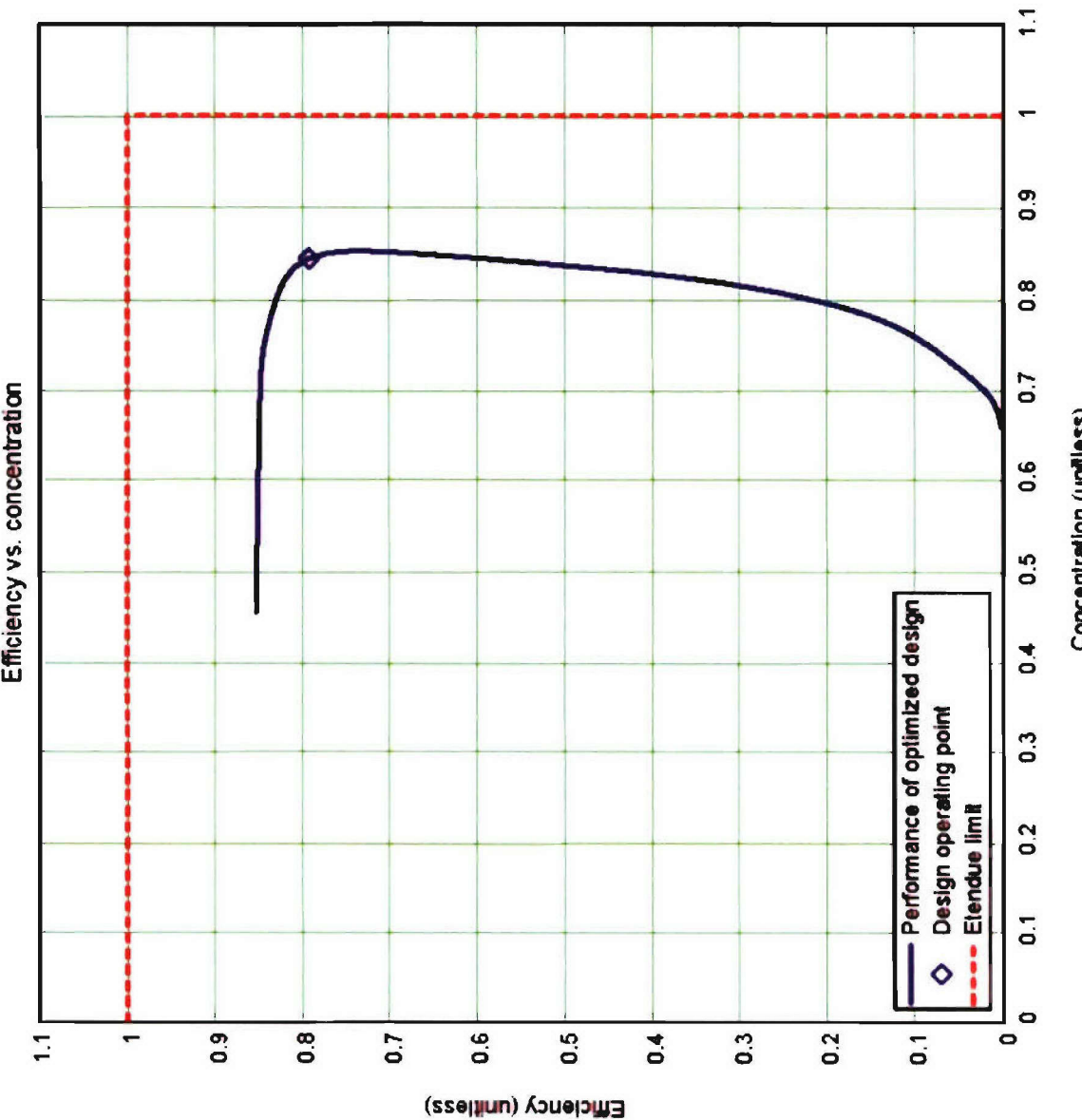
(étendue limit based on available source étendue)

# Micro-optics design R02: renorm. efficiency vs. concentration



(efficiency based on available source étendue)

## Micro-optics design R02: total efficiency versus concentration



(efficiency based on total source étendue)

**Non-axisymmetric micro-optics, with reflective coating  
and 0.0-mm source clearance**

## Optimized non-axisymmetric micro-optics, with reflective coating and 0.0-mm source clearance



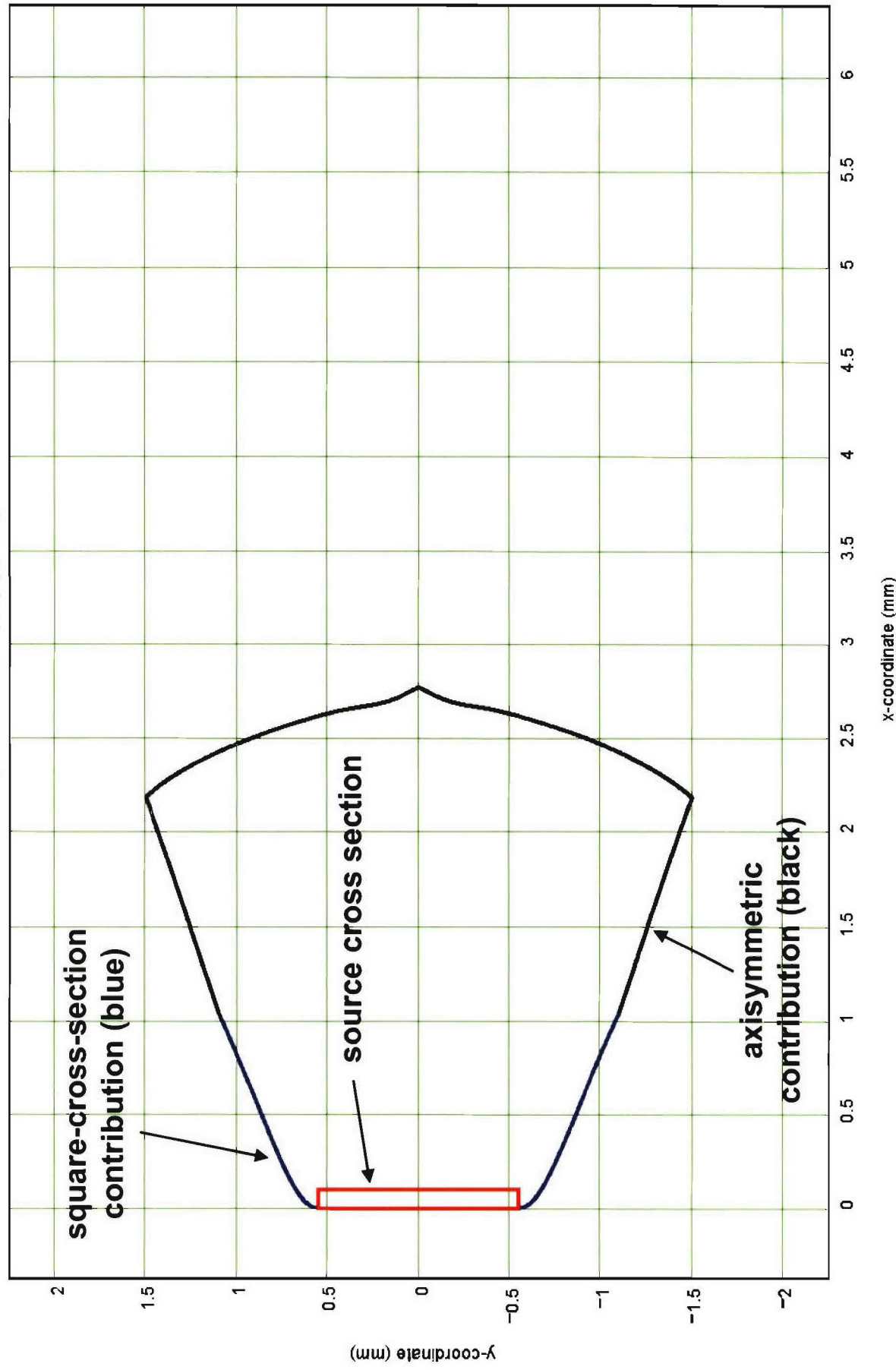
An Employee-Owned Company

- Design designation: M02.
- Shape of reflective section of micro-optics combines square-cross-section and axisymmetric contributions.
- Refractive surface is axisymmetric
- Optical surface is allowed to contact LED light source.
- Maximum diameter of micro-optics: 3.0 mm.
- Refractive index: 1.51.
- Optimized for reflective surface having 95% reflectance.
- Optimized for refractive surface having 100% transmittance.
- Length: 2.77 mm.
- Performance plots assume 100% reflectance for reflective surface and 100% transmittance for refractive surface.

# Cross section of design M02

Case = "M02"

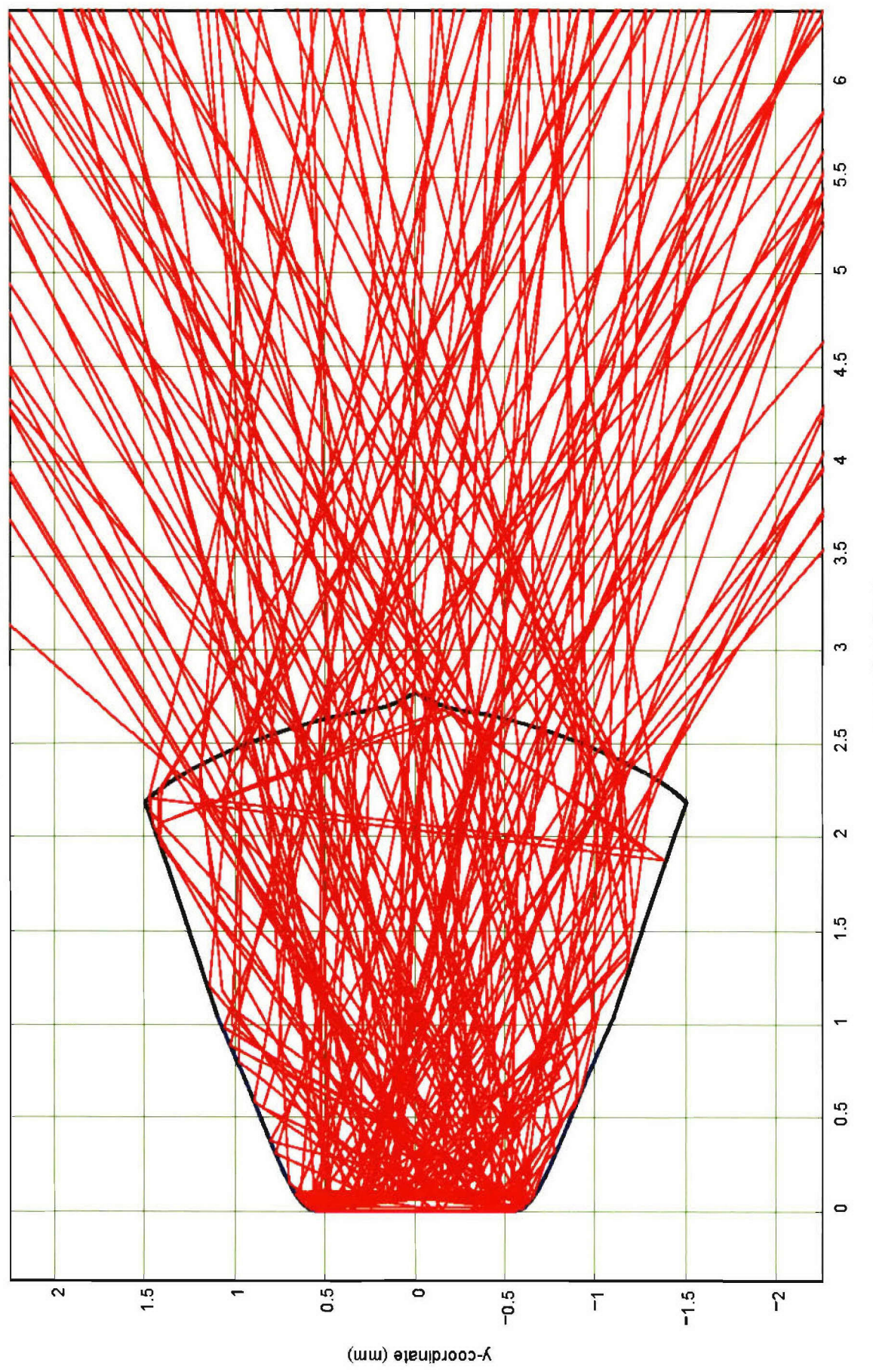
Optimized lens shape (x,y-plane)



## Cross section of design M02, with traced rays

Case = "M02"

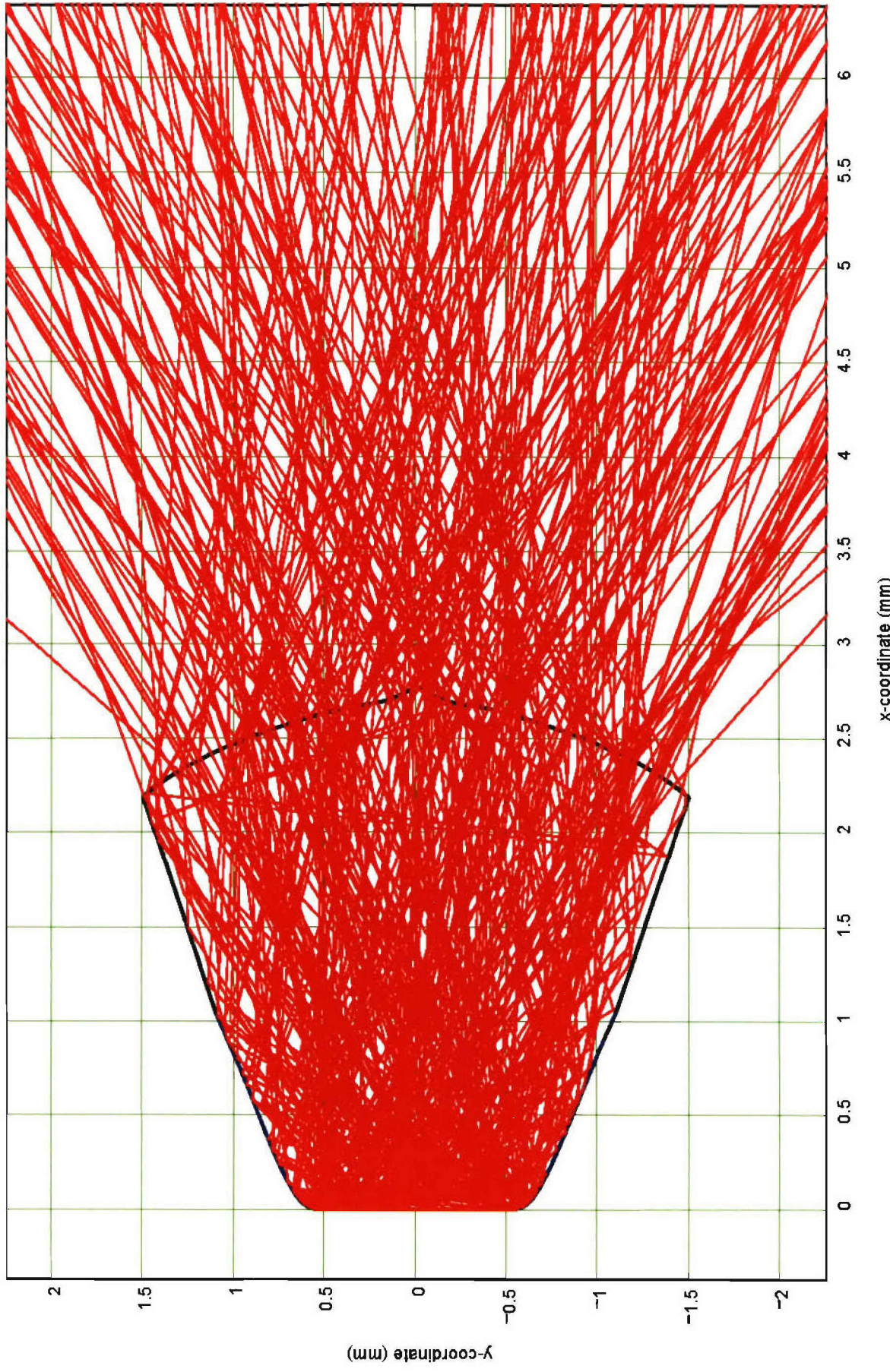
Optimized lens shape (x,y-plane)



## Cross section of design M02, with larger number of traced rays

Case = "M02"

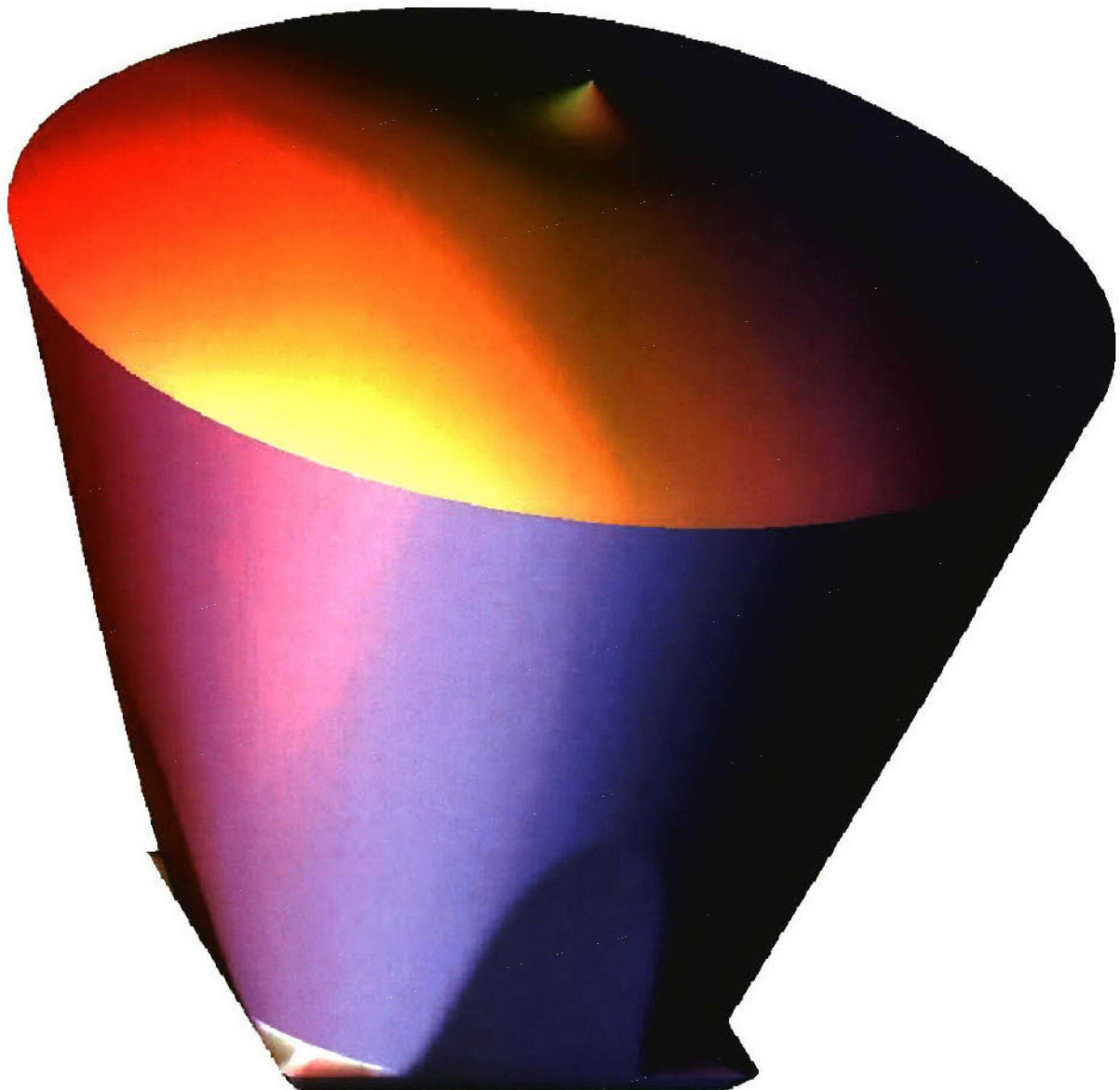
Optimized lens shape (x,y-plane)



## Three-dimensional representation of design M02



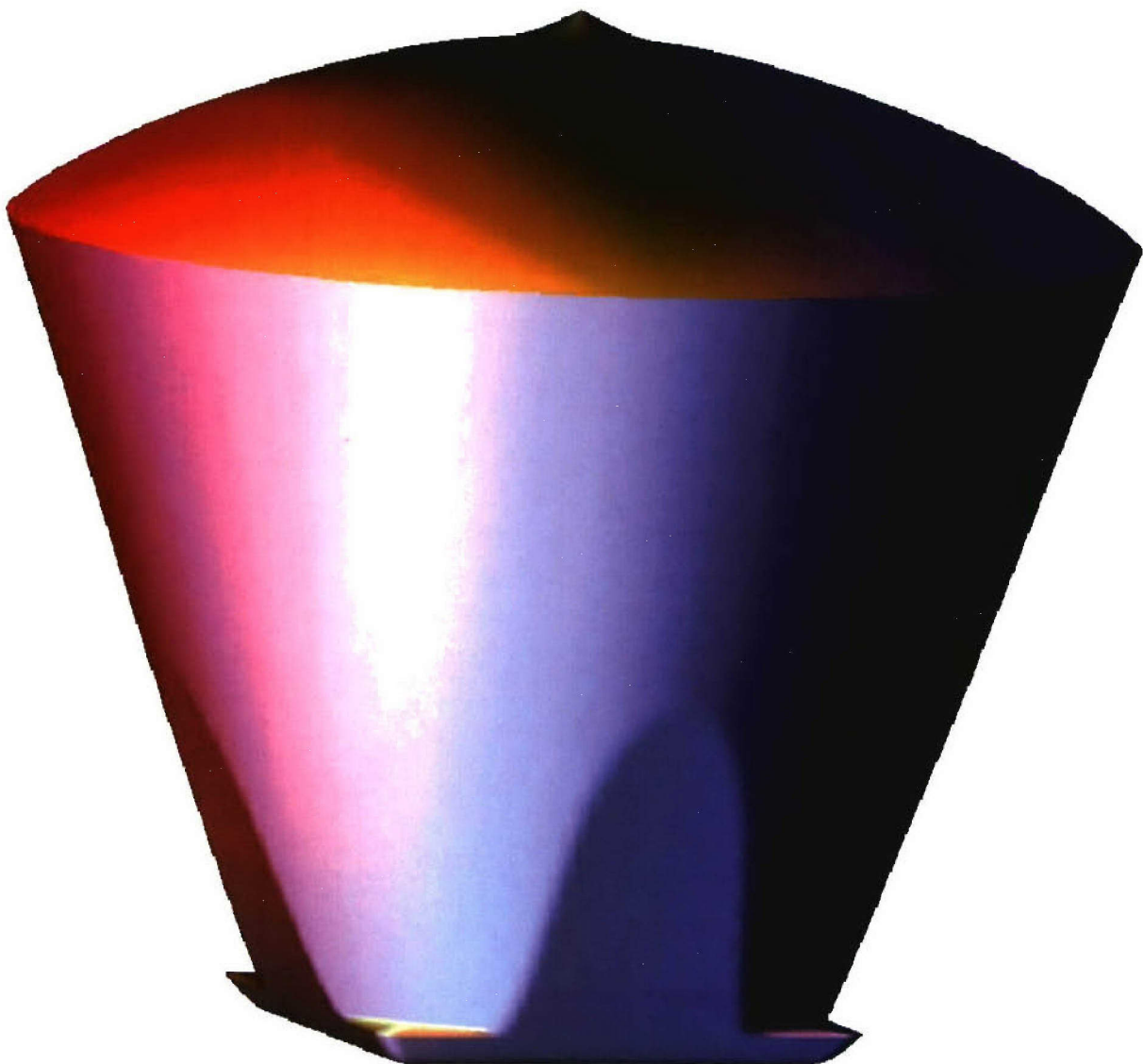
An Employee-Owned Company



## Three-dimensional representation of design M02 (different view)



An Employee-Owned Company



## Total source étendue versus available source étendue

- Surface area of source:  $1.65 \text{ mm}^2$ .
- Projected solid angle of source:  $3.1416 \text{ sr}$ .
- Refractive index in which source is immersed:  $1.51$ .

• Total source étendue:  $11.82 \text{ mm}^2\text{-sr}$ .

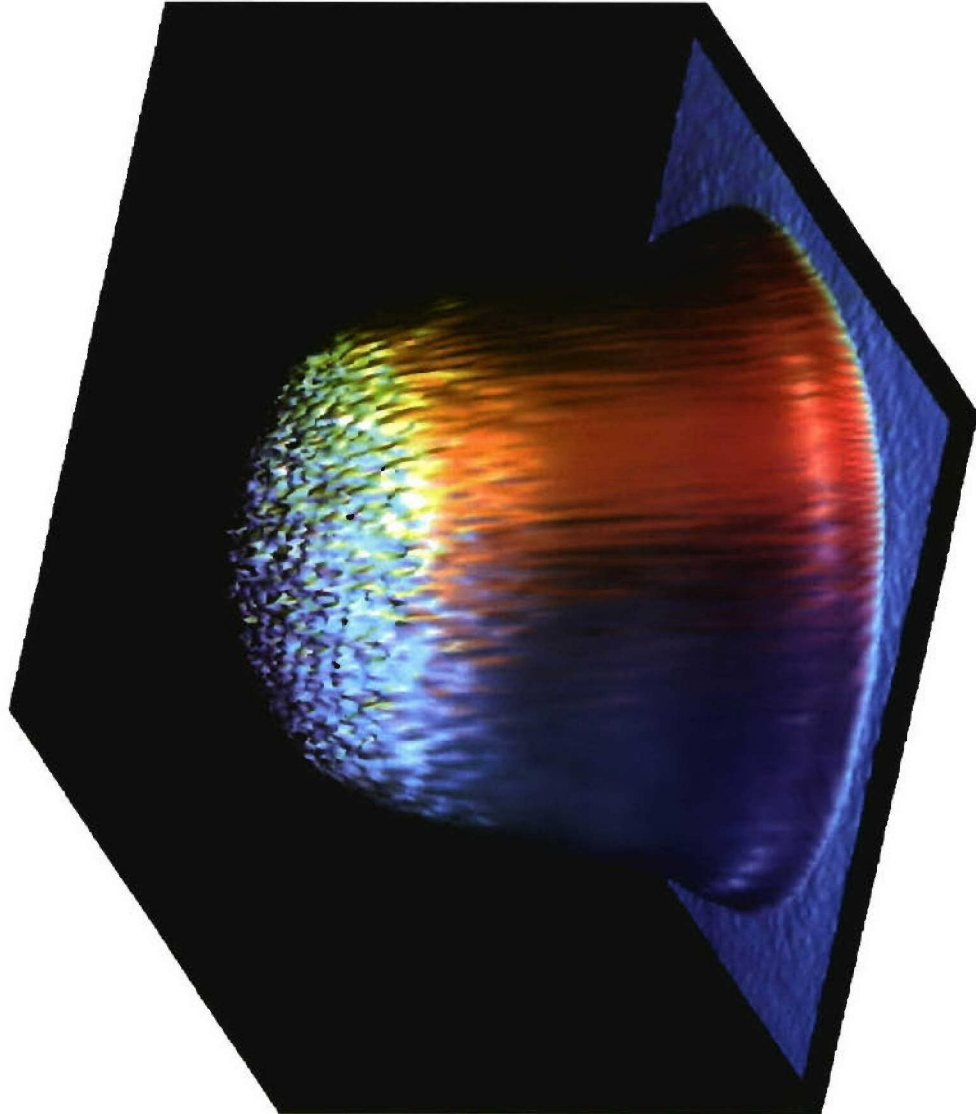
- Since there are no source-clearance requirements in this case, 100% of source étendue is actually available.

• Available source étendue:  $11.82 \text{ mm}^2\text{-sr}$ .

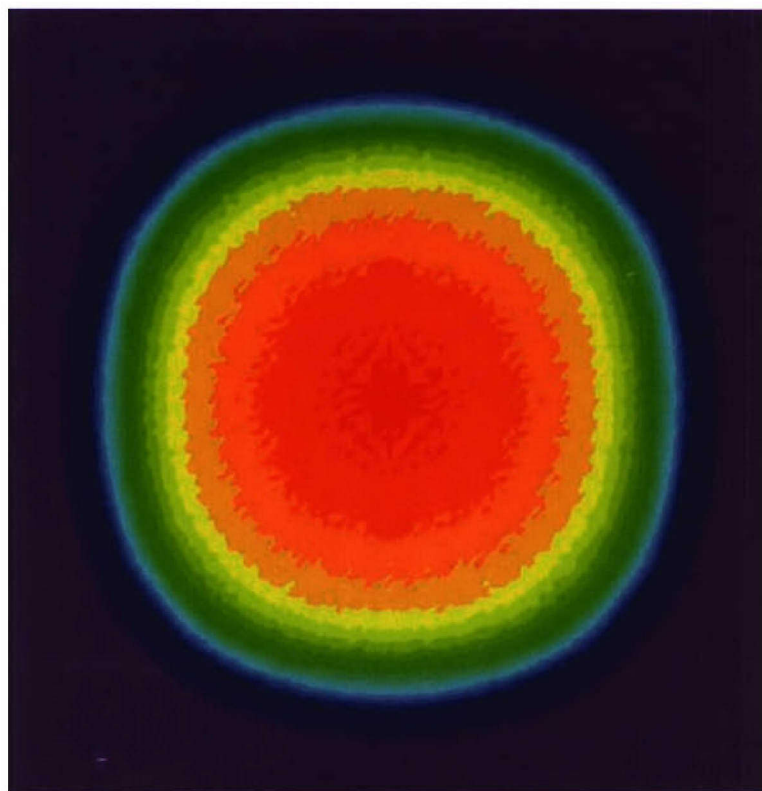
## Micro-optics design M02: intensity distribution



An Employee-Owned Company



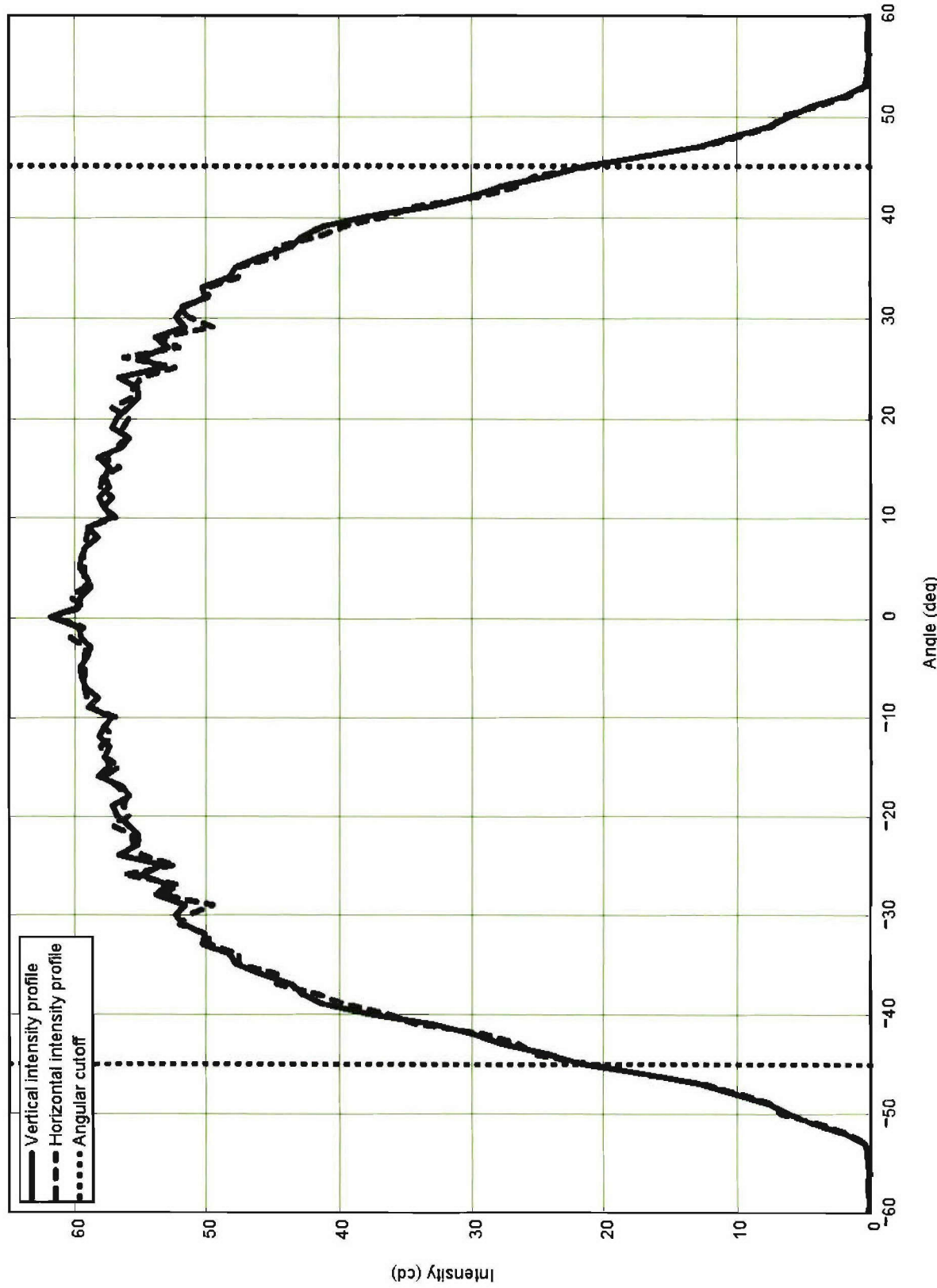
(surface plot)



(pseudo-color contour plot)

## Micro-optics design M02: intensity profiles

Case M02: Vertical and horizontal intensity profiles



# Micro-optics design M02: radial intensity distribution

Case = "M02"

Intensity as a function of angle

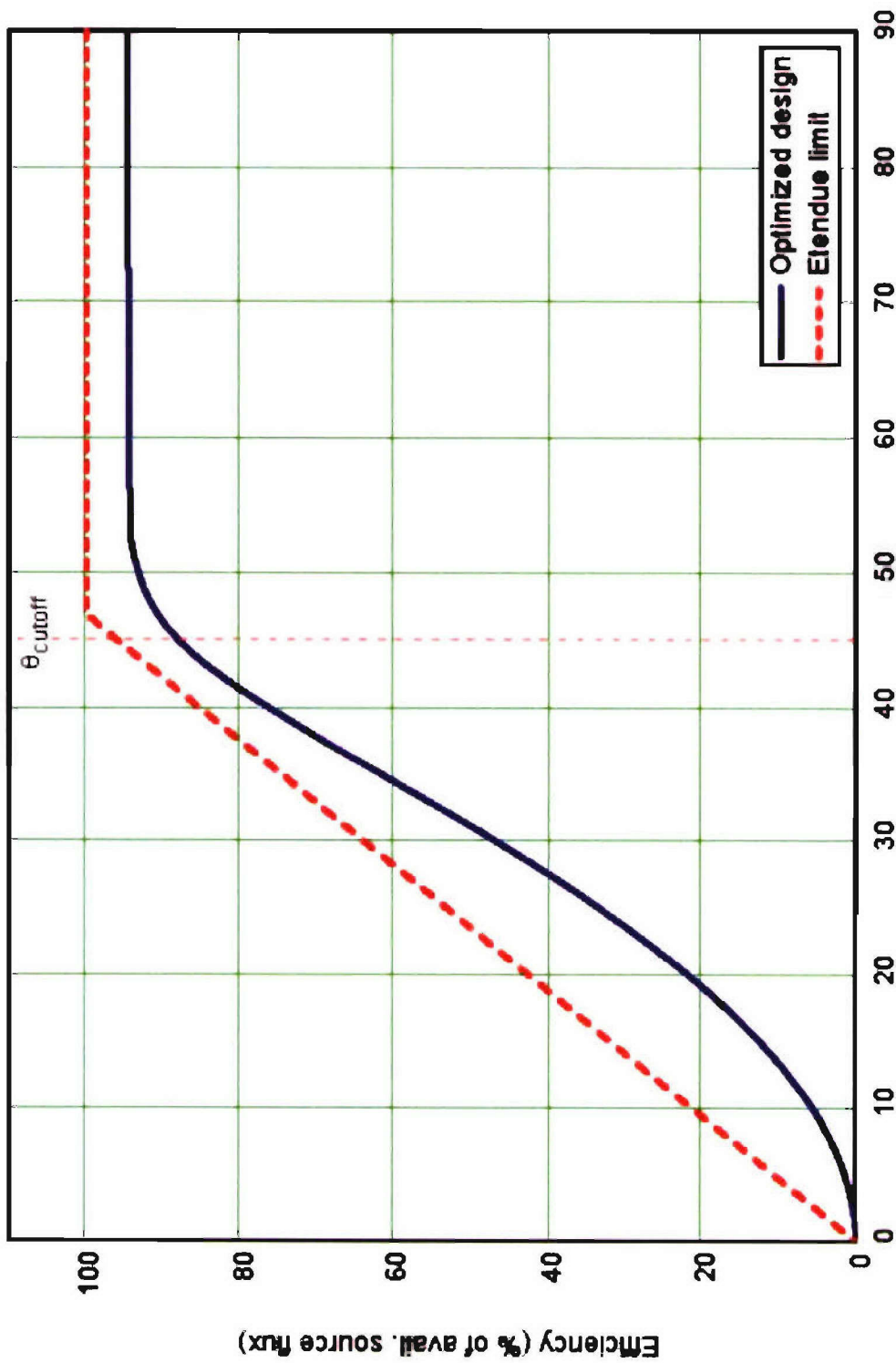


Angle off axis (degrees)

intensity output averaged over annular angular bins as a function of angle off axis)

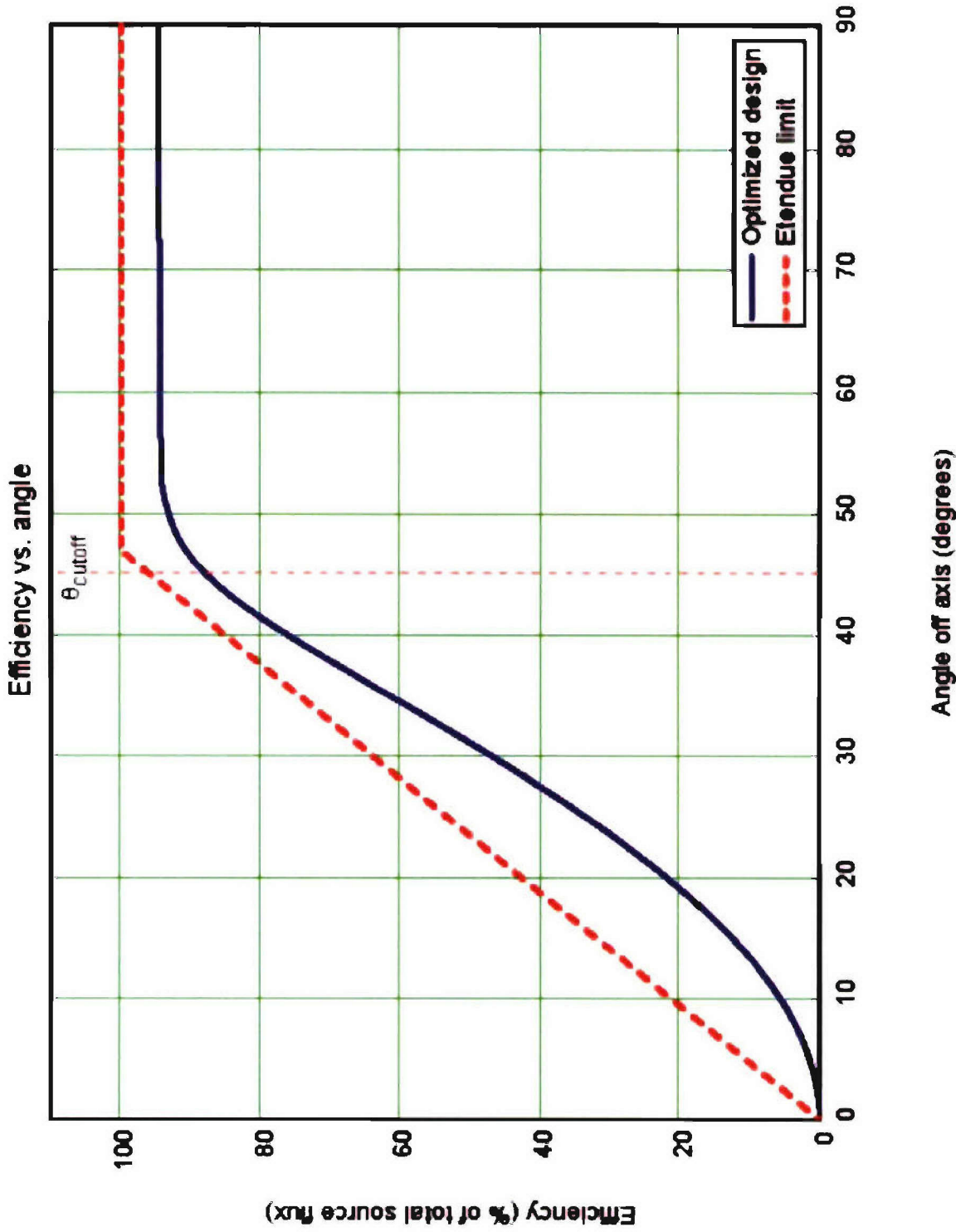
## Micro-optics design M02: renormalized efficiency versus angle

Efficiency vs. angle



(efficiency as a percentage of available source étendue)

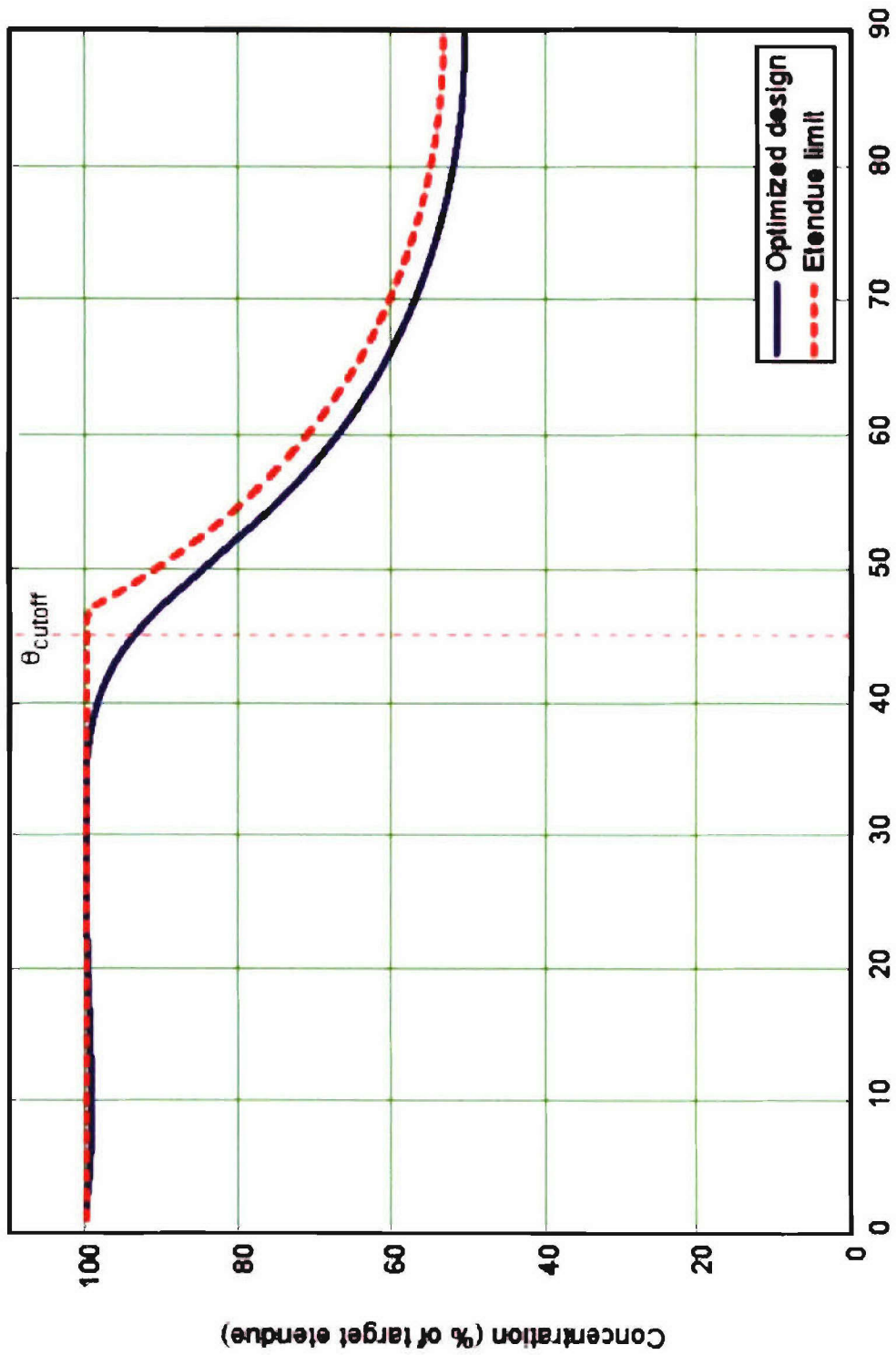
## Micro-optics design M02: total efficiency versus angle



(efficiency as a percentage of total source étendue)

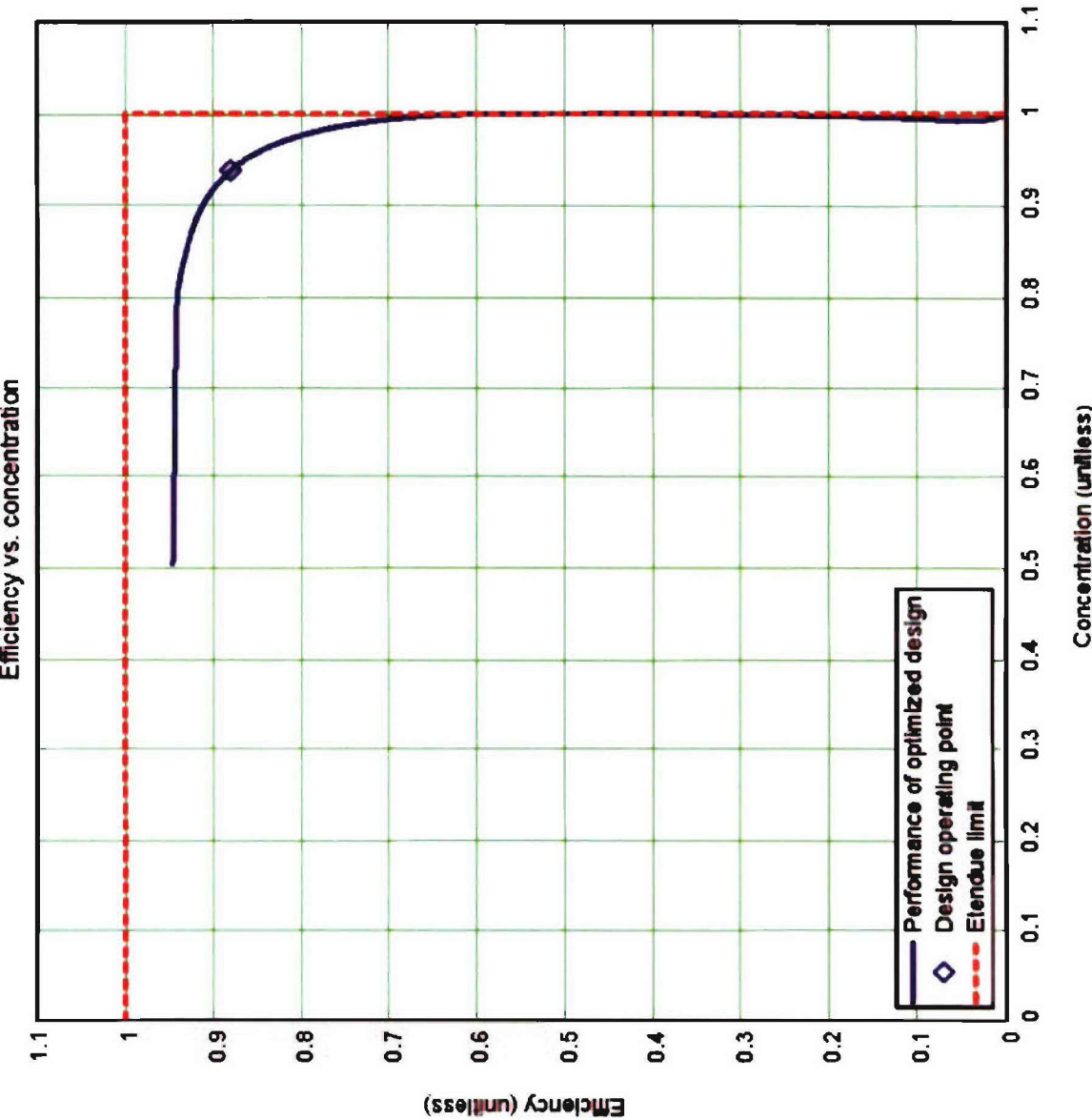
## Micro-optics design M02: concentration versus angle

Concentration vs. angle



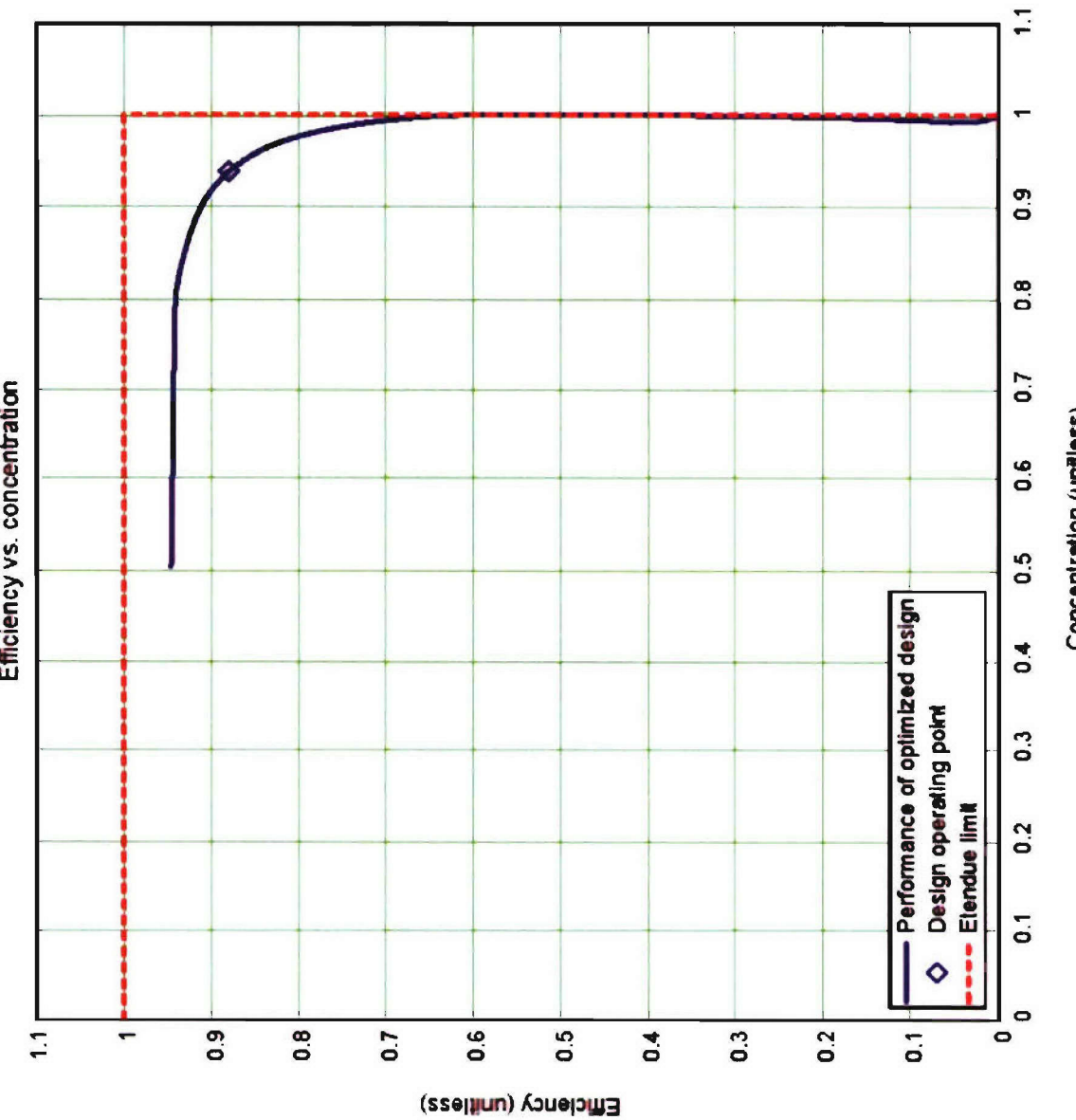
(étendue limit based on available source étendue)

## Micro-optics design M02: renorm. efficiency vs. concentration



(efficiency based on available source étendue)

## Micro-optics design M02: total efficiency versus concentration



(efficiency based on total source étendue)

# Summary of results

- Axisymmetric designs (C01 and G01) use refractive index of 1.50.
- Index was changed to 1.51 for non-axisymmetric designs (M02, R02, and H03).
- For higher index, source étendue is 1.3% higher than for axisymmetric designs.
- Due to source étendue difference, efficiency results for axisymmetric designs are not directly comparable to non-axisymmetric designs.
- Can compensate by reducing acceptance half angle for axisymmetric designs to provide same source-to-target étendue ratio as for non-axisymmetric designs.
- Required compensated acceptance half angle for axisymmetric cases:  $44.6^\circ$ .

Case	Source Clearance (mm)	Non-axisymmetric metric	Efficiency (%), relative to total étendue			Efficiency (%), relative to available étendue		
			Uncoated	95% reflectance	100% reflectance	Uncoated	95% reflectance	100% reflectance
M02	0.0	Yes	N.A.	84.2	88.1	N.A.	84.2	88.1
R02	0.1	Yes	N.A.	76.2	79.3	N.A.	82.6	86.0
H03	0.2	Yes	N.A.	68.0	70.5	N.A.	75.7	78.5
C01	0.2	No	N.A.	67.8	70.8	N.A.	76.5	79.9
G01	0.2	No	61.9	N.A.	N.A.	69.8	N.A.	N.A.

# Lengths of micro-optics designs

Case	Source Clearance (mm)	Non-axisymmetric	Length (mm)
M02	0.0	Yes	2.77
R02	0.1	Yes	2.79
H03	0.2	Yes	2.66
C01	0.2	No	4.99
G01	0.2	No	6.06

## Aspect ratios (length to diameter) of micro-optics designs

Case	Source Clearance (mm)	Non-axisymmetric	Aspect Ratio (unitless)
M02	0.0	Yes	0.92
R02	0.1	Yes	0.93
H03	0.2	Yes	0.89
C01	0.2	No	1.66
G01	0.2	No	2.02

## Conclusions

---

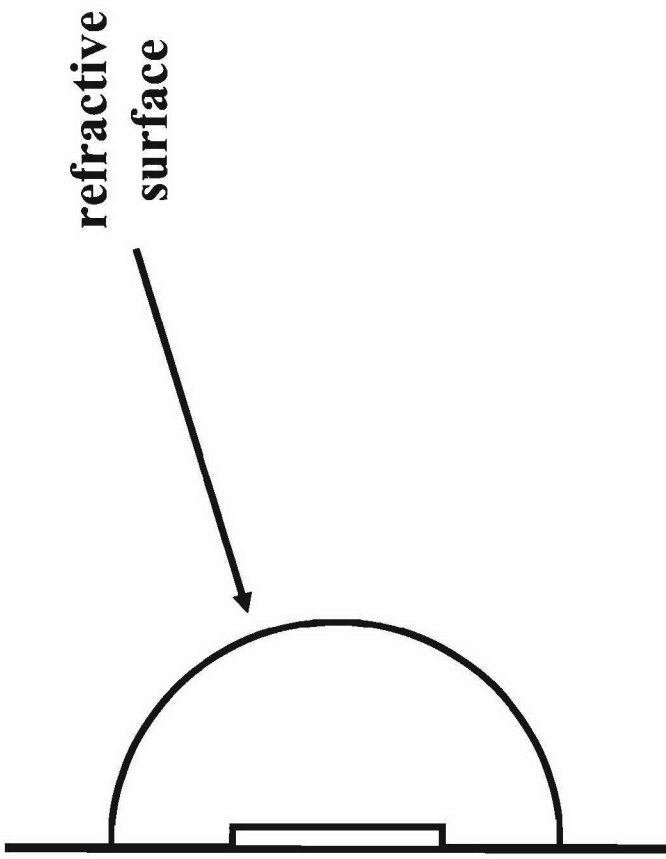


- Existing LEDs incorporate encapsulant dome shapes that are not optimized for light extraction and disperse flux over  $2\pi$  steradians. It is generally difficult to design illumination optics to work with such large collection angles.
- In addition to improving the collection efficiency, pre-compressing the LED output with a special micro-optic element could potentially improve flux-transfer efficiency of the downstream optics, as well as greatly simplify their design and consequently reduce development and manufacturing costs.
- We have demonstrated high efficiency axisymmetric and non-axisymmetric micro-optics designs. Sharp angular beam cutoffs have also been achieved.
- The non-axisymmetric design (H03) with a 0.2-mm source clearance provides comparable performance to the axisymmetric design (C01), but with only half the length.
- Source clearance distances below 0.2 mm can provide significantly improved flux-transfer efficiencies.
- Using symmetry breaking and global optimization we have demonstrated that micro-optics lens designs can achieve a highly efficient pre-compression of the light output of an LED with a geometry that is no more intrusive than a conventional encapsulant dome.

## Appendix: Results with encapsulant dome

## Optical performance of encapsulant dome

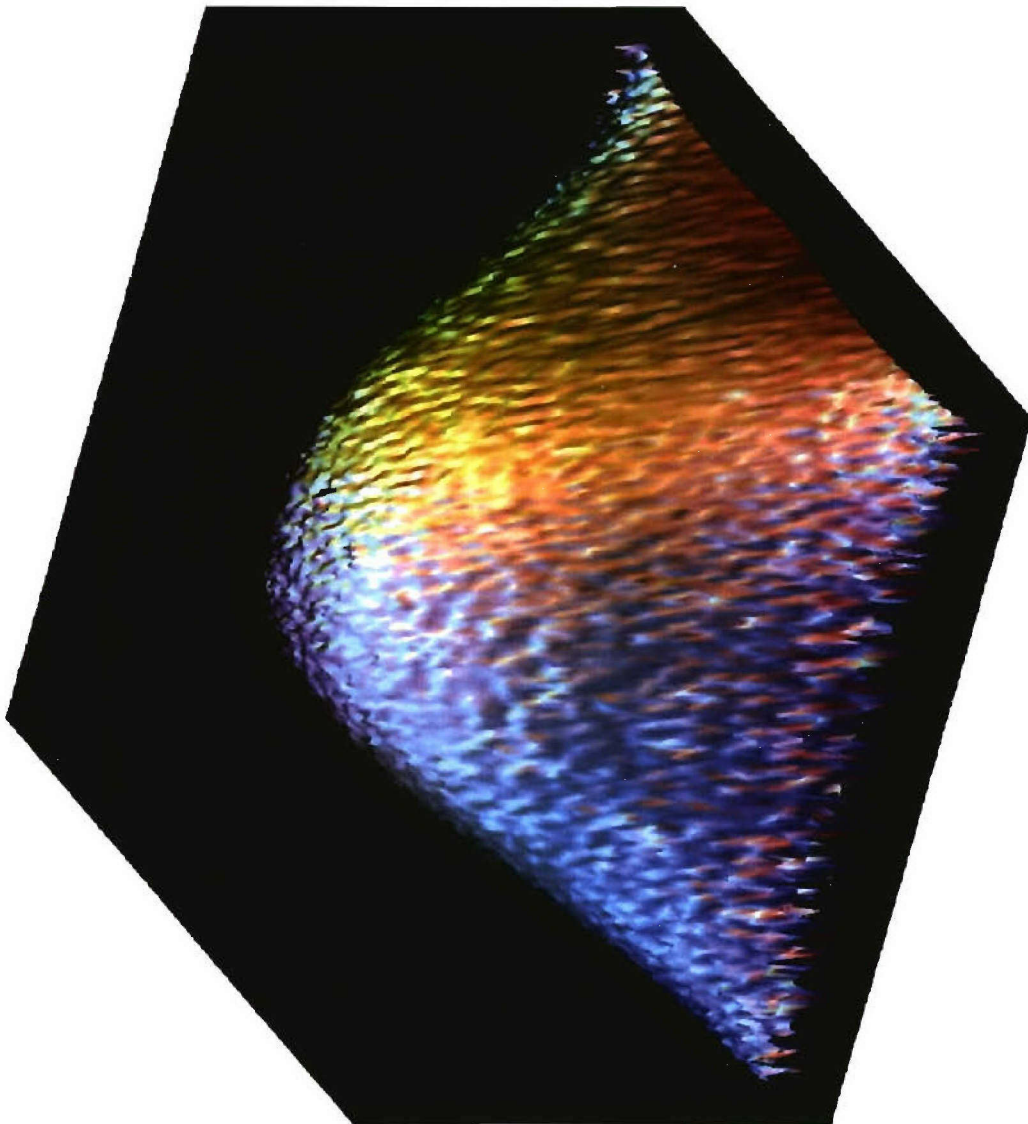
- Design designation: DM0.
- Dome shape: hemispherical, centered on optical axis in substrate plane.
- Dome diameter: 5.6 mm.
- Refractive index: 1.5.
- Assumed transmittance of refractive surface: 100%.
- Assumed target for étendue-limit calculations: 5.6-mm diameter circular aperture.



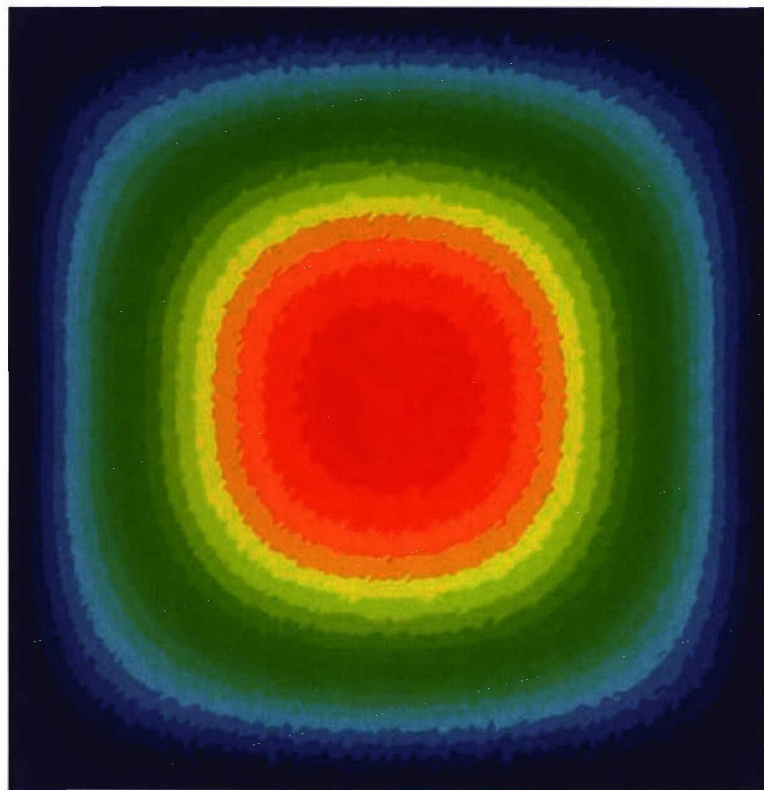
## Encapsulant dome DM0: intensity distribution



An Employee-Owned Company



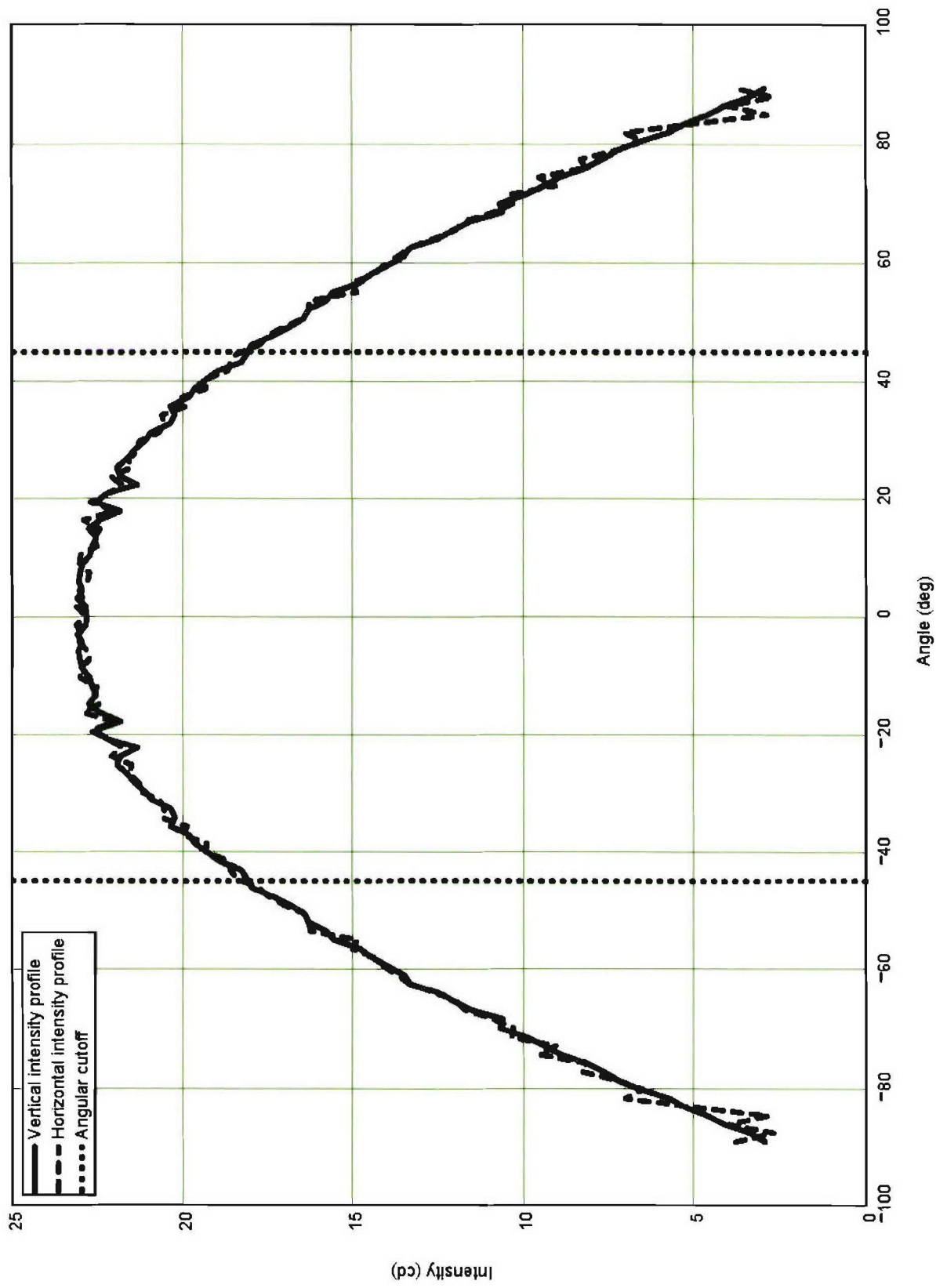
(surface plot)



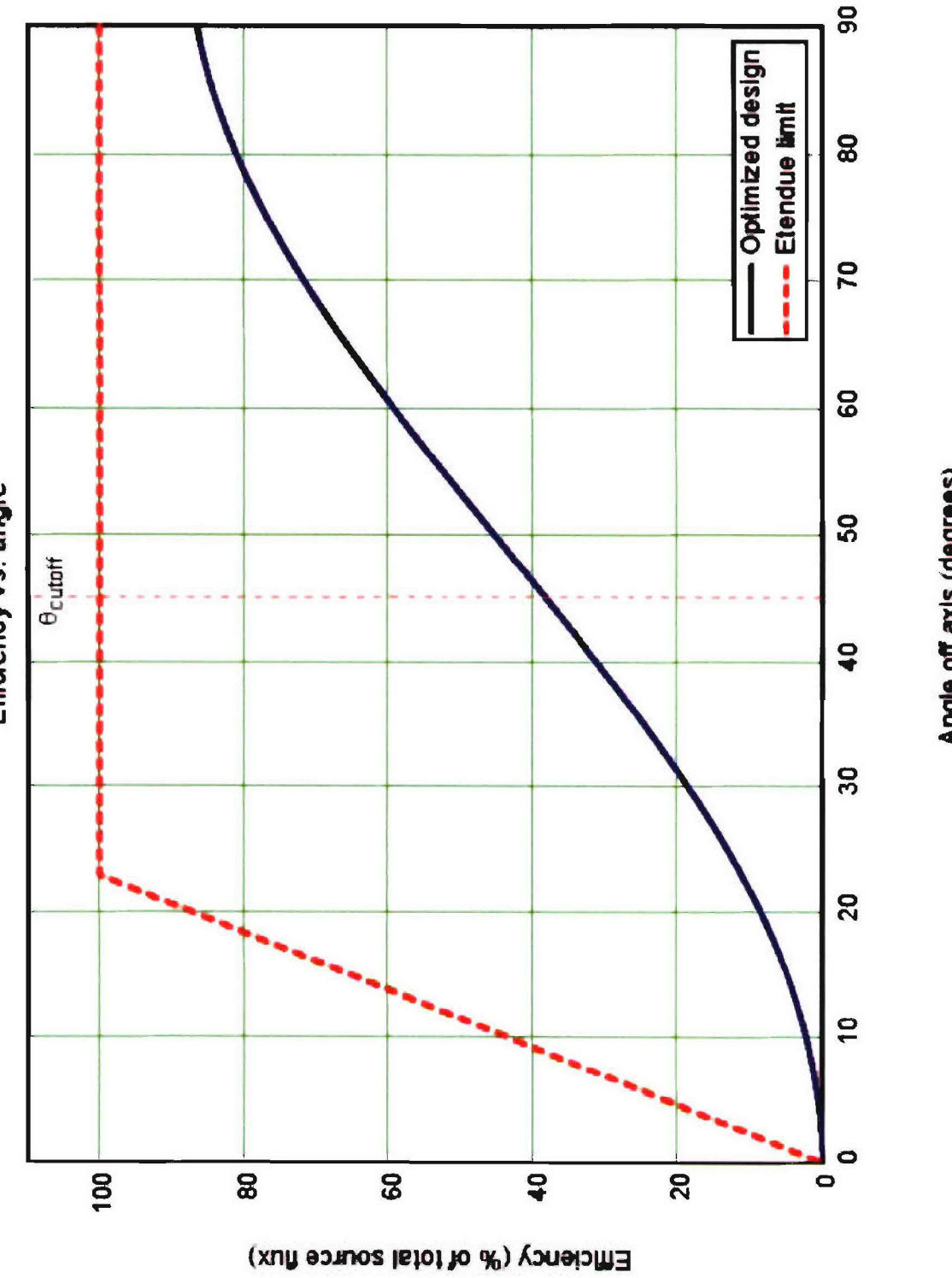
(pseudo-color contour plot)

## Encapsulant dome DM0: intensity profiles

Case DM0: Vertical and horizontal intensity profiles



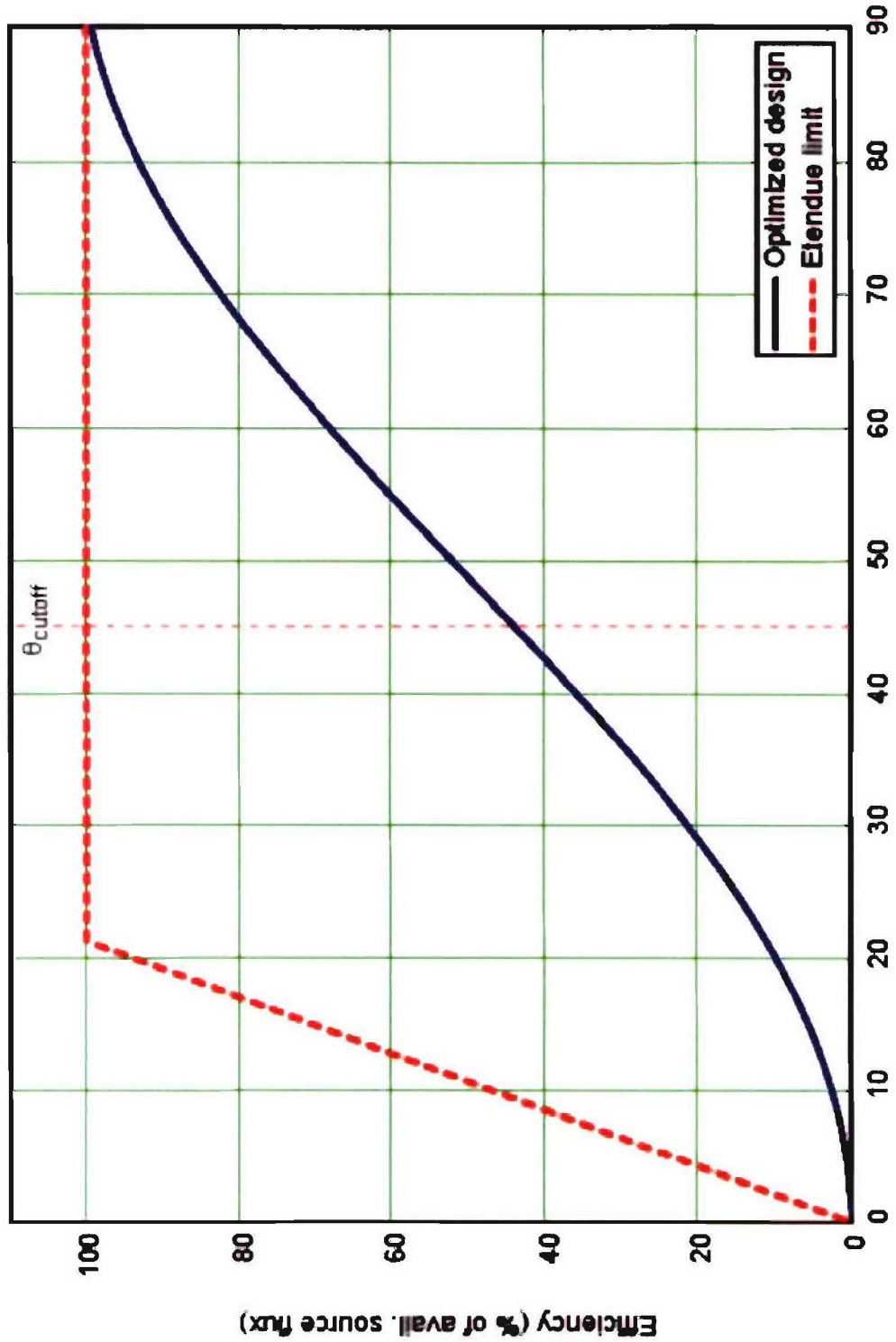
## Encapsulant dome DM0: total efficiency versus angle



(efficiency as a percentage of total source étendue)

# Encapsulant dome DM0: renormalized efficiency versus angle

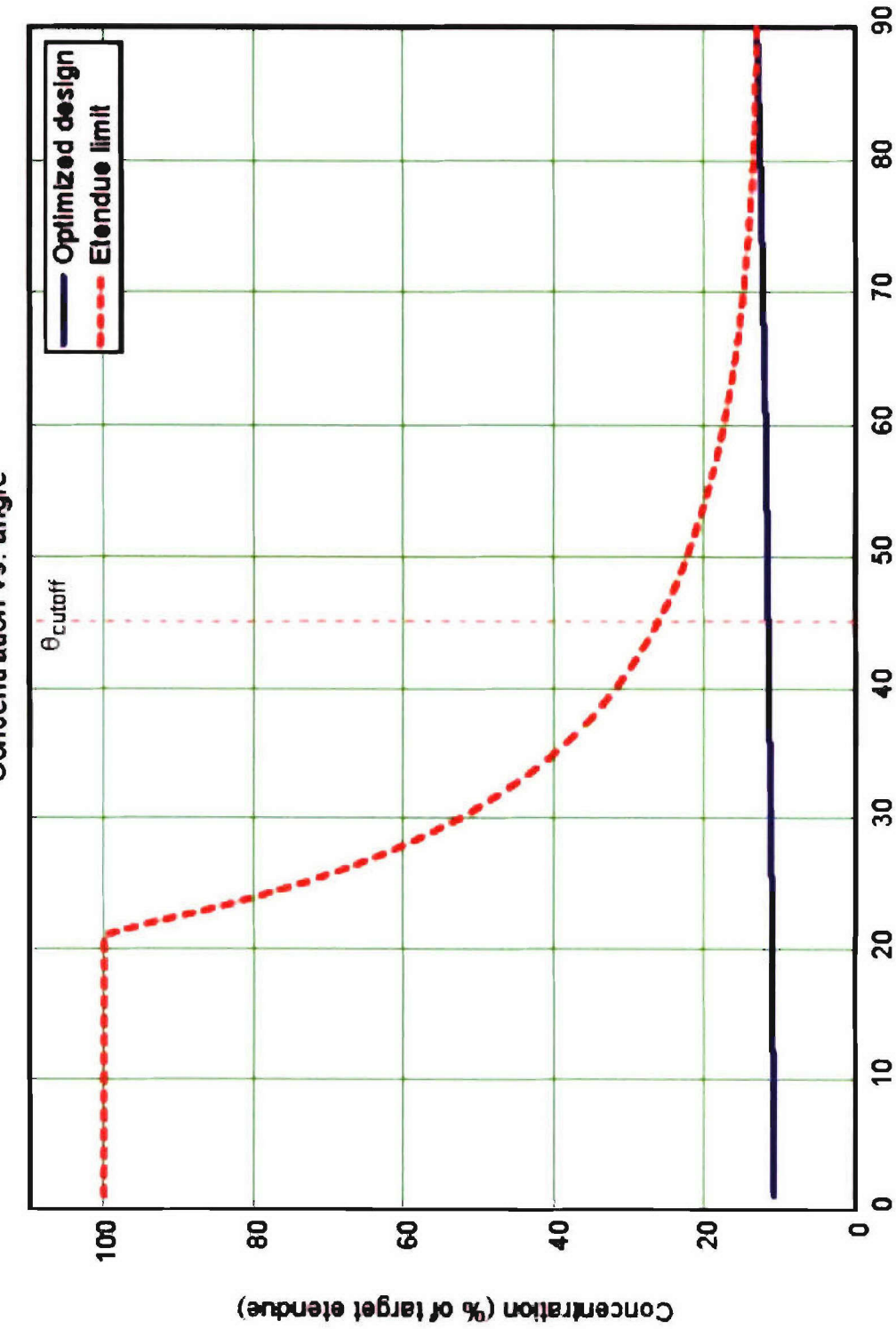
Efficiency vs. angle



Angle off axis (degrees)

Efficiency as a percentage of total source étendue  
(efficiency as a percentage of total source étendue  
minus étendue obstructed by substrate)

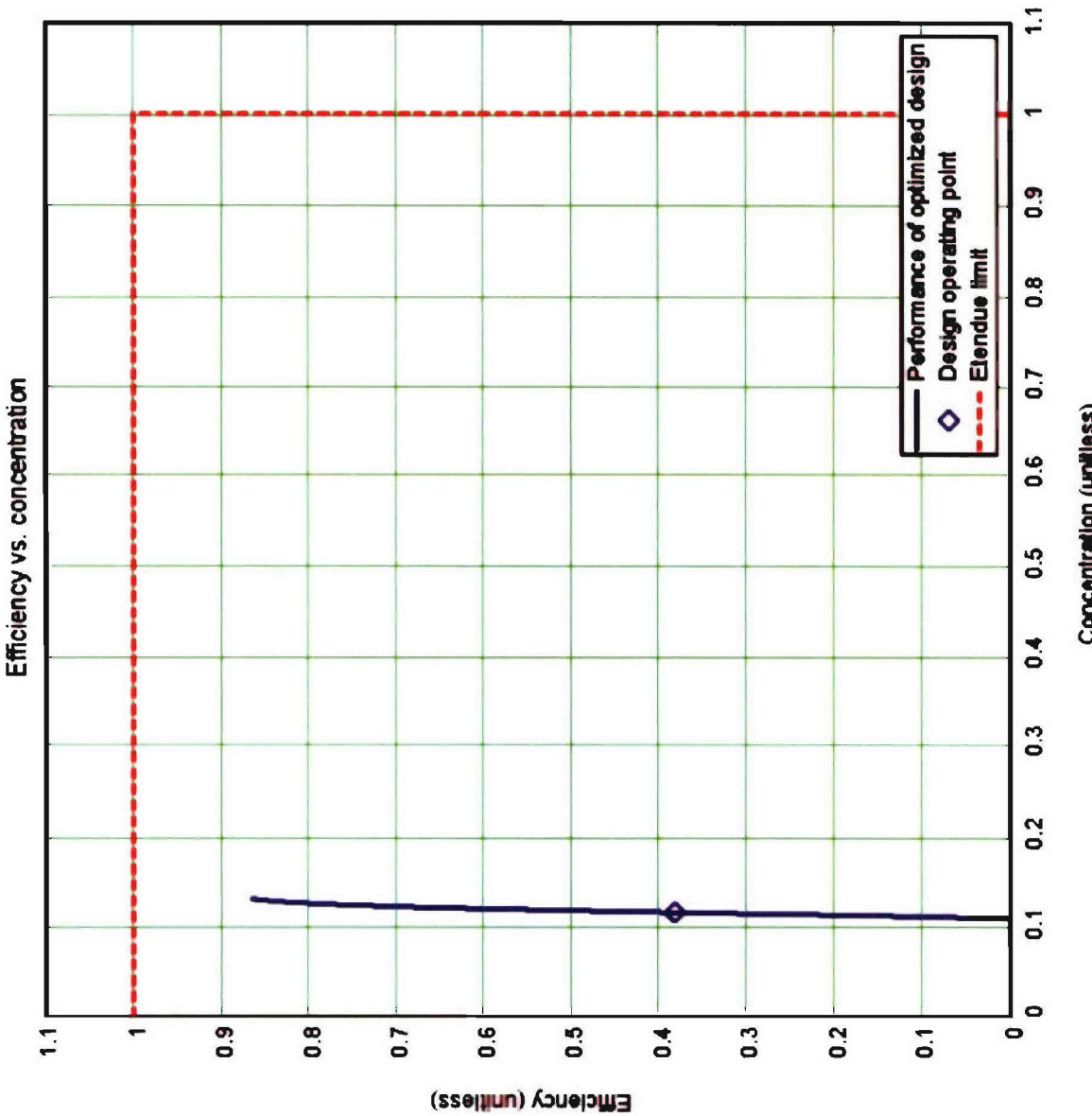
## Encapsulant dome DM0: concentration versus angle



Angle off axis (degrees)

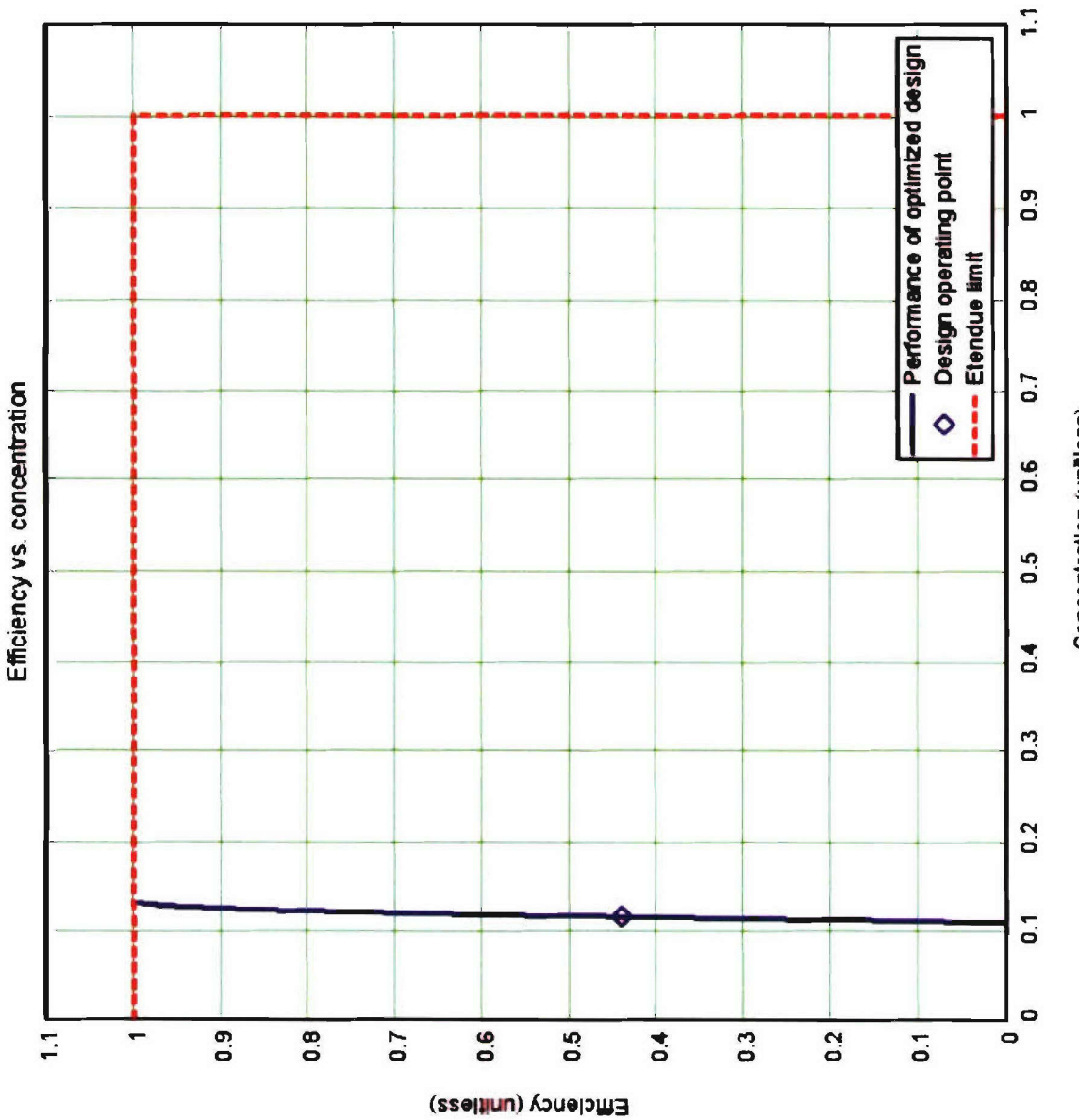
(étendue limit based on total source étendue minus étendue obstructed by substrate)

# Encapsulant dome DMO: total efficiency versus concentration



(étendue limit based on total source étendue)

## Encapsulant dome DM0: renorm. efficiency vs. concentration

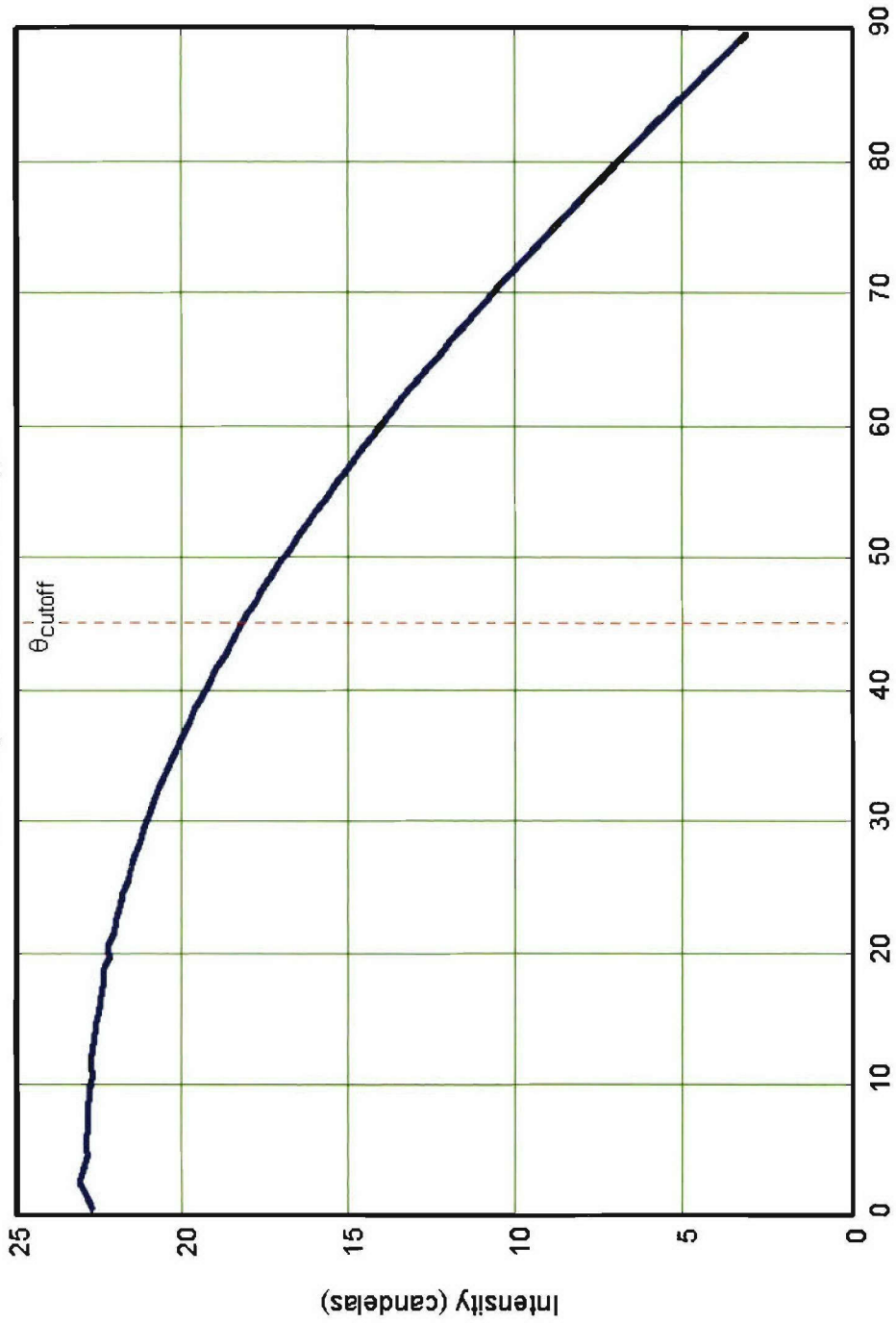


(éendue limit based on total source étendue  
minus étendue obstructed by substrate)

# Encapsulant dome DM0: radial intensity distribution

Case = "DM0"

Intensity as a function of angle



Angle off axis (degrees)

(intensity output averaged over annular angular bins as a function of angle off axis)